Dark and Light: Unifying the Origins of Dark and Visible Matter

Citation
Shuve, Brian. 2012. Dark and Light: Unifying the Origins of Dark and Visible Matter. Doctoral dissertation, Harvard University.

Permanent link
http://nrs.harvard.edu/urn-3:HUL.InstRepos:9284844

Terms of Use

Share Your Story

Accessibility

Thesis advisor   Author

Lisa Randall   Brian James Shuve

Dark and Light: Unifying the Origins of Dark and Visible Matter

Abstract

The Standard Model of particle physics can account for neither the dark matter dominating the universe's matter density, nor the baryon asymmetry that leads to the visible matter density. This dissertation explores models of new physics that connect dark matter to baryogenesis and can naturally account for the observed quantities of both types of matter. Special emphasis is given to models incorporating new weak-scale physics, as such models often predict signatures at present and upcoming experiments and can potentially be connected to solutions of the hierarchy problem.

In one class of models we study, the dark matter abundance is determined by a dark matter asymmetry connected to the baryon asymmetry. In such models, the separate dark matter, baryon, and lepton number global symmetries observed today are individually broken at or above the weak scale and lead to mixing of dark matter and Standard Model fields in the early universe. This can happen generically, with dark matter-visible matter mass mixing induced by large background energies or moduli in the early universe, and can also arise at the electroweak phase transition. Mass mixing models of asymmetric dark matter can readily accommodate dark matter masses ranging from 1 GeV to 100 TeV and expand the scope of possible relationships between the dark and visible sectors.

We also consider models of symmetric dark matter in which the annihilation of dark

matter particles in the early universe generates the observed baryon asymmetry. This process, called "WIMPy baryogenesis", naturally accommodates weak-scale dark matter and explains the observed dark matter density with only order-one couplings. WIMPy baryogenesis is a new model of baryogenesis at the weak scale, avoiding problems with high reheat temperatures in supersymmetric theories, and yielding observable consequences in ongoing and future experiments for some models.

Contents

Citations to Previously Published Work

Chapter 2 is based on work that appeared in the paper:

> "Emergent Dark Matter, Baryon, and Lepton Numbers", Yanou Cui, Lisa Randall, and Brian Shuve, JHEP **1108**, 073 (2011), `arXiv:1106.4834 [hep-ph]`.

Chapter 3 is based on work that appeared in the paper:

> "A WIMPy Baryogenesis Miracle", Yanou Cui, Lisa Randall, and Brian Shuve, JHEP **1204**, 075 (2012), `arXiv:1112.2704 [hep-ph]`.

Electronic preprints (shown in `typewriter font`) are available on the Internet at the following URL:

> `http://arXiv.org`

Acknowledgments

I would like to thank first and foremost my doctoral advisor, Lisa Randall. She has taught me how to think like a physicist: what questions to ask, how to get at the heart of what's really interesting about a physical problem, and how being persistent can pay dividends. I have also learned much physics from her class and our conversations, and I'm greatly appreciative of everything she's taught me.

I would also like to acknowledge the support of the other members of my doctoral committee. I owe a debt of gratitude to Matt Schwartz for the guidance he has provided through my Ph.D., his consistent presence in the high energy theory area, as well as the frequent physics help and comments he has given to me. I would also like to thank John Huth for providing me with excellent advice on experimental matters and for acting as a liaison with other experimentalists, and Melissa Franklin for her support through my entire at Harvard. and for stepping in to help with my defence. Howard Georgi provided me with invaluable support and guidance during the early years of my Ph.D., and I very much enjoyed my collaborations and conversations with him.

I am especially grateful for my other collaborators, particularly Yanou Cui, with whom I worked on the papers included in this dissertation, and Matt Buckley, Randy Kelley, and Dave Krohn, with whom I have worked on other projects. They have been excellent mentors, and I very much enjoyed our conversations on all matters related to physics or otherwise. I would also like to thank my academic siblings, David Simmons-Duffin and Dilani Kahawala, for their ongoing support, as well as others to whom I am greatly indebted: Tarek Anous, Irene Bredberg, Chi-Ming Chang, Yang-Ting Chien, Clay Cordova, Carol Davis, Laura Jeanty, Mike Kagan, Tina Lin, Tongyan Lin, John Mason, Eleanor Millman, Eddie Schlafly, Eli Visbal, and the many others in the physics department who have supported me

during my time at Harvard.

Much of the work presented in this dissertation was done in the stimulating environment at Currier House, where I have had the pleasure of spending the last three years. I am grateful to the Housemasters, Richard Wrangham and Elizabeth Ross, for the opportunity to be a part of the community and for providing much encouragement and support. I am equally indebted to the tutorial staff, administrators, and many of the students for making possible an enjoyable and productive three years.

My family has been a source of limitless support and encouragement over the course of my Ph.D: my mother Angela, my father John, my brother Karl and sister-in-law Melissa, niece Catriona, and step-mother Pamela. Without them, I would not have made it this far, and I am greatly appreciative of each of them. I would also like to thank my friends for keeping me sane and on-track, and for the wonderful times we spent together.

Finally, I want to thank my partner, David. He has been my rock for the past two and a half years, and I can't express how much he means to me, and how grateful I am for his support.

Dedicated to David.

Chapter 1

Introduction

The Standard Model of particle physics is one of the most successful physical theories of the modern era. It has withstood experimental scrutiny over a wide range of energy scales, and experiments at the Large Hadron Collider (LHC) continue to uphold its predictions. There do exist anomalies (in the muon anomalous magnetic dipole moment [1], the top quark forward-backward asymmetry measured at the Tevatron [2], and flavor violation in the charm sector at LHCb [3], among others), but they do not yet point to a conclusive break-down of the Standard Model effective field theory. In fact, electroweak precision tests strongly constrain models of new physics [4], and tests of flavor violation seem to indicate that the approximate flavor symmetries of the Standard Model hold to energies much higher than the scale of electroweak symmetry breaking (up to $\sim 10^4$ TeV) [5].

Astrophysical measurements do, however, tell us that there must exist physics beyond the Standard Model. Only about 1/6 of the matter energy density in the universe is made up of baryons and other visible matter, whereas the remaining 5/6 is comprised of dark matter particles [6]. Dark matter has only been observed through its gravitational interactions, yet

a number of its properties can be inferred: it is electrically neutral, stable on cosmological time-scales, has limited interactions with Standard Model particles and with other dark matter particles, and was likely cold at the time of its decoupling to prevent washout of small-scale structure[1]. With no Standard Model particles satisfying these conditions, the existence of dark matter is a sure sign of physics beyond the Standard Model.

Although many candidates for dark matter exist, the most common category by far is the weakly interacting massive particle (WIMP). One reason for this is that many models solving the hierarchy problem and stabilizing the Higgs mass predict new, stable, neutral particles at the weak scale that are viable dark matter candidates. Furthermore, the thermal relic abundance of a weakly interacting particle with a mass of $\mathcal{O}(100 \text{ GeV})$ is consistent with the observed dark matter energy density; this is known as the "WIMP miracle".

The parameter space of WIMP dark matter models is constrained by colliders, direct detection, and indirect detection experiments. The strongest limits by far come from direct detection experiments, which exclude (for some masses) spin-independent WIMP-nucleon cross sections above 10^{-44} cm^2 [8, 9], many orders of magnitude below cross sections mediated by electroweak gauge bosons, and comparable to cross sections mediated by the Higgs boson. Cosmic ray searches and studies of the cosmic microwave background (CMB) spectrum constrain the mass of a conventional WIMP to be above ~ 10 GeV [10], whereas monojet searches at the Tevatron and LHC rule out mediator masses at scales below a few hundred GeV [11]. While such experimental constraints can be evaded in a number of ways, such as if dark matter scattering is velocity-suppressed or couples dominantly to leptons [10], the narrowing viable parameter space and the absence of any discovery of new weak-scale

---

[1]For a recent review, see [7] and references therein.

states at the LHC suggest that the dark matter particle may not be a conventional WIMP, and it inspires us to look beyond the canonical examples of WIMP dark matter, considering in particular examples where dark matter can be connected to other beyond-the-Standard-Model phenomena.

Another question that cannot be resolved within the Standard Model is that of the origin of the baryon asymmetry[2]. While baryon number violation occurs in the Standard Model through transitions between different gauge field vacua (i.e. sphalerons and instantons), the CP violation and departure from thermal equilibrium at the electroweak phase transition are too small to generate the observed asymmetry. The very existence of visible matter at the densities we observe is therefore evidence in favor of physics beyond the Standard Model, and much effort has been expended in building viable models of baryogenesis. Unlike theories of dark matter, however, there is no *a priori* reason to believe that baryogenesis is connected in any way to the weak scale. In fact, many theories of baryogenesis, such as leptogenesis, are constrained to occur at scales well above the weak scale [13], making any experimental probe of the underlying physics nearly impossible. Only a few mechanisms for weak-scale baryogenesis are currently known [14, 15].

Given two known consequences of new physics, namely the existence of dark matter and the origin of the baryon asymmetry, it is important to consider whether they have a common origin. This is not a new idea: the oldest proposal dates from the mid-eighties and proposes that electroweak baryogenesis creates an asymmetry simultaneously in baryons and in a technibaryon dark matter sector [16]. Many of the earliest models, such as the one proposed by Nussinov in [16], have since been ruled out by direct detection experiments, but there

---

[2]For a review of baryogenesis, see [12] and references therein.

has been much progress recently in understanding the ways in which dark matter can be connected to baryogenesis [17, 18, 19, 20, 21, 22, 23, 24, 25, 26, 27]. The most commonly studied class of models is that of asymmetric dark matter [17], in which the dark matter abundance is not determined through thermal freeze-out but instead with an asymmetry connected to the baryon asymmetry, and it has been shown that dark matter masses ranging from keV to TeV can be accommodated within this framework [18, 19]. Asymmetric dark matter models can avoid constraints from indirect detection experiments and CMB studies, which both study late-time dark matter annihilation [10], and can provide a dynamical explanation for the similar energy densities of dark matter and baryons.

In this dissertation, we present two papers that extend the literature on possible connections between dark matter and baryogenesis. In Chapter 2, we study new ways in which the dark matter and baryon asymmetries in asymmetric dark matter models can be related [27]. As in many asymmetric dark matter models, separate dark matter, baryon, and lepton number symmetries are broken at high scales (ranging from the weak scale to the Planck scale) and only emerge at lower energies. We observe that such a global symmetry structure allows the mixing of dark matter and visible sector fields in the early universe, and we show that such mixing can occur generically in a range of scenarios. In particular, dark matter-baryon mixing induced by Planck-scale operators can be important and can lead to a relation between dark matter and baryon asymmetries even in models with no other connections between the dark and visible sectors. We further consider models where the separate dark matter, baryon, and lepton number symmetries emerge at the electroweak phase transition, calculating the effects of mass-mixing on the dark and visible sector asymmetries and showing the phenomenological implications for the LHC and dark matter detection

experiments.

We also propose one of the first models of *symmetric* dark matter connected to baryogenesis [28]. In Chapter 3, we demonstrate that dark matter annihilation can itself generate the observed baryon asymmetry in a process called "WIMPy baryogenesis". In WIMPy baryogenesis, the correct dark matter density is obtained for TeV-scale dark matter according to the WIMP miracle, while CP- and baryon-number-violating couplings to Standard Model fields allow for the creation of a baryon asymmetry. Since baryogenesis occurs at the weak scale, the theory avoids any problems associated with high reheat temperatures in supersymmetric theories. Many of the models also lead to observable consequences in upcoming experiments. Testing the precise mechanism of baryogenesis, however, remains a challenge.

Chapter 2

Emergent Dark Matter, Baryon, and Lepton Numbers

2.1 Introduction

Asymmetric dark matter models [17] have the potential to explain the fact that the energy in dark matter and ordinary matter are notably comparable. Suggested explanations involve the co-generation of an asymmetry in both dark matter and baryonic sectors by the decay of heavy fields [20, 21] or the Affleck-Dine mechanism [22]. Many others involve higher-dimensional operators that transfer asymmetries between the two, as was first explored in [16] and more recently in [17, 18, 23, 24, 25, 26]. Although it seems reasonable that dark matter number and baryon or lepton number might not be exactly preserved in the early universe, most such models require new ingredients (scales or fields) to accommodate higher-dimensional operators that lead to requisite relationships between the dark matter and ordinary matter densities. Although conceptually compelling, these models leave open

the question of whether we really expect the operators that violate baryon or lepton and dark matter numbers to exactly the right degree to really exist. Much more convincing would be models where there is mass mixing in the early universe arising from renormalizable interactions or operators suppressed only by the Planck scale, although ultimately, it is experiments that will hopefully shed light on the precise nature of the dark sector and its connection to the Standard Model.

In this Chapter, we show that it is possible that lepton (and hence baryon) number and dark matter number are not independent in the early universe. Mass mixing between dark-matter-number-carrying and lepton-number-carrying particles allows asymmetries to be established for both dark matter and lepton numbers. This mixing, of course, must turn off at later times when we know that the two symmetries must be independently preserved. The mechanism therefore requires fields whose value at high temperature differ from their low-temperature values so that in the late universe, dark matter and lepton numbers are independent symmetries and separately conserved.

The mass parameters in the models we present are linked to scales we know should be associated with new fields or interactions, namely the Planck scale and the electroweak scale (although in some cases we invoke also leptogenesis or grand unification scales). Furthermore, mass mixing can allow for novel relationships between the asymmetries in the dark and visible sectors when asymmetry transfer processes are out of equilibrium or the mass mixing shuts off rapidly in a first-order phase transition, allowing for deviations from the often-cited "predicted" value of the dark matter mass of ~ 5 GeV.

In our models, the mass mixing is active during a period of time after a fundamental $B - L$ asymmetry is generated but vanishes at late times to ensure stability of the dark matter.

This is the opposite of the usual chronology of phase transitions, where finite-temperature corrections keep the system in the symmetric phase at early times and a vacuum expectation value (VEV) arises at later times. There are at least two situations when symmetries are broken in the early universe and restored at late times. One involves multiple fields where one field initially stabilizes another field away from its minimum but no longer does so below a critical value [29]. Two stage phase transitions in a two Higgs model were first discussed in [30]. A similar idea is exploited in hybrid inflation models, [31], but the fields in our models are confined to the minima of the potential and involve no slow roll. We present models with multiple-stage phase transitions in Section 2.2. The second possibility is temperature-dependent background fields in the early universe that turn off as the universe cools. Examples include moduli field VEVs and the background energy density in the early universe. When these background fields are active, Planck-suppressed higher-dimensional operators can induce mass mixing at early times. We present both supersymmetric and non-supersymmetric models in Section 2.3.

2.2   Two-stage phase transition

2.2.1   Overview

Canonical examples of phase transitions in the early universe involve a transition from the symmetric phase at high temperatures to a broken phase at low temperatures. In Weinberg's pioneering work on symmetry breaking at finite temperature [29], examples were presented where the reverse is true: a symmetry broken at high temperatures is restored at later times. Typically, there exist multiple scalar fields and multiple stages to such phase transitions. In

this Chapter, we first discuss one simple example of a two Higgs doublet model originally considered in the context of electroweak baryogenesis [30], although our results can be generalized in a relatively straightforward manner. The models in the following section are more generic, but have slightly more technically complicated dynamics and work for a more restricted parameter range.

In the two Higgs set-up, a $B - L$ asymmetry is established at temperatures above a few hundred GeV. The precise mechanism is irrelevant to our analysis. At high temperatures $T \gg 100$ GeV, the universe is in an electroweak symmetric phase. As the universe cools to $T \sim 100$ GeV, the electroweak phase transition occurs, proceeding in two stages. In the first stage, a non-Standard Model scalar Φ acquires a VEV while the Higgs remains confined to the origin. When Φ gets a VEV, it induces mass mixing between the dark sector and the left-handed Standard Model leptons. During this period, the lepton asymmetry gets shifted into an asymmetry involving the high-temperature mass eigenstates, which are linear combinations of the zero-temperature dark matter and lepton fields.

At later time, a minimum develops along the Standard Model Higgs H direction with a lower energy than the initial vacuum. In the new vacuum, the Standard Model Higgs develops a VEV but Φ is confined to the origin by the potential induced by the large Standard Model Higgs VEV. Bubbles of the new vacuum form in a first-order phase transition. Because this phase transition occurs very rapidly, mass mixing shuts off before thermal interactions can adjust the asymmetry. This allows for non-trivial mixing of the asymmetry between the dark and visible sectors. In one scenario, the mixing can populate heavy dark sector fields that have been thermally suppressed in the previous stage, in which case the relationship between the final dark matter and lepton asymmetries is determined by the mixing angle at

the time of the first-order phase transition. In another scenario, it is determined purely by thermal factors.

In this two Higgs model, the second Higgs plays two important roles. First, it allows a field value that turns on and off before the fields enter the true electroweak-symmetry-breaking vacuum with the zero temperature Higgs VEV. Second, the Φ scalar is initially trapped far from the origin and allows for a first-order phase transition so the asymmetry in the dark matter gets established immediately.

We introduce only $\mathcal{O}(1)$ couplings and mass scales in the theory that are connected to the weak scale. We do not attempt to solve the hierarchy problem, but presume the model can be embedded in models that do have solutions (for instance, in supersymmetric models in which both scalars get their masses from supersymmetry breaking).

2.2.2 Asymmetry transfer during phase transition

The mechanism of asymmetry transfer by mass mixing is largely independent of the specific details of the two Higgs model, and we postpone a discussion of the field content, interactions, and phase transition to Section 2.2.3 and appendices A and B. For now, we consider general models with a doublet scalar Φ with a Yukawa coupling y_X to a vector-like dark matter particle, X, and a left-handed lepton L. During the intermediate stage of the electroweak phase transition, the real part of the scalar Φ has a VEV that induces mass mixing between X and L,

$$m_{XL}(T) = y_X \, v_\Phi(T). \tag{2.1}$$

If Φ does not acquire a VEV, an unbroken $\mathrm{U}(1)_{X-\Phi}$ symmetry would persist through the entire universe's evolution. At late times, after Φ had decayed away entirely, the solution to

the chemical potential relations would be $\mu_\Phi = \mu_X = 0$, and there would be no late time X asymmetry. Thus, the mass mixing stage is vital to ensuring a non-zero asymmetry at late times.

Although the model contains three generations of X and L, for simplicity and to retain only the essential elements of the mass mixing transfer mechanism, we consider only the case where one flavor of L and X have a large mixing. This could be obtained, for example, by hierarchical Yukawa couplings of the same form as in the Standard Model. The discussion can be easily generalized to the case of arbitrary mixings between flavor states.

The vector-like dark matter has a Dirac mass m_X. The mass matrix in the $(X, \bar{X}, L^0)$ basis, including the dynamically induced mixing term $m_{XL}(T)$ is

$$
\mathcal{M} = \begin{pmatrix} 0 & m_X & m_{XL}(T) \\ m_X & 0 & 0 \\ m_{XL}(T) & 0 & 0 \end{pmatrix}, \tag{2.2}
$$

which gives two degenerate states with mass $M = \sqrt{m_X^2 + m_{XL}^2}$ and a massless state. The mass basis states are

$$
|L'\rangle = -\sin\theta|\bar{X}\rangle + \cos\theta|L^0\rangle, \tag{2.3}
$$

$$
|\bar{X}'\rangle = \cos\theta|\bar{X}\rangle + \sin\theta|L^0\rangle, \tag{2.4}
$$

$$
|X\rangle, \tag{2.5}
$$

with the $|L'\rangle$ state being the massless state and the $|X\rangle$, $|\bar{X}\rangle$ states having mass M. The

mixing angle is

$$\sin \theta = \frac{m_{XL}}{\sqrt{m_X^2 + m_{XL}^2}}. \tag{2.6}$$

In the interaction basis, the rate of asymmetry transfer between L and X is approximately [32]

$$\Gamma_{L \to X} = \Gamma_0 \sin^2 2\theta \sin^2 \left(\frac{M^2}{6T\Gamma_0} \right), \tag{2.7}$$

which is explained in Section 2.3.2. This formula says that the net transfer rate is the oscillation rate that occurs before a thermal interaction, multiplied by the thermal interaction rate. Γ_0 is the rate at which scattering events occur, averaged between X and L. The system is in chemical equilibrium for the mass scales and couplings considered in this section if $y_X \gtrsim 10^{-6}$.

The gauge interaction of L^0 with charged leptons appears in the mass basis as

$$\mathcal{L}_{\text{gauge}} = \frac{1}{2}(L^-)^\dagger \gamma^\mu (1 - \gamma^5) W_\mu^- \left(\cos\theta\, L' + \sin\theta \bar{X}' \right). \tag{2.8}$$

The rate of interactions of $\bar{X}'$ is $\sin^2\theta$ times the usual weak interaction rate. Since the Hubble constant is very small at the time of the electroweak phase transition, for any non-negligible value of θ, $\bar{X}'$ is in thermal equilibrium due to gauge interactions. Since L^- carries lepton number of $+1$, $\bar{X}'$ and L' carry lepton number of $+1$ as well. The Yukawa interaction

$$\mathcal{L} \supset y_X \, \Phi \, X L = y_X \, \Phi \, X (-\sin\theta \bar{X}' + \cos\theta L') \tag{2.9}$$

gives X a lepton number -1. The interactions in our model are sufficient to keep the dark matter in thermal and chemical equilibrium.

We define the asymmetries in each field as $\Delta n_{L'}$, $\Delta n_{\bar{X}'}$ and Δn_X. The asymmetries in the fields are (for $T < M$)

$$\Delta n_{L'} = \frac{1}{3} \mu_L T^2, \tag{2.10}$$

$$\Delta n_{\bar{X}'} = -\Delta n_X = \sqrt{\frac{2TM^3}{\pi^3}} \mu_L \, e^{-M/T} \qquad (M \gg T), \tag{2.11}$$

$$= \frac{1}{3} \mu_L T^2 \qquad\qquad (M \ll T). \tag{2.12}$$

where μ_L is the chemical potential for lepton number. μ_L is fixed because the baryon and lepton numbers have already equilibriated due to sphaleron processes active prior to the electroweak phase transition. At the time of the second stage of the phase transition, the weak gauge boson masses are large enough that sphaleron processes are exponentially suppressed.

These relations are valid as long as the mixing is turned on. At a temperature T_{N}, bubble nucleation occurs and the system moves to the true vacuum via a strongly first-order phase transition. The dynamics of the phase transition are discussed in Appendix B. Therefore, in the moment immediately following the phase transition, the particles are still in the same state that they were in prior to the phase transition (according to the instantaneous approximation), but their masses are now fixed by the new vacuum. In particular, the mass mixing has shut off. The abundances of X, $\bar{X}$, and L^0 are fixed by the abundances of the

mass eigenstates at decoupling. In particular,

$$\Delta n_L = \cos^2\theta \Delta n_{L'} + \sin^2\theta \Delta n_{\bar{X}'}, \tag{2.13}$$

$$\Delta n_{\bar{X}} = \sin^2\theta \Delta n_{L'} + \cos^2\theta \Delta n_{\bar{X}'}, \tag{2.14}$$

$$\Delta n_X = -\Delta n_{\bar{X}'} \tag{2.15}$$

We now define the total dark matter and baryon numbers (obtained from summing over all charged fields) as

$$\Delta_X = \Delta n_X - \Delta n_{\bar{X}}, \tag{2.16}$$

$$\Delta_B = \Delta n_B - \Delta n_{\bar{B}}. \tag{2.17}$$

The ratio of X number to Δn_L is

$$\frac{\Delta_X}{\Delta n_L} = -\frac{(1+\cos^2\theta)\Delta n_{\bar{X}'} + \sin^2\theta \Delta n_{L'}}{\cos^2\theta \Delta n_{L'} + \sin^2\theta \Delta n_{\bar{X}'}}. \tag{2.18}$$

Once the phase transition completes, there is a conserved global $U(1)_{X-\Phi}$ symmetry. Since $\Delta n_\Phi = 0$ at the time of bubble nucleation, and Φ decays to X at late times, the zero temperature value of Δ_X is identical to that immediately after the phase transition occurs.

Depending on parameters, the ratio of the X and L asymmetries in (2.18) can be consistent with both light dark matter with a mass of $\sim$ GeV, or with heavier dark matter masses in the range $200 - 500$ GeV (other models consistent with heavier asymmetric dark matter can be found in [18, 21, 23]). For the heavy case, the final asymmetry ratio is dependent on which terms dominate (2.18). We identify three distinct limits:

1. **Relativistic** X. In the relativistic limit, when $T_N \gg m_X$, m_{XL}, there is no thermal suppression in the X_1 distribution and we have $\Delta n_{L'} = \Delta n_{\bar{X}'}$. Equation (2.18) reduces to

$$\frac{\Delta_X}{\Delta n_L} \approx -\frac{2}{3}. \tag{2.19}$$

This is consistent with light dark matter, $m_X \approx 3.3$ GeV, which we calculate from (2.23) below and by imposing $\Omega_X = 5\Omega_B$.

2. **Thermally-suppressed** X. In the non-relativistic limit $m_X \gg T_N$, then $\Delta n_{\bar{X}'} \ll \Delta n_{L'}$. In the thermal-suppression-dominated limit, $\Delta n_{\bar{X}'}/\Delta n_{L'} \gg \tan^2\theta$ and

$$\frac{\Delta_X}{\Delta n_L} \approx -6\sqrt{\frac{2M^3}{\pi^3 T^3}}\, e^{-M/T}. \tag{2.20}$$

This relation is the same as the one appropriate to asymmetry transfer via higher-dimensional operators that freeze out when X is non-relativistic [18]. This is the relevant limit when the ϕ VEV at T_N or the Yukawa coupling y_X is small.

3. **Mixing-angle-suppressed** X. The other type of non-relativistic solution is when $\Delta n_{\bar{X}'}/\Delta n_{L'} \ll \tan^2\theta$ and the solution is mixing-angle-dominated. In this case, the final ratio of X/L asymmetries is independent of $\Delta n_{\bar{X}'}$ and is determined only by the mixing angle,

$$\frac{\Delta_X}{\Delta n_L} = -\tan^2\theta. \tag{2.21}$$

This is a novel relationship and unique to models with mass mixing. Unlike the thermal-suppression-dominated limit, this result is only weakly dependent on T_N, since the expression for the ϕ VEV (A.4) is effectively temperature independent at low T.

We show below that, when the mixing is large ($y_X \gtrsim 1$), both the mixing angle and thermal suppression terms in (2.18) are relevant.

We now relate the baryon number to the X number using the relationship between baryon and lepton numbers in the early universe [33],

$$\frac{\Delta_B}{\Delta_L} = -\frac{4}{3}\frac{6N_\mathrm{f} + 3}{14N_\mathrm{f} + 9}, \tag{2.22}$$

where N_f is the number of Standard Model flavors. The baryon number to X number in each of the above cases is

1.

$$\frac{\Delta_X}{\Delta_\mathrm{B}} = \frac{2}{3}, \tag{2.23}$$

2.

$$\frac{\Delta_X}{\Delta_\mathrm{B}} = \frac{3}{\frac{2}{3}\sqrt{\frac{\pi^3 T^3}{2M^3}}\, e^{M/T} - 4}, \tag{2.24}$$

3.

$$\frac{\Delta_X}{\Delta_\mathrm{B}} = \frac{3\tan^2\theta}{4(1 - \tan^2\theta)}. \tag{2.25}$$

2.2.3   Field content and interactions

We now describe our model in more detail. It contains:

- The Standard Model fields, including and most relevant, the Higgs H and left-handed leptons L_i.

- The dark matter fields, which are three vector-like fermions X_i carrying a lepton flavor index.

- An additional doublet scalar Φ with hypercharge $+1/2$. The mass of Φ satisfies $m_\Phi > m_X$ so that X is stable.

There exists a Z_2 symmetry, under which Φ and X are charged but Standard Model fields are not. This makes X absolutely stable at late times, since $\langle \Phi \rangle = 0$ in the true vacuum and the Z_2 symmetry is unbroken. The symmetry also excludes the term $H\Phi^\dagger$, which would give Φ a tadpole when H gets a VEV.

The new terms of the Lagrangian are

$$\mathcal{L} \supset m_X X_i \bar{X}_i + y_X \, \Phi X_i L_i + V(H, \Phi) + \text{h.c.}, \tag{2.26}$$

where

$$V(T = 0) = 4k_1 |H|^4 - 4\mu_1^2 |H|^2 + 4k_2 |\Phi|^4 - 4\mu_2^2 |\Phi|^2 + 4k_3 |\Phi|^2 |H|^2, \tag{2.27}$$

using the notation of [30] that is convenient in the basis of real scalar fields. In addition to ensuring dark matter stability, the Z_2 symmetry excludes an $H\Phi^\dagger$ term, which would give Φ a tadpole when H gets a VEV.

With the convention in (2.27), perturbativity requires that $k_1, k_2 < 0.8$ and $k_3 < 3.1$. There are additional constraints to avoid hitting a Landau pole below the GUT scale, but this is highly dependent on what other fields couple to H and Φ (for example, the quartic terms could have large contributions from integrating out other weak scale particles) so we do not consider this as a constraint.

At $T = 0$, Φ must be stabilized at the origin, while H should have its measured VEV of $v = 246$ GeV. The vacua of the theory are determined by finding the critical points of the potential. To do so, it is simplest to move to the basis of real fields. Because $\text{U}(1)_{\text{em}}$

remains unbroken, the VEVs can be rotated purely into the neutral components of H and Φ. Furthermore, assuming that the potential is CP-conserving (for simplicity), only the real components of Φ and H can get VEVs. Therefore, we make the substitution

$$\Phi = \frac{1}{\sqrt{2}} \begin{pmatrix} \phi \\ 0 \end{pmatrix}, \quad H = \frac{1}{\sqrt{2}} \begin{pmatrix} h \\ 0 \end{pmatrix}, \tag{2.28}$$

giving the zero temperature potential

$$V(T=0) = k_1 h^4 - 2\mu_1^2 h^2 + k_2 \phi^4 - 2\mu_2^2 \phi^2 + k_3 \phi^2 h^2. \tag{2.29}$$

Because we are interested in the evolution of the field values as the universe cools, we also need to include thermal contributions to the masses of H and Φ. These thermal corrections are proportional to T and dominate over the tree-level masses for $T \gg \mu$. Ultimately, these corrections determine how the phase transition proceeds. We can write the finite temperature potential as

$$V(T) = k_1 h^4 - 2\mu_1^2 h^2 + k_2 \phi^4 - 2\mu_2^2 \phi^2 + k_3 \phi^2 h^2 + \frac{1}{2}\alpha_1 T^2 h^2 + \frac{1}{2}\alpha_2 T^2 \phi^2, \tag{2.30}$$

where

$$\alpha_1 = 2k_1 + \frac{2}{3}k_3 + \frac{e^2(1 + 2\cos^2 \theta_{\mathrm{W}})}{\sin^2 2\theta_{\mathrm{W}}} + \frac{1}{2}y_t^2, \tag{2.31}$$

$$\alpha_2 = 2k_2 + \frac{2}{3}k_3 + \frac{e^2(1 + 2\cos^2 \theta_{\mathrm{W}})}{\sin^2 2\theta_{\mathrm{W}}} + \frac{1}{6}y_X^2. \tag{2.32}$$

The light quark and lepton Yukawa couplings are sufficiently small that only the top Yukawa needs to be considered for corrections to the h mass.

We give the details of the vacua and constraints on the parameters in Appendix A. The first of the two most important results is the constraint leading to a two stage phase transition,

$$\sqrt{\frac{k_1}{k_2}} < \frac{\mu_1^2}{\mu_2^2} < \frac{\alpha_1}{\alpha_2}, \tag{2.33}$$

which comes from requiring that the ϕ direction become unstable at the origin before h, while also requiring that the Standard Model Higgs vacuum have lower energy than the $\phi \neq 0$ vacuum. The other main requirement is that ϕ be stabilized to the origin in the true vacuum,

$$m_\phi^2 = 2\mu_1^2 \frac{k_3}{k_1} - 4\mu_2^2 > 0. \tag{2.34}$$

2.2.4   Numerical results

We present numerical results for a scan of parameters leading to a two stage phase transition. The most relevant result for us is the temperature T_N at which bubble nucleation occurs for a given set of parameters. This determines which of the three limits (relativistic, thermal-suppression-dominated or mixing-angle-dominated) is most relevant and hence the dark matter mass consistent with $\Omega_{DM} = 5\,\Omega_{baryon}$. We present details of the calculation of T_N in Appendix B.

The necessary and sufficient conditions for asymmetry transfer through a two stage phase transition are:

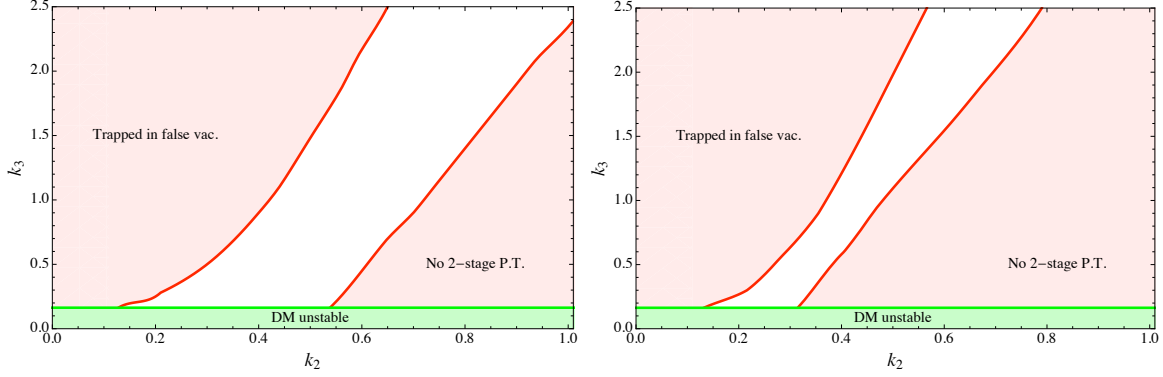- The constraints (2.33) are satisfied.

Figure 2.1: Unshaded regions in the $k_2 - k_3$ plane give rise to a two stage phase transition and a viable dark matter asymmetry through mass mixing for light dark matter. Each parameter point is consistent with dark matter of mass 3.3 GeV. The other parameters are held fixed at $\mu_2 = 54$ GeV for both plots, $y_X = 0.5$ (left) and $y_X = 1.7$ (right). In the left shaded region (red), the barrier between vacua is too large for rapid bubble nucleation and the system remains trapped in the false vacuum. In the right shaded region (also red), the $\phi \neq 0$ direction is not a stable vacuum. In the bottom shaded region (green), the scalar mass m_ϕ is excluded by LEP.

- The bubble nucleation temperature $T_N > 0$, and the wall velocity is large enough that the transition is strongly first-order (see Appendix B).

- The mass $m_\phi > m_X$ in the final vacuum so that X is stable, where m_ϕ is given in (2.34).

There is also a constraint coming from LEP searches for new doublet scalars (specifically sleptons, from which there is a bound $m_\phi \gtrsim 90$ GeV [34]).

The Standard Model Higgs mass parameter, μ_1, is fixed to be $\mu_1 = 42$ GeV by a Higgs boson mass of 120 GeV in the final vacuum, while the quartic coupling k_1 is fixed by the VEV $\langle h \rangle = 246$ GeV. We have a four-dimensional parameter space, consisting of the ϕ quartic self-coupling k_2, the $\phi - h$ mixed quartic coupling k_3, the ϕ mass parameter μ_2, and the Yukawa coupling y_X.
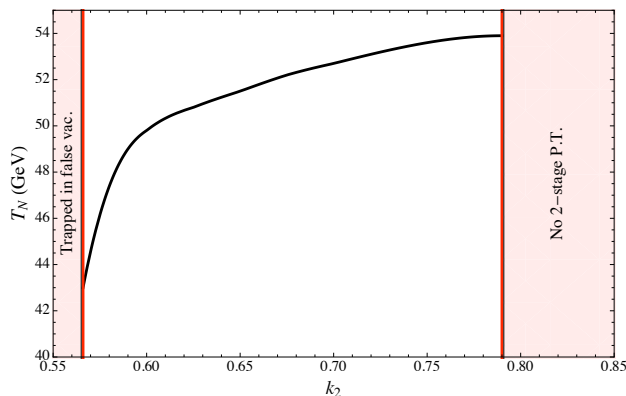
Figure 2.2: Relationship between the temperature of the first-order phase transition T_N and the ϕ quartic coupling k_2. The other parameters are held fixed at $k_3 = 1.5$, $y_X = 1.7$ and $\mu_2 = 54$ GeV. No first-order phase transition takes place in the shaded regions.

The allowed values of μ_2 come from the constraint (2.33). The range is $\mu_2 = 25 - 100$ GeV, which is precisely the range we expect if μ_1 and μ_2 have a common origin. Since perturbativity limits $k_2 \lesssim 0.8$, the upper bound of $\mu_2 < 100$ GeV follows from (2.33). The lower bound $\mu_2 > 25$ GeV comes from the fact that the ratio α_1/α_2 is fixed by the Standard Model interactions when $y_X, k_2, k_3 \to 0$. The parameter space for a viable two stage phase transition is small close to either bound on μ_2, so we present all of our results with an intermediate, representative value of $\mu_2 = 54$ GeV and scan over other parameters.

The Yukawa coupling is selected to be $\mathcal{O}(1)$. In this case, the symmetric component of X annihilates through the Yukawa interaction (see Section 2.2.5).

We now present, in turn, the parameters consistent with the three dark matter scenarios discussed above.

1. **Relativistic X.** In general, $T_N \gg 3.3$ GeV, so light 3.3 GeV dark matter is consistent with any choice of parameters leading to a two stage phase transition. We show in Figure 2.1 a region of parameter space in the $k_2 - k_3$ plane (with $\mu_2 = 54$ GeV and

two values of $y_X = 0.5, 1.7$) with a two stage phase transition and light dark matter.

In the right shaded region, the couplings k_2 give a large contribution to the thermal mass of ϕ, stabilizing the ϕ direction and leading the system to condense directly into the true, $h \neq 0$ vacuum. In this case, the ϕ VEV is never non-zero. For smaller values of k_2, the VEV $\langle \phi \rangle \approx \mu_2/\sqrt{k_2}$ increases and the barrier between vacua becomes larger. In the left shaded region, the barrier is so large that bubble nucleation never occurs and the system remains stuck in the false vacuum. The tunneling temperatures are shown in Figure 2.2.

In the shaded region at the bottom, m_ϕ from (2.34) is smaller than the LEP bound.

2. **Thermally-suppressed** X. The relation (2.24) dictates the X masses consistent with a given tunneling temperature T_N. We present results in Figure 2.3 as a function of the parameters k_2, k_3, with $\mu_2 = 54$ GeV and $y_X = 0.5$. The Yukawa coupling is small enough that the mixing angle contribution to the asymmetry is always smaller than the thermal terms. For Yukawa couplings $y_X \gtrsim 1$, both mixing angle and thermal suppressions are relevant and we address this case in point #3.

The entire unshaded region is consistent with dark matter with a thermally-suppressed asymmetry, and the dashed contours illustrate a few representative values of m_X between 300 and 450 GeV. The outer side shaded regions represent the same constraints as the relativistic case. For small values of k_3, m_ϕ becomes smaller than the value of m_X giving the correct dark matter density, making the dark matter unstable. In the inner shaded region on the left, the mixing angle contribution to $\Delta_X/\Delta_\mathrm{B}$ dominates over the thermally-suppressed terms.
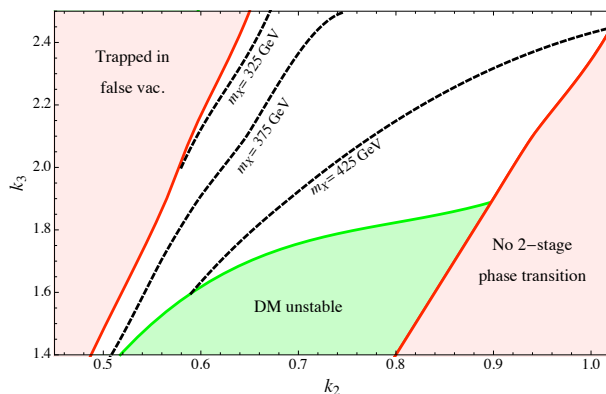
Figure 2.3: Regions in the $k_2 - k_3$ plane where the final X asymmetry is dominated by thermal suppression. The unshaded region is the viable parameter space. Other parameters are held fixed at $\mu_2 = 54$ GeV and $y_X = 0.5$. Dashed contours show representative X masses associated with each point in parameter space (from left to right, 325 GeV, 375 GeV, 425 GeV). The outer shaded regions to the side (red) do not give rise to a two stage phase transition, while the shaded bottom region (green) violates the condition $m_X < m_\phi$, rendering X unstable.

We find a range of dark matter masses $300 - 500$ GeV for the given parameters. When we scan over other values of μ_2, we find a range $\sim 250 - 550$ GeV, although most of the parameter space lies in the $300 - 450$ range. According to (2.33), a smaller value of μ_2 gives a two stage phase transition with smaller values of k_2, shifting the band in Figure 2.3 to the left (to smaller values of k_2). Smaller values of y_X decrease the value of α_2, allowing larger values of k_2 and relaxing the upper bound on k_2 from (2.33).

This range of masses is the expected range for the two Higgs model since the bubble nucleation temperature $T_N \lesssim 2\mu_1$ from (B.1), and this restricts $m_\phi \lesssim 550$ GeV. For stability, the X mass can never exceed the ϕ mass, and the largest possible value of m_ϕ with perturbative quartic couplings is about 550 GeV. The lower bound on masses comes from the fact that the vast majority of points in parameter space with a two stage phase transition have tunneling temperature $T_N \gtrsim 35$ GeV (when the vacua
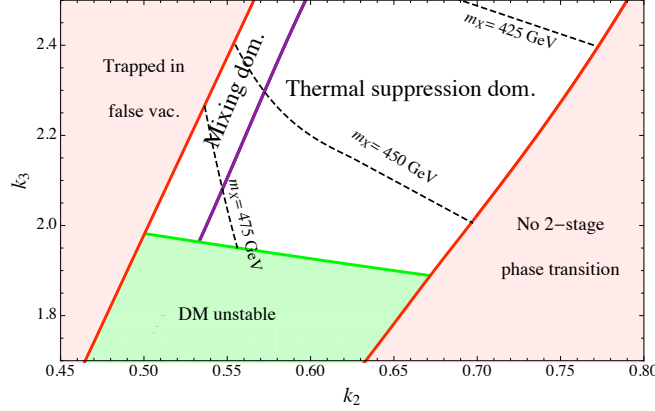
Figure 2.4: Regions in the $k_2 - k_3$ plane with $y_X = 1.7$ and $\mu_2 = 54$ GeV consistent with weak scale dark matter. The mixing angle contribution is relevant for all points. The unshaded region is the viable parameter space. Dashed contours show representative X masses associated with each point in parameter space (from left to right, 425 GeV, 450 GeV, 475 GeV). The two inner, unshaded regions show parameters where the mixing angle (left) and thermal suppression (right) are respectively dominant. The outer shaded regions (red) do not give rise to a two stage phase transition. In the lower shaded region (green), the $m_X < m_\phi$ condition is violated.

become degenerate at a temperature lower than this, the energy barrier is typically large enough that the system remains trapped in the false vacuum). Thus, when the final asymmetry in X is determined by thermal suppression, the range of allowed dark matter masses is $250 \lesssim m_X \lesssim 550$ GeV.

3. **Mixing-angle-suppressed** X. We present results in Figure 2.4 as a function of the parameters k_2, k_3, with $\mu_2 = 54$ GeV and $y_X = 1.7$[1]. Dark matter is consistent with the unshaded region, with dashed contours showing representative values (425 GeV, 450 GeV, 475 GeV). The outer shaded regions do not give rise to a two stage phase transition for the reasons outlined in the relativistic discussion. In the lower shaded

---

[1]For $y_X = 0.5$ considered in the first two cases, the mixing angle is always too small to give a significant contribution to the asymmetry.

region (green), the X mass consistent with the asymmetry transfer is larger than m_ϕ, making the dark matter unstable.

We mark the regions where the mixing angle and thermal suppression terms in (2.18) dominate. Dark matter masses range from $400 - 500$ GeV with the parameters chosen. Comparing with Figure 2.3, the presence of the large mass mixing significantly changes the asymmetry, even in regions where thermal terms are largest. This favors heavy dark matter, $\mathcal{O}(400 \text{ GeV})$, as the large X mass suppresses both the mixing angle and thermal contributions and results in the correct dark matter abundance, even in the presence of two sources of asymmetry transfer.

The range of parameters with dominant mixing angle is much more restricted than for relativistic or thermally-suppressed dark matter. The reason is that, except for small k_2, tunneling occurs shortly after the vacua become degenerate and when the ϕ VEV is small. This typically leads to a mixing angle that is smaller than the Boltzmann suppression factor.

To summarize, with a two Higgs model with a two stage phase transition, the relationship between the baryon and dark matter asymmetries can be determined by thermal effects and/or the mixing angle. With large mass mixing $(y_X \gtrsim 1)$, the mixing angle contribution to the asymmetry is always important, and the ratio of $\Delta_X/\Delta_\mathrm{B}$ deviates from the predictions of earlier work where only thermal suppression is relevant. The model is consistent with a wide range of dark matter masses, from 5 GeV in the relativistic case to 300-500 GeV in the thermally-dominated and mixing-angle-dominated regimes.

Note that for this model the transfer is always in equilibrium and the thermal scattering rate is always comparable to the oscillation rate.

2.2.5   Annihilation of the symmetric component

In addition to generating the correct dark matter asymmetry, the coupling must be large enough that the symmetric component annihilates efficiently so that the late-time X density is dominated by the asymmetric component. Our model provides a built-in mechanism for symmetric X annihilation via the t-channel scalar exchange process process $X\bar{X}^\dagger \to LL^\dagger$. The cross section for this process is

$$\sigma = \frac{y_X^4}{16\pi} \cdot \frac{m_X^2}{m_\phi^4}. \tag{2.35}$$

The requirement that the symmetric number density of X at freeze-out be less than the asymmetric component constrains the Yukawa coupling. For masses in the $\mathcal{O}(100 \text{ GeV})$ range, this requires $x \equiv m_X/T_{\text{freeze-out}} \sim 25$ and,

$$y_X^4 > (6.6 \times 10^3) \left(\frac{m_\phi^4 \, e^x}{M_{\text{Pl}} \, m_X^3 \sqrt{x}} \right). \tag{2.36}$$

For values $m_X \sim m_\phi \sim \mathcal{O}(500 \text{ GeV})$, this gives the constraint $y_X > 0.45$. This is satisfied for the parameters considered above and is true over much of the parameter space consistent with asymmetric dark matter where the X asymmetry comes from mass mixing.

When $m_X = 3.3$ GeV, the suppression in the cross section from $(m_X/m_\phi)^2$ can be very large. When m_ϕ is at its lowest bound of 90 GeV, then $y_X \gtrsim 0.6$. For larger values of m_ϕ, then $y_X > 1$ to ensure the annihilation of the symmetric component. There may also exist other annihilation channels (for example, if there is a U(1)$'$ under which X and ϕ are charged) to further deplete the symmetric component.

2.2.6 Phenomenology

While the dark matter in this model is a singlet under the Standard Model gauge group, the model also contains a new charged field, the doublet scalar ϕ. This leads to a loop-suppressed coupling of X to nucleons, as described in [35, 17]. The direct detection cross section is the same as [23],

$$\sigma_{\text{dd}} \approx (4 \times 10^{-46} \text{ cm}^2) \left(\frac{Z/A}{0.4} \right)^2 \left(\frac{500 \text{ GeV}}{m_\phi/y_X} \right), \qquad (2.37)$$

where $m_\phi/y_X \approx 10 - 1000$ GeV in the two Higgs model ($m_\phi \approx 100 - 500$ GeV and $y_X \approx 0.5 - 10$). This cross section should be tested by the next generation of detectors. The one-loop interaction with nucleons is dominant over direct interactions with electrons in the detector, due to the small mass of the electron and therefore the small recoil energy [36].

The doublets can be pair produced at the LHC by s-channel weak gauge bosons. The neutral component ϕ^0 decays to $X + \nu$, while the charged components decays to $X + \ell^\pm$. The decay of $\phi^\pm \to \phi^0 + W^\pm$ is suppressed by the small mass splitting (induced by electroweak symmetry breaking loops) between components of the doublet.

The charged component is easiest to find. Given the approximate lepton-X flavor symmetry, the signature is two oppositely-charged leptons of the same flavor plus missing energy. This is exactly analogous to searches for charged left-handed sleptons in the MSSM, with X being analogous to the neutralino LSP. In the case of sleptons, assuming no degeneracy with the LSP ($m_{\chi^0} \ll m_{\tilde{\ell}}$), the LHC will be capable of finding left-handed sleptons at the LHC at the 5σ level with masses up to 350 GeV with an integrated luminosity of 100 fb^{-1} at 14 TeV [37]. In our case, the doublet masses are in the range $100 - 500$ GeV, so there is

the possibility of detection at the LHC, although discovery will require a long running time.

This model can be differentiated from supersymmetric models because the decay chains should be different. Furthermore, this is a more challenging search than gluino or squark searches, so by the time of detection of the doublets, we should already know whether or not supersymmetry is present at the weak scale.

Other possible signatures are the production of two ϕ^0, which results in a monojet + missing energy signature, or the production of $\phi^+\phi^0$, with a signature of one lepton + missing energy. Both are difficult to distinguish from the Standard Model background, and we find it unlikely that either is promising.

Our model is an asymmetric leptophilic dark matter model [23] and can therefore have suppressed indirect detection signals. The fact that the late-time dark matter density is dominated by the asymmetric component means that there may be insufficient anti-dark-matter in the late universe for there to be an appreciable annihilation signal. As shown in earlier works, the symmetric component could, however, be replenished by a small X Majorana mass [38] or there could be some remnant of the symmetric component due to annihilation freeze-out [25]. Therefore, the detection of excesses in cosmic spectra does not rule out this model. As shown in [23], the annihilation cross section (2.35) for weak scale dark matter is $\langle \sigma_{\mathrm{ann}} v \rangle \approx 10^{-24}$ cm^3/s, which is consistent with the PAMELA and Fermi anomalies for $m_X = 400$ GeV, $m_\phi = 500$ GeV and $y_X = 1$ [23].

2.3 Mass Mixing via Planck-Scale-Suppressed Operators

2.3.1 Overview

Our second and more generic scenario exploits large VEVs that we expect in the early universe. Examples of fields that are likely to have large, non-zero values include moduli, flat directions in supersymmetric theories, and Goldstone bosons. At finite temperature and density, the kinetic energies of relativistic fields also have sizable background values. Generically, all such fields should couple to any other existing fields through Planck-suppressed operators. Since we do not expect such operators to respect any particular global symmetry, these operators should lead to the mixing of dark matter and lepton quantum numbers. While theories with moduli and flat directions are most likely supersymmetric, mixing due to background energy is also present in non-supersymmetric theories.

The key point to take away for all models of mixing by Planck-suppressed operators is that mixing between different sectors *does* occur due to Planck-scale physics (assuming gauge-invariant combinations of fields). Therefore, asymmetry transfer between sectors also occurs if the asymmetry generation happens early in the universe's history. This is the dominant effect if the dark and Standard Model sectors are very isolated, and is still expected to be present as a sub-leading effect if other fields mediate dark-matter-number-violating interactions between the two sectors.

We consider both fermionic and scalar dark matter candidates. Since lower-dimensional operators lead to less-suppressed mixing, scalar dark matter proves to be particularly important when the mixing would otherwise be too small, such as when induced by thermal kinetic

terms and field VEVs, which are temperature-suppressed and therefore generically smaller than those for moduli. For operators involving string moduli and other flat directions, both fermion and scalar mixing can lead to a large transfer of asymmetry between sectors.

For simplicity, we consider models in which the dark matter is a Standard Model gauge singlet in order to avoid direct detection bounds. This implies that the field mixing with the dark matter is also a Standard Model gauge singlet[2]. One option for the field mixing with dark matter is the right-handed neutrino in a model with Dirac neutrino masses, which carries lepton number. While we choose this example to work out the concrete details of mass mixing, the general framework is also compatible with Majorana leptogenesis (or GUT baryogenesis) in theories with additional lepton-number-carrying gauge singlets. As will be discussed later, models with heavy moduli can dilute the dark matter and baryon asymmetries. In the framework of Dirac leptogenesis, the dilution can be compensated by resonance enhancement, which is not generic. A more general alternative is to have Affleck-Dine leptogenesis (or baryogenesis) along a flat-direction as a composition of singlet $L(B)$ and SM leptons (baryons). Alternatively, the moduli can be light enough to be stable over the lifetime of the universe.

We focus on the case where a $B - L$ symmetry is created via Dirac leptogenesis [39]. In such models, no net lepton number is created but an equal and opposite lepton number is sequestered in the LH and RH neutrino sectors. The processes that equilibriate the two sectors have rates that are suppressed by neutrino masses and so do not come into equilibrium until well after the time of the electroweak phase transition. The asymmetry stored in the RH (s)neutrinos can then be transferred to the dark sector via mass mixing terms and provide

---

[2]The dark matter can carry a gauge charge as long as the field with which it mixes is also charged.

for a connection between the dark matter and baryon asymmetries.

For our models, we take the field content to be the MSSM as well as the new components outlined below. First, there are the dark matter and singlet lepton fields:

- Three generations of singlet RH neutrino chiral superfields N_i.

- Chiral superfields X and $\bar{X}$, which comprise the dark matter.

We also assume in this model the existence of fields responsible for Dirac leptogenesis, as outlined in Appendix C:

- At least two generations of heavy vector-like doublets ψ and $\bar{\psi}$, whose decay generates the $B - L$ asymmetry.

- A singlet field χ which is necessary for generating an asymmetry in both LH and RH neutrinos.

- A U(1)$_N$ symmetry that forbids direct coupling between the LH Standard Model lepton L and the RH neutrino N. It can also permit the annihilation of the symmetric component of X if gauged. The gauge symmetry is anomaly-free with charges $Q(X) = 1$, $Q(N) = -1$, $Q(\psi) = 1$ and $Q(\chi) = 1$ with two additional fields, either in the lepton or dark sectors.

Note that the new matter content is similar to that for models of Majorana leptogenesis (and a dark matter sector). But in this case the right-handed neutrinos are light and additional fields are present to generate the $B - L$ asymmetry through their decay.

The tree-level, renormalizable superpotential is

$$W = M_\psi \bar{\psi}\psi + y_u Q H_u \bar{u} + y_d Q H_d \bar{d} + y_N N H_u \psi + y_L L \chi \bar{\psi}. \tag{2.38}$$

The model possesses a Peccei-Quinn-type symmetry that forbids $\bar{X}X$ mass terms. These mass scales can be generated dynamically at later times, possibly through SUSY breaking. We then expect that the X masses (for both the fermions and scalars) are ultimately set by the soft SUSY scale.

2.3.2   Mass mixing formalism

In Section 2.2, we worked in the mass eigenstate basis. This is appropriate because the mass mixing in the two Higgs case is nearly temperature-independent around the decoupling temperatures (particularly when compared to the rate of the first-order phase transition), making the mass eigenbasis temperature independent as well. The system also consists of a mixture of relativistic and non-relativistic states, and the mass basis adequately describes the Boltzmann suppression of the heavy states. Finally, the system is fully mixed, meaning that the rate of the asymmetry transfer given by (2.7) is in equilibrium ($\gg H$) and the chemical potentials for X and N track their equilibrium values.

By contrast, the VEVs inducing mass mixing for these models with Planck-suppressed operators are highly temperature-dependent. In fact, there is no phase transition, with VEVs typically proportional to some power of T and turning off gradually. Because the mass mixing changes with time, the mass basis is only an instantaneous eigenbasis. To avoid continually changing basis over the course of the time evolution, it is simplest to use interaction eigenstates.

At early times when the Planck-suppressed mass mixing operators are active, the fields are also highly relativistic. This is precisely the limit in which the standard neutrino oscillation formalism is valid. This section is dedicated to the overview of how distributions of particles

with mass mixing evolve over time. A good review of this material can be found in [40]. We first present fermion mixing and then discuss scalars.

We first review the story with pure coherent oscillation, which is directly analogous to neutrino oscillation. For Weyl fermions ψ_α, $\alpha = 1, \dots, N$, the mass part of the Hamiltonian is

$$\mathcal{H}_{\text{mass}} = \frac{1}{2} M_{\alpha\beta} \psi_\alpha \psi_\beta + \text{h.c.}. \tag{2.39}$$

We assume no mass degeneracies in order to simplify the results. We use Greek letters to label flavor eigenstates and Latin letters to label mass eigenstates. The mass eigenvalues M_i^2 are found by diagonalizing the matrix $M^\dagger M$. The rotation matrix U that diagonalizes M satisfies

$$\sum_{\alpha,\beta} U_{i\alpha}^\dagger (M^\dagger M)_{\alpha\beta} U_{\beta j} = M_i^2 \delta_{ij}. \tag{2.40}$$

The relationship between the mass basis and the flavor basis is

$$|\psi_\alpha\rangle = \sum_i U_{\alpha i} |\psi_i\rangle. \tag{2.41}$$

During a particle's propagation between interaction points, it can be described by a wavefunction in standard quantum mechanics. After a time t, the probability of oscillation from flavor state α to β is given by $\mathcal{P}_{\alpha \to \beta}(t) = |\langle \psi_\beta(t) | \psi_\alpha(0) \rangle|^2$. Expanding the states in the mass basis and performing space-time evolution using the operator $e^{-iHt + i\mathbf{p}\cdot\mathbf{x}}$ gives, in the relativistic limit,

$$\mathcal{P}_{\alpha \to \beta}(t) = \text{Re} \left[\sum_{i,j} U_{\alpha i} U_{\alpha j}^* U_{\beta i}^* U_{\beta j} \exp\left(-i \frac{M_i^2 - M_j^2}{2E} t \right) \right], \tag{2.42}$$

where $\alpha \neq \beta$. The case where $\alpha = \beta$ is simply found by subtracting the probability of oscillating into anything else.

For the special case of two fields, we can write U in terms of a single mixing angle,

$$U = \begin{pmatrix} \cos\theta & \sin\theta \\ -\sin\theta & \cos\theta \end{pmatrix}. \tag{2.43}$$

The oscillation probability then reduces to the familiar form

$$\mathcal{P}_{\alpha \to \beta}(t) = \sin^2 2\theta \; \sin^2 \left(\frac{M_2^2 - M_1^2}{4E} t \right). \tag{2.44}$$

We compute the exact rate at which the asymmetry is transferred between sectors by mass mixing using the density matrix formalism for fermions and scalars. Before doing so, we present a good, approximate formula for the rate of asymmetry transfer that agrees with the density matrix results in two important limits discussed in Sections 2.3.2 and 2.3.2. This formula will be useful in understanding how the asymmetry rate depends on the mass eigenvalues and mixing angle. We derived all of our numerical results in Section 2.3 using the density matrix formalism.

In an environment where frequent scatterings occur, as is typical in the early universe, oscillation is interrupted by interactions with other states. This decoheres the system and can be thought of as collapsing the ψ wavefunction into one of its interaction eigenstates. Interactions are occurring at a total average rate Γ_0,

$$\Gamma_0 = \frac{1}{2} \left(\Gamma_\alpha + \Gamma_\beta \right), \tag{2.45}$$

where Γ_α is the total rate with which species α interacts with the thermal background. The mean free path is $1/\Gamma_0$. The rate that species α changes into species β is going to be given by this interaction rate, multiplied by the probability of oscillation:

$$\Gamma_{\alpha \to \beta} = \Gamma_0 \, \sin^2 2\theta \, \sin^2 \left(\frac{M_2^2 - M_1^2}{4 \, E \, \Gamma_0} \right) \equiv \Gamma_0 \, \sin^2 2\theta \, \sin^2 \left(\frac{\epsilon}{2\Gamma_0} \right), \qquad (2.46)$$

where $\epsilon = (M_2^2 - M_1^2)/2E$. Equation (2.46) is easy to understand and is a good approximation to the actual evolution of various species in a thermal background and we use it frequently. If $\Gamma_{\alpha \to \beta} > H$, the mixing is in equilibrium. Otherwise, we can obtain an order-of-magnitude estimate of the amount of transfer from species α to β by the quantity $\Gamma_{\alpha \to \beta}/H$ evaluated at the time the asymmetry is generated in one sector.

The $\alpha \to \beta$ transfer can proceed in two different ways associated with different limits of (2.46). Which regime the system is in is independent of whether or not the mixing is in equilibrium. When $\epsilon/\Gamma_0 \gg 1$, the oscillation length is much shorter than the mean free path and so a larger amount of α particles are transferred per collision. As a result, fewer collisions are necessary to bring the system into equilibrium. The opposite limit, $\epsilon/\Gamma_0 \ll 1$, occurs when collisions occur very rapidly compared to the oscillation time scale and few α particles are converted to β particles per collision. Nevertheless, the transfer process can still be in equilibrium if the mixing angle is large. We encounter examples of both limiting cases in Sections 2.3.3 and 2.3.4.

The evolution of the different flavor states, taking into account oscillations and coherence-destroying thermal interactions, can be performed in a unified framework using the density matrix formalism [32, 41, 42]. The system begins in some state ρ_0, where the diagonal components give the iniital relative abundances of each particle type and the off-diagonal

components represent any coherences present in the initial state. The time evolution of the density matrix is given by the equation

$$i\dot{\rho} = [H^{(\mathrm{R})}, \rho] - i\{H^{(\mathrm{I})}, \rho\}, \tag{2.47}$$

where $H^{(\mathrm{R})}$ is the real part of the Hamiltonian calculated to leading order and includes masses and interactions with the thermal background, while $H^{(\mathrm{I})}$ consists of the imaginary part of the background potential consisting of absorptive interactions with the background that cause the system to decohere. Integrating (2.47) yields the final abundance of each species. In Sections 2.3.2 and 2.3.2, we give (2.47) in component form for scalar and fermion mixing and show that, in the limit of time-independent temperature and mixing, the result reduces to (2.46).

We are interested in determining the evolution of an asymmetry that is stored entirely in one sector and subsequently migrates to a different sector through oscillations. Since the evolution equations are linear, it is appropriate to consider only the asymmetric components. The initial density matrix at the time the asymmetry is generated and that we use in our analysis is $\rho_0 = \mathrm{diag}(1, 0, 0, \ldots, 0)$, where the 1 is the diagonal component of the species housing the asymmetry.

At finite temperature and density, particularly temperatures where $T > M_i$, finite temperature contributions to the background potential must be included in the mass mixing formulae (we assume that both sectors are in kinetic equilibrium so that there is a common temperature between them). Considering again the 2×2 case, the effective masses from

thermal corrections for both fermions and scalars in the interaction basis are

$$|M(T)|^2 - |M(0)|^2 = \begin{pmatrix} \lambda_1^2 T^2 & 0 \\ 0 & \lambda_2^2 T^2 \end{pmatrix}, \tag{2.48}$$

where λ_1 and λ_2 are effective couplings parameterizing all interactions with the background plasma[3]. In Section 2.3.3, we relate λ_1 and λ_2 to the couplings of specific models.

Using $E \approx 3T$ at finite temperature and density in the ultra-relativistic limit, we get the Hamiltonian

$$H_{\alpha\beta} = 3T \, \delta_{\alpha\beta} + \frac{|M(T)|^2_{\alpha\beta}}{6T}. \tag{2.49}$$

In the case that there exist common interactions between the sectors that are in thermal equilibrium, T is the same for all fields. The mixing angle and energy eigenvalue splitting are unchanged when a term proportional to the identity is subtracted, so we can subtract the $T \, \delta_{\alpha\beta}$ term from (2.49).

We now derive results for the particular cases of scalars and fermions.

Scalars

Let the tree-level, diagonal elements of M_{ij} be denoted by μ_i. Then, the total mass-squared matrix is

$$|M(T)|^2 = \begin{pmatrix} \mu_1^2 + \lambda_1^2 T^2 & M_{12}^2 \\ M_{12}^2 & \mu_2^2 + \lambda_2^2 T^2 \end{pmatrix}. \tag{2.50}$$

---

[3]For fermions, finite temperature corrections do not give rise to a mass term in the Lagrangian due to chiral symmetry, but they do give rise to an effective potential that can be considered as a contribution to the $M^\dagger M$ matrix

The mass eigenvalues and mixing angle are

$$
2m_\pm^2 = \lambda_1^2 T^2 + \lambda_2^2 T^2 + \mu_1^2 + \mu_2^2 \pm \sqrt{(\lambda_{21}^2 T^2 + \mu_2^2 - \mu_1^2)^2 + 4M_{12}^4}, \tag{2.51}
$$

$$
\sin\theta = \frac{\sqrt{2}M_{12}^2}{\sqrt{(\lambda_{21}^2 T^2 + \mu_2^2 - \mu_1^2)(\lambda_{21}^2 T^2 + \mu_2^2 - \mu_1^2 + \sqrt{(\lambda_{21}^2 T^2 + \mu_2^2 - \mu_1^2)^2 + 4M_{12}^4}) + 4M_{12}^4}}, \tag{2.52}
$$

where $\lambda_{21}^2 = \lambda_2^2 - \lambda_1^2$.

The Hamiltonian (2.49) is

$$
H = \frac{1}{6}\begin{pmatrix} \mu_1^2 + \lambda_1^2 T^2 & M_{12}^2 \\ M_{12}^2 & \mu_2^2 + \lambda_2^2 T^2 \end{pmatrix}. \tag{2.53}
$$

and

$$
\rho = \begin{pmatrix} \rho_{11} & \rho_{12} \\ \rho_{21} & \rho_{22} \end{pmatrix}. \tag{2.54}
$$

The density matrix evolution equations (2.47) in component form are [42]

$$
\begin{pmatrix} \dot{\rho}_{11} \\ \dot{\rho}_{22} \\ \dot{\rho}_{12} \\ \dot{\rho}_{21} \end{pmatrix} = A \begin{pmatrix} \rho_{11} \\ \rho_{22} \\ \rho_{12} \\ \rho_{21} \end{pmatrix}, \tag{2.55}
$$

where

$$A = \begin{pmatrix} 0 & 0 & iM_{12}^2 & -iM_{12}^2 \\ 0 & 0 & -iM_{12}^2 & iM_{12}^2 \\ iM_{12}^2 & -iM_{12}^2 & -2\Gamma_0 T + i\left[\mu_2^2 - \mu_1^2 - \lambda_{21}^2 T^2\right] & 0 \\ -iM_{12}^2 & iM_{12}^2 & 0 & -2\Gamma_0 T - i\left[\mu_2^2 - \mu_1^2 - \lambda_{21}^2 T^2\right] \end{pmatrix}.$$

In this case, (2.45) gives

$$\Gamma_0 = \frac{1}{2}\left(\Gamma_1 + \Gamma_2\right). \tag{2.56}$$

Note that the previous formula applies also in the limit that M_{12} and T are independent of time, in which case we have a linear system of first-order differential equations. The solutions are exponential functions, with the coefficients in the exponential being given by the eigenvalues of the matrix in (2.55). There is one zero eigenvalue, representing the equilibrium distribution, and the approach to chemical equilibrium (i.e. the asymmetries being equal in both fields) is given by the smallest of the eigenvalues, denoted by γ_{slow}. Defining

$$\epsilon \equiv \frac{m_+^2 - m_-^2}{6T}, \tag{2.57}$$

the solutions can be found analytically in the limits $\Gamma_0 \ll \epsilon$ and $\Gamma_0 \gg \epsilon$. The solutions are

$$\gamma_{\text{slow}} = 2\Gamma_0 \sin^2\theta \cos^2\theta, \quad \Gamma_0 \ll \epsilon, \tag{2.58}$$

$$\gamma_{\text{slow}} = \sin^2\theta \cos^2\theta \frac{\epsilon^2}{\Gamma_0}, \quad \Gamma_0 \gg \epsilon, \tag{2.59}$$

which reproduces (2.46) in the same limits. This confirms our physical picture of transfer via mass mixing and interactions with the background, and also checks equation (2.46).

Since all of the parameters in our theory are actually time-dependent, the system never reaches chemical equilibrium if $\gamma_{\text{slow}} < H$. There is a significant parameter space for the models in Sections 2.3.3 and 2.3.4 for which this is true. In this case, the amount of asymmetry transferred between sectors is approximately γ_{slow}/H.

Fermions

Suppose we have three Weyl fermions with a Dirac mass μ between ψ_1 and ψ_2 and a Dirac mass mixing M_{13} between ψ_1 and ψ_3. The mass-squared matrix is

$$|M(T)|^2 = \begin{pmatrix} \mu^2 + M_{13}^2 + \lambda_1^2 T^2 & 0 & 0 \\ 0 & \mu^2 + \lambda_2^2 T^2 & \mu M_{13} \\ 0 & \mu M_{13} & M_{13}^2 + \lambda_3^2 T^2 \end{pmatrix}. \tag{2.60}$$

Unlike in the scalar case, the tree-level mass μ appears in the off-diagonal terms. The matrix is block diagonal and only the lower 2×2 sector is mixed. The mass eigenvalues and mixing angle are

$$2m_{\pm}^2 = \mu^2 + M_{13}^2 + (\lambda_2^2 + \lambda_3^2)T^2 \pm \sqrt{\mu^4 + (M_{13}^2 + \lambda_{32}^2 T^2)^2 + 2\mu^2(M_{13}^2 - \lambda_{32}^2 T^2)}, \tag{2.61}$$

$$\sin\theta = \frac{\sqrt{2}\mu M_{13}}{\sqrt{A + M_{13}^4 + (\mu^2 - \lambda_{32}^2 T^2 - M_{13}^2)\sqrt{\mu^4 + 2\mu^2(M_{13}^2 - \lambda_{32}^2 T^2) + (M_{13}^2 + \lambda_{32}^2 T^2)^2}}}, \tag{2.62}$$

where

$$A = (\mu^2 - \lambda_{32}^2 T^2)^2 + 2M_{13}^2(\mu^2 + \lambda_{32}^2 T^2). \tag{2.63}$$

The Hamiltonian is

$$H = \frac{1}{6T} \begin{pmatrix} \mu^2 + M_{13}^2 + \lambda_1^2 T^2 & 0 & 0 \\ 0 & \mu^2 + \lambda_2^2 T^2 & \mu M_{13} \\ 0 & \mu M_{13} & M_{13}^2 + \lambda_3^2 T^2 \end{pmatrix}. \tag{2.64}$$

The density matrix is

$$\rho = \begin{pmatrix} \rho_{11} & \rho_{12} & \rho_{13} \\ \rho_{21} & \rho_{22} & \rho_{23} \\ \rho_{31} & \rho_{32} & \rho_{33} \end{pmatrix}. \tag{2.65}$$

Because H is block diagonal, the density matrix evolution equations involving ψ_1 decouple from those independent of ψ_1, giving three independent systems of equations,

$$\begin{pmatrix} \dot{\rho}_{22} \\ \dot{\rho}_{33} \\ \dot{\rho}_{23} \\ \dot{\rho}_{32} \end{pmatrix} = B \begin{pmatrix} \rho_{22} \\ \rho_{33} \\ \rho_{23} \\ \rho_{32} \end{pmatrix},$$

$$\begin{pmatrix} \dot{\rho}_{12} \\ \dot{\rho}_{13} \end{pmatrix} = \frac{1}{6T} \begin{pmatrix} -6\Gamma_0' T - i M_{13}^2 & i\mu M_{13} \\ i\mu M_{13} & -6\Gamma_0'' T - i\mu^2 \end{pmatrix} \begin{pmatrix} \rho_{12} \\ \rho_{13} \end{pmatrix},$$

$$\dot{\rho}_{11} = 0, \tag{2.66}$$

where

$$
B = \frac{1}{6T}
\begin{pmatrix}
0 & 0 & i\mu M_{13} & -i\mu M_{13} \\
0 & 0 & -i\mu M_{13} & i\mu M_{13} \\
i\mu M_{13} & -i\mu M_{13} & -6\Gamma_0 T + i(\mu^2 - M_{13}^2 - \lambda_{32}^2 T^2) & 0 \\
-i\mu M_{13} & i\mu M_{13} & 0 & -6\Gamma_0 T - i(\mu^2 - M_{13}^2 - \lambda_{32}^2 T^2)
\end{pmatrix}.
$$

$$(2.67)$$

The equations for ρ_{21} and ρ_{31} are found by taking the conjugate of those for ρ_{12} and ρ_{13}.

Because there are now three particle types, we have three rates and

$$
\Gamma_0 = \frac{1}{2}\left(\Gamma_2 + \Gamma_3\right), \tag{2.68}
$$

$$
\Gamma_0' = \frac{1}{2}\left(\Gamma_1 + \Gamma_2\right), \tag{2.69}
$$

$$
\Gamma_0'' = \frac{1}{2}\left(\Gamma_1 + \Gamma_3\right). \tag{2.70}
$$

Since ρ_{11} is conserved, we can only have transfer between particles of species 2 and 3, and

therefore only the first system of equations in (2.66) is relevant for our purposes.

As in the scalar case, the analytic solution to (2.66) in the case of time-independent T

and M_{13} is

$$
\gamma_{\text{slow}} = 2\Gamma_0 \sin^2\theta \cos^2\theta, \quad \Gamma_0 \ll \epsilon, \tag{2.71}
$$

$$
\gamma_{\text{slow}} = \sin^2\theta \cos^2\theta \, \frac{\epsilon^2}{\Gamma_0}, \quad \Gamma_0 \gg \epsilon, \tag{2.72}
$$

which reproduces (2.46).

2.3.3 Moduli-induced mass mixing

Overview

One class of fields that are expected to have large background values at early times are moduli fields; examples include string moduli or Polonyi fields for supersymmetry (SUSY) breaking. As their potentials are exactly flat at the perturbative level in SUSY, moduli can be found at finite temperature far from their zero-temperature minima. Such fields can have VEVs as large as M_{Pl} following inflation. The moduli subsequently roll down to their true minima, which would be established by SUSY-breaking terms in the potential. During this period of rolling, the VEVs can induce large mass mixing terms between other fields in the theory.

Note that moduli decay can create entropy that would dilute both lepton and dark matter numbers. We assume that either decay occurs very late (as with light moduli) with Dirac leptogenesis or that a more efficient means of baryogenesis (such as Affleck-Dine baryogenesis) applies. Dirac leptogenesis can be efficient as well with resonance enhancement, but it is less generic. We show that both light and heavy moduli are possible in Section 2.3.3. For clarity, we use bold-face when discussing the cases of heavy and light moduli.

We consider the dark matter to be a vector-like pair of superfields $X, \bar{X}$ with tree-level mass μ_{tree}. Mass mixing arises from Planck-suppressed higher-dimensional operators. Mass mixing between X and N generically occurs for both fermions and their scalar counterparts.

For **heavy moduli**, mixing between fermion components and a modulus ϕ, mixing can come from superpotential terms such as

$$\Delta W = \frac{c\,\phi^2}{M_{\mathrm{Pl}}}XN + \text{h.c.},\tag{2.73}$$

which gives a mixing

$$m_{XN} = \frac{c\,\phi^2}{M_{\mathrm{Pl}}}.$$ (2.74)

Since the Hamiltonian contains the squared mass matrices, the relevant mixing term is not m_{XN} but the product

$$m^2_{\mathrm{mix}} = \mu_{\mathrm{tree}}\,m_{XN} = \frac{c\,\mu_{\mathrm{tree}}\phi^2}{M_{\mathrm{Pl}}}.$$ (2.75)

The dark matter is stable if $\mu_{\mathrm{tree}} < 2m_\phi$.

Superpotential terms also generate mixing between the scalar components of X and N. In the presence of a spurion field S with SUSY-breaking $\mathcal{F}$-term, an allowed operator is

$$\Delta W = \frac{c_{\mathrm{s}}\,S\phi^2}{M_{\mathrm{Pl}}^2}XN + \mathrm{h.c.},$$ (2.76)

If $\mathcal{F}_S$ is responsible for SUSY breaking in the MSSM, the mixing is

$$m^2_{XN} = \frac{c_{\mathrm{s}}\,m_{3/2}\,\phi^2}{M_{\mathrm{Pl}}}.$$ (2.77)

We compare the mixing term in the squared mass matrix (2.77) with the fermion case (2.75). The ratio of fermion to scalar mixing is $\mu_{\mathrm{tree}}/m_{3/2}$.

The late-time dark matter particle can be either scalar or fermion, depending on the details of the model. It is, however, irrelevant at late times whether the dominant mixing was through scalars or fermions, since interactions within the X sector (most importantly, those responsible for annihilation of the symmetric component) equilibrate the asymmetry among the scalar and fermion components.

We expect that higher-dimensional couplings to moduli fields also contribute to $X\bar{X}$ mass

terms. For the fermion case,

$$\Delta W = \frac{c_X \, \phi^2}{M_{\text{Pl}}} X\bar{X} + \text{h.c.}. \tag{2.78}$$

This operator doesn't violate dark matter or lepton numbers, but is relevant to the mixing angle. The resulting diagonal mass is

$$\mu_X = \mu_{\text{tree}} + \frac{c_X \, \phi^2}{M_{\text{Pl}}} \equiv \mu_{\text{tree}} + \kappa \, m_{XN}. \tag{2.79}$$

Since both $X\bar{X}$ and XN get masses from the moduli VEV, we express everything in terms of m_{XN} and the proportionality constant $\kappa = m_{X\bar{X}}/m_{XN}$, which we expect to be $\mathcal{O}(1)$ since both masses arise from the same moduli fields and operators of the same dimension. For scalars, the corresponding diagonal mass term is

$$\mu^2_{X\,\text{scalar}} = \mu^2_{\text{tree}} + \frac{\kappa \, c_{\text{s}} \, m_{3/2} \, \phi^2}{M_{\text{Pl}}}. \tag{2.80}$$

In the scalar case, the diagonal mass does not contribute to the off-diagonal component of the mass-squared matrix, m^2_{XN}. We show in Section 2.3.3 that the asymmetry transfer rate does not depend on $\mu^2_{X\,\text{scalar}}$.

For **light moduli**, the condition $m_X < 2m_\phi$ is not satisfied. The fermion decay rate is

$$\Gamma_X \approx \frac{m^3_X}{M^2_{\text{Pl}}}, \tag{2.81}$$

and the X lifetime would be much below the bound of $\tau > 10^{26}$ seconds [43]. For this model,

we assume a Z_3 symmetry that only allows higher-dimensional operators such as

$$\Delta W_{\text{light}} = \frac{c\,\phi^3}{M_{\text{Pl}}^2} XN + \text{h.c.,} \tag{2.82}$$

which gives a mixing

$$m_{XN} = \frac{c\,\phi^3}{M_{\text{Pl}}^2}. \tag{2.83}$$

The diagonal component of the mass-squared matrix is

$$m_{\text{mix}}^2 = \frac{c\,\mu_X\phi^3}{M_{\text{Pl}}^2}. \tag{2.84}$$

The corresponding superpotential term for scalar mixing is

$$\Delta W = \frac{c\,S\phi^3}{M_{\text{Pl}}^3} XN + \text{h.c.,} \tag{2.85}$$

which gives a mixing term in the mass-squared matrix

$$m_{XN}^2 = \frac{c\,m_{3/2}\phi^3}{M_{\text{Pl}}^2}. \tag{2.86}$$

As with heavy moduli, the ratio of fermion to scalar mixing is $\mu_X/m_{3/2}$. The decay width is

$$\Gamma_X \approx \frac{m_X^5}{M_{\text{Pl}}^4}, \tag{2.87}$$

safely satisfying the constraints for $m_X \sim$ GeV-TeV. The mixing term for scalars is the SUSY-breaking spurion S coupled to (2.82).

We present a toy model for the potential of **moduli of any mass** [44]:

$$V = (m_\phi^2 - a^2 H^2)|\phi|^2 + \frac{1}{2M_{\mathrm{Pl}}^2}(m_\phi^2 + b^2 H^2)|\phi|^4, \tag{2.88}$$

where H is the Hubble scale. The m_ϕ^2 and H^2 mass terms arise from SUSY breaking due to MSSM SUSY breaking terms and finite-temperature effects, respectively. At early times, the minimum of this potential lies at

$$\langle\phi\rangle = M_{\mathrm{Pl}}\sqrt{\frac{a^2 H(t)^2 - m_\phi^2}{b^2 H(t)^2 + m_\phi^2}}. \tag{2.89}$$

At the critical time t_{c}, when $H(t_{\mathrm{c}}) = m_\phi/a$, the minimum of the potential disappears. Because of damping in the equations of motion, ϕ is unable to efficiently track the minimum of the potential near t_{c} and is left at some finite value. After the critical time, it begins to oscillate with a power-law-damped envelope, rolling toward the true minimum of $\phi = 0$. Its equation of motion is

$$\ddot{\phi} + 3H\dot{\phi} + 2(m_\phi^2 - a^2 H^2)\phi + \frac{2}{M_{\mathrm{Pl}}^2}(m_\phi^2 + b^2 H^2)\phi^3 = 0 \tag{2.90}$$

To obtain the asymmetry transfer rate, we must also specify the interactions in the theory. The simplest model that allows for the annihilation of the symmetric component of X is a U(1)$'$ gauge interaction with coupling g under which X and N are oppositely charged. In the most minimal scenario, N also has Yukawa interactions (with coupling y) from leptogenesis.

We then have, in the notation of section 2.3.2,

$$\lambda_X^2 = g^2/8, \tag{2.91}$$

$$\lambda_N^2 = g^2/8 + y^2/8, \tag{2.92}$$

$$\lambda_{NX}^2 = y^2/8. \tag{2.93}$$

The Yukawa coupling y depends on the model of leptogenesis. For Dirac leptogenesis, the effective coupling is $y = \mathrm{Max}(y_L^2, y_N^2) T_{\mathrm{lep}}^2 / M_\psi^2$ with $T_{\mathrm{lep}} < M_\psi$. For Affleck-Dine leptogenesis, $y = (T_{\mathrm{lep}}/M_{\mathrm{Pl}})^n$, where n is the dimension of the operator lifting the flat direction.

Because of its importance, we repeat the analytic estimate of the transfer rate (2.46):

$$\Gamma_{N \to X} = \Gamma_0 \sin^2 2\theta \sin^2 \left(\frac{\epsilon}{2\Gamma_0} \right).$$

Three parameters influence the transfer rate: the mass eigenstate energy splitting $\epsilon = (m_+^2 - m_-^2)/6T$, the mixing angle θ (both of which are explicitly given in eqs.(2.61,2.62)), and the thermal scattering rate $\Gamma_0 \approx \frac{1}{8\pi^3}(g^4 + y^2)T$. The asymmetry transfer rate is reduced for small mixing angles and small mass splittings. Note that in the limit where $\epsilon \gg \Gamma_0$, the oscillation is rapid and $\sin^2 \left(\frac{\epsilon}{2\Gamma_0} \right) \to 1/2$ takes on its average value.

There are constraints associated with the couplings and scales in theory. They are:

- Leptogenesis should occur after reheating to avoid diluting the lepton asymmetry with the massive quantity of entropy released by inflaton decay.

- In order to ensure efficient depletion of the symmetric component of X, the X annihilation coupling should be $g \sim \mathcal{O}(1)$.

- $y \ll 1$ for the heavy field in leptogenesis to decay out of equilibrium.

- $T > m_{XN}$ to avoid thermal suppression of X and N fields.

Evolution of ϕ

The evolution of ϕ (2.90) depends on its mass. We present the evolution of ϕ for both heavy moduli ($m_\phi \gtrsim 50$ TeV) and light moduli ($m_\phi \lesssim 10$ MeV). We justify these mass ranges in Section 2.3.3.

We first consider **heavy moduli**, ϕ oscillation begins when $H \approx m_\phi$. For $m_\phi \gtrsim 50$ TeV and $T_{\rm RH} \lesssim 10^{12}$ GeV, oscillation will begin prior to inflaton decay. In between the time t_c when oscillation begins and reheating, the cosmic background density is matter dominated by inflaton and moduli fields that scale as massive matter. This gives an approximate solution to the ϕ evolution:

$$\phi \approx \phi_0 \frac{\sin(m_\phi t)}{(m_\phi t)}, \tag{2.94}$$

where $\phi_0 \sim M_{\rm Pl}$.

At the critical time $t_{\rm c}$, $H \approx m_\phi$ and $\langle \phi \rangle = M_{\rm Pl}$, so the ϕ and inflaton fields have comparable energy densities. Before the inflaton decays, both ρ_ϕ and $\rho_{\rm inf}$ scale identically with T, so their densities are also comparable at the time of reheating. Setting $\rho_\phi = \rho_{\rm inf}$ at the time of reheating establishes the relationship between temperature and time in the subsequent ϕ-dominated stage of the universe's evolution. Assuming the inflaton decays entirely to radiation, equating the inflaton and moduli densities gives

$$\frac{\pi^2}{30} g_* T_{\rm RH}^4 \approx m_\phi^2 \, \phi(t_{\rm RH})^2. \tag{2.95}$$

The background remains matter dominated and the relation (2.94) stays valid until the time of moduli decay, and during this epoch the temperature-time relation is

$$T = T_{\mathrm{RH}}(t_{\mathrm{RH}}/t)^{2/3}. \tag{2.96}$$

The solution to the evolution of ϕ for heavy moduli is

$$\phi \approx \frac{a}{b} M_{\mathrm{Pl}} \left(\frac{t_c}{t} \right) \approx \frac{a}{b} M_{\mathrm{Pl}} \left(\frac{t_c}{t_{RH}} \right) \left(\frac{T}{T_{RH}} \right)^{3/2}. \tag{2.97}$$

The mass mixing follows from (2.74) and (2.77). Asymmetry transfer from N to X begins only at the time at which leptogenesis occurs, t_{lep}. Because m_{XN} turns off as T^3, the dark matter asymmetry is essentially established at t_{lep}. The mass mixing values m_{XN} clearly depend on the model input parameters a, b, c, and t_{lep}.

We now turn to **light moduli**. In this case, oscillation must begin before $H = m_\phi$ to avoid having ϕ overclose the universe. One possibility is that the ϕ negative mass-squared predominantly comes from inflaton couplings that decay at reheating (see Section 2.3.3) for details. Oscillation then begins at the time of reheating.

For all values of T_{RH} and light m_ϕ satisfying the overclosure bound (2.116), oscillation begins only after reheating. As a result, the universe is radiation-dominated during the time of leptogenesis and mass-mixing, in contrast to the matter-dominated scenario for heavy moduli. In a radiation-dominated universe, T and t are related by [45]

$$t = \frac{0.301 M_{\mathrm{Pl}}}{\sqrt{g_*} T^2} \tag{2.98}$$

and the ϕ evolution is

$$\phi \approx \frac{a}{b} M_{\mathrm{Pl}} \left(\frac{t_{\mathrm{RH}}}{t} \right)^{3/4} \approx \frac{a}{b} M_{\mathrm{Pl}} \left(\frac{T}{T_{\mathrm{RH}}} \right)^{3/2}. \tag{2.99}$$

The mass mixing is obtained from (2.83) for fermions and (2.86) for scalars.

Analytic approximations

We derive approximations that directly link the parameters from moduli mixing to the mixing angle and mass eigenvalue splittings in Section 2.3.2. There are three relevant limits for the mass eigenvalue splitting ϵ and $\sin\theta$. These are $m_{XN} \gg \mu_X$, $m_{XN} \ll \mu_X$, and $m_{XN} \sim \mu_X$.

The results for fermions follow from equations (2.61) and (2.62):

$$\epsilon = \frac{\mu_X^2}{6T}, \quad \sin\theta = \frac{m_{XN}}{\mu_X}, \quad \mu_X \gg m_{XN}; \tag{2.100}$$

$$\epsilon = \frac{m_{XN}^2}{6T}, \quad \sin\theta = \frac{\mu_X}{m_{XN}}, \quad \mu_X \ll m_{XN}; \tag{2.101}$$

$$\epsilon = \frac{m_{XN}^2}{3T}, \quad \sin\theta = \frac{1}{\sqrt{2}}, \quad \mu_X = m_{XN}. \tag{2.102}$$

The overall thermal interaction rate is $\Gamma_0 \approx g^4 T/8\pi^3$. When the gauge coupling is $\mathcal{O}(1)$ (as needed for annihilation of the symmetric component of dark matter), $m_{XN}, \mu_X < T$ in order to avoid thermal suppression. This means that typically $\epsilon \lesssim \Gamma_0$ and the asymmetry transfer rate in each limit (2.46) reduces to the same quantity,

$$\Gamma_{N\to X} = \frac{4\sin^2\theta \cos^2\theta \epsilon^2}{2\Gamma_0} \approx \frac{m_{XN}^2 \mu_X^2}{18T^2 \Gamma_0} \approx \frac{\mu_X^2 \phi^4}{3T^2 \Gamma_0 M_{\mathrm{Pl}}^2} \tag{2.103}$$

For $\kappa = 1$ (i.e. including higher-dimensional corrections to the diagonal mass) and $m_{XN} \gg \mu_{\text{tree}}$, this rate $> H$ and the system is in chemical equilibrium for $m_{XN} \sim T$, while it is out of chemical equilibrium for lower mixings. In this limit,

$$\Gamma_{N \to X} \approx \frac{\phi^8}{3T^2 \Gamma_0 M_{\text{Pl}}^4}. \tag{2.104}$$

Since ϕ is proportional to $(T/T_{\text{RH}})^3$, if reheating and leptogenesis occur around the same scale, the asymmetry transfer is in equilibrium and chemical equilibrium is reached. If, however, there is a large hierarchy between T_{RH} and T_{lep}, the transfer rate is suppressed.

In the case of scalars, from equations (2.51) and (2.52):

$$\epsilon = \frac{\mu_X^2}{6T}, \qquad \sin\theta = \frac{m_{XN}^2}{2\mu_X^2}, \qquad \mu_X \gg m_{XN}; \tag{2.105}$$

$$\epsilon = \frac{m_{XN}^2}{3T}, \qquad \sin\theta = \frac{1}{\sqrt{2}}, \qquad \mu_X \ll m_{XN}; \tag{2.106}$$

$$\epsilon = \frac{\sqrt{5}m_{XN}^2}{6T}, \qquad \sin\theta = \frac{\sqrt{2}}{\sqrt{5-\sqrt{5}}}, \qquad \mu_X = m_{XN}. \tag{2.107}$$

For similar reasons to the fermion case, when m_{XN}, $\mu_X < T$, the asymmetry transfer rate (2.46) in all three limits is approximately

$$\Gamma_{N \to X} = \frac{4\sin^2\theta \cos^2\theta \epsilon^2}{2\Gamma_0} \approx \frac{m_{XN}^4}{18T^2\Gamma_0} \approx \frac{m_{3/2}^2\phi^4}{18T^2\Gamma_0 M_{\text{Pl}}^2}. \tag{2.108}$$

Once again, when leptogenesis occurs close to the scale of reheating, m_{XN} is large and the system is in chemical equilibrium. At lower leptogenesis scales and smaller values of m_{XN}, the system is out of chemical equilibrium.

We can compare the transfer rate from mixing between fermions and scalars:

$$\frac{\Gamma_{N \to X,\,\text{scalar}}}{\Gamma_{N \to X,\,\text{fermion}}} = \frac{m_{3/2}^2}{\mu_X^2}. \tag{2.109}$$

Therefore, scalars give the dominant contribution to mixing if $m_{3/2} \gg \mu_X$, and fermions give the dominant contribution if $\mu_X \gg m_{3/2}$. Of course, the heavier of the two state will decay to the lighter state, which is the dark matter.

Numerical results

To confirm our approximate results, we numerically solve the density matrix evolution equations to determine the magnitude of the $N \to X$ asymmetry transfer. We summarize the results below. The dark matter density is $\Omega_{\text{DM}} \approx (5-6)\Omega_{\text{B}}$. We choose parameters so that $\Omega_{\text{DM}} = 5\Omega_{\text{B}}$.

We begin with **heavy moduli**. ϕ oscillation begins before reheating for $m_\phi \gtrsim 50$ TeV, and ϕ is damped from its initial value of M_{Pl} by the time of reheating. For $T_{\text{RH}} \sim 10^{10}$ GeV, reheating occurs only shortly after oscillation begins and ϕ is not much damped from M_{Pl}. As a result, fermion mass mixing is $> T$ and fermionic modes are suppressed, allowing the scalar mixing to dominate the asymmetry transfer.

With smaller reheating temperatures, $T \sim 10^8$ TeV, ϕ is sufficiently damped at reheating that fermionic modes are not thermally suppressed. In this case, either scalar or fermion mixing can dominate, depending on the ratio of $\mu_X/m_{3/2}$, according to (2.109).

We present our results in terms of benchmark points for a high reheat temperature of $T_{\text{RH}} = 10^{10}$ GeV and a lower reheat temperature of $T_{\text{RH}} = 10^8$ GeV. We use $m_\phi = 50$ TeV for both cases.

For $T_{\mathrm{RH}} = 10^8$ GeV and all leptogenesis scales $T_{\mathrm{lep}} < T_{\mathrm{RH}}$, fermion mixing $m_{XN} < T$ and so we must consider both scalar and fermion mixing. With $a = b = 1$, $c = \kappa = 2$, some benchmark points are

1. $T_{\mathrm{lep}} = 10^8$ GeV and $m_X = 5$ GeV. The dominant mixing is from fermions because

   $\mu_X \approx 5 \times 10^5$ GeV $> m_{3/2} \approx 5 \times 10^4$ GeV.

2. $T_{\mathrm{lep}} = 10^7$ GeV and $m_X = 90$ GeV. The dominant mixing is from scalars because

   $\mu_X \approx 90$ GeV $\ll m_{3/2}$.

The transfer rate is fast enough to bring X and N into chemical equilibrium for point #1 above, consistent with ~ 5 GeV dark matter. The transferred asymmetry is suppressed for point #2, consistent with heavier dark matter. Heavier masses $\gtrsim 100$ GeV are consistent with later leptogenesis times.

For $T_{\mathrm{RH}} = 10^{10}$ GeV, with $a = b = 1$ and $c = \kappa = 0.1$:

- For leptogenesis scales 5×10^8 GeV $< T_{\mathrm{lep}} < T_{\mathrm{RH}}$, fermion mass mixing is $> T$ and fermionic modes are suppressed. Mixing from scalars gives:

  $T_{\mathrm{lep}} = 10^8 - 10^{10}$ GeV and $m_X = 5$ GeV.

- Below $T_{\mathrm{lep}} = 5 \times 10^8$ GeV:

  1. $T_{\mathrm{lep}} = 5 \times 10^8$ GeV and $m_X \sim 5$ GeV. Mixing is dominated by fermions because

     $\mu_X \approx 3 \times 10^8$ GeV $\gg m_{3/2}$.

  2. $T_{\mathrm{lep}} = 5 \times 10^7$ GeV and $m_X \sim 5$ GeV. Mixing is dominated by fermions because

     $\mu_X \approx 3 \times 10^5$ GeV $> m_{3/2}$.

Scalar mixing dominates for $T_{\text{lep}} \lesssim 10^7$ GeV and asymmetry transfer is suppressed, consistent with X masses up to 100 TeV depending on the leptogenesis time. Note that, even though the gap between the reheat temperature and leptogenesis scale is wider in this example than for the low reheat case, the ϕ VEV (and hence mass mixing) is still large enough to keep the system in chemical equilibrium at $T_{\text{lep}} = 5 \times 10^7$ GeV. The reason is that, with a higher temperature, the reheat time is also earlier and so the *time* of leptogenesis is earlier than it would be with a lower reheat temperature. Since $\phi \sim 1/t$, this leads to a larger mixing.

To summarize our findings for heavy moduli, asymmetry transfer from higher-dimensional moduli couplings to XN is consistent with dark matter masses ranging from 5 GeV to the weak scale over a range of reheat temperatures and leptogenesis scales. We generally expect scalar mixing to dominate when $m_{XN} > T$ and the fermion modes are suppressed. With lower T_{lep}, fermion mixing dominates over scalar mixing when m_{XN} is just below T, while scalar mixing dominates once again at low T_{lep} because m_{XN} is small and the scalar mixing has an $m_{3/2}$ enhancement.

Moving on to **light moduli**, $\phi = M_{\text{Pl}}$ at the time of reheating. Therefore, if leptogenesis occurs at or near the reheat temperature, the fermion X and N are thermally suppressed and the dominant asymmetry transfer happens between scalars. The scalar mixing is small because $m_{3/2} \sim m_\phi$ is small in this case, and the resulting transfer is out of equilibrium. In fact, for the points shown below, mixing from scalars alone cannot transfer enough asymmetry to be consistent with a dark matter mass below 100 TeV, which is the upper limit for fields whose symmetric components can be annihilated by perturbative couplings.

We present benchmark points for reheat temperatures $T_{\mathrm{RH}} = 10^9$ GeV and $T_{\mathrm{RH}} = 10^{11}$ GeV. We begin with $T_{\mathrm{RH}} = 10^9$ GeV and $m_\phi = 3$ keV, which is the largest moduli mass consistent with decay and overclosure constraints.

- For leptogenesis scales 2×10^6 GeV $< T_{\mathrm{lep}} < T_{\mathrm{RH}}$, fermion mass mixing is $> T$ and fermionic modes are suppressed. Mixing from scalars is highly out-of-equilibrium and transfers no appreciable asymmetry.

- For leptogenesis scales $T_{\mathrm{lep}} < 2 \times 10^6$ GeV, fermion mixing is dominant. The asymmetry transferred to X drops with T_{lep}. Some benchmark points are

  1. $T_{\mathrm{lep}} = 2 \times 10^6$ GeV and $m_X = 5$ GeV.

  2. $T_{\mathrm{lep}} = 5 \times 10^5$ GeV and $m_X = 5$ GeV.

  3. $T_{\mathrm{lep}} = 10^5$ GeV and $m_X = 160$ GeV.

For the first two benchmark points, mixing is large and chemical equilibrium is attained as outlined in the previous paragraph. The transfer rate is suppressed for lower T_{lep} and so $\Delta_X \ll \Delta_{\mathrm{B}}$ for the last case. Higher X masses are consistent with lower T_{lep}, but in practice, it is very difficult to achieve leptogenesis at such a low scale.

For a high reheat temperature of $T_{\mathrm{RH}} = 10^{11}$ GeV, with $a = b = c = \kappa = 1$. As before, we use $m_\phi = 3$ keV.

- For leptogenesis scales 8×10^8 GeV $< T_{\mathrm{lep}} < T_{\mathrm{RH}}$, fermion mass mixing is $> T$ and fermionic modes are suppressed. Mixing from scalars is highly out-of-equilibrium and transfers no appreciable asymmetry.

- For leptogenesis scales $T_{\mathrm{lep}} < 8 \times 10^8$ GeV, fermion mixing is dominant. The asymmetry drops with T_{lep}. Some benchmark points are

1. $T_{\text{lep}} = 7 \times 10^8$ GeV and $m_X \sim 5$ GeV.

2. $T_{\text{lep}} = 5 \times 10^8$ GeV and $m_X \sim 5$ GeV.

3. $T_{\text{lep}} = 10^8$ GeV and $m_X = 2.2$ TeV.

4. $T_{\text{lep}} = 3 \times 10^7$ GeV and $m_X = 80$ TeV.

For the first two points, $\Gamma_{N \to X} > H$ and the system is in chemical equilibrium, leading to $n_X \approx n_{\text{B}}$ and $m_X \sim 5$ GeV. For the latter two, the transfer rate is suppressed and $n_X \ll n_{\text{B}}$, consistent with X above the weak scale.

There are two principal differences between the results for light and heavy moduli. Since the modulus mass is tied to $m_{3/2}$, the ratio of soft scales between light and heavy moduli is $\sim$ keV/TeV $\sim 10^{-9}$. As a result, scalar mixing is much more highly suppressed with light moduli. The second difference is that, for light moduli, ϕ only begins oscillation at reheating, whereas for heavy moduli oscillation begins before reheating. This means that the ϕ VEV is larger for light moduli, leading to larger fermion mixing.

For both light and heavy moduli in the limit $\Gamma_0 \ll H$, the particles do not undergo any scatterings with the thermal background in a Hubble volume. This means that X and N remain in a coherent state given by the oscillation between the two states. The asymmetry transferred in this case is dependent only on the mixing angle. The requirement that $\Gamma_0 \ll H$ is, however, at odds with the condition that the symmetric component of the dark matter be efficiently depleted. Therefore, the scenario of oscillation with no thermal scatterings is not a viable asymmetric dark matter model.

In summary, we have presented a number of scenarios where mixing between dark matter and lepton-number-carrying fields is induced by moduli VEVs. Depending on the reheat temperature and scale of leptogenesis, the mixing can be very rapid, bringing the two sectors

into chemical equilibrium and transferring an X asymmetry consistent with GeV-scale dark matter. Alternatively, the mixing can be suppressed, leading to dark matter at the weak scale or heavier. The mixing suppression can be very large, but the largest possible dark matter masses are ~ 100 TeV, above which point the symmetric component of X cannot be annihilated by perturbative couplings.

Moduli cosmology

Moduli are gravitationally coupled and therefore long-lived, with characteristic decay widths

$$\Gamma_\phi \approx \frac{m_\phi^3}{8\pi M_{\mathrm{Pl}}^2}. \tag{2.110}$$

As a result, moduli tend to dominate the energy density of the universe until the time of their decay. The entropy accompanying moduli decay can greatly dilute any existing relics, including the baryon asymmetry. Furthermore, if moduli decay occurs after Big-Bang Nucleosynthesis (BBN), the resulting entropy generation alters the predictions for the light element abundances and such a scenario is in conflict with observations. There are two possibilities: either moduli decay reheats the universe to above the scale of BBN (about 5 MeV), or they are stable to the present day. These possibilities require heavy moduli and light moduli, respectively.

Assuming that the energy of the universe is moduli-dominated for the case of heavy moduli, the reheat temperature T_1 from moduli decay is given by

$$T_1 = \left(\frac{30 m_\phi^2 \, \phi(t = 1/\Gamma_\phi)^2}{\pi^2 g_*} \right)^{1/4}. \tag{2.111}$$

Since $T_1 > T_{\text{BBN}} \approx 5$ MeV, we determine that $m_\phi \gtrsim 50$ TeV.

The temperature immediately before ϕ decay is

$$T_0 = T_{\text{RH}}(t_{\text{RH}}\Gamma_\phi)^{2/3}. \tag{2.112}$$

The generated entropy (and hence the dilution of particle relics) is

$$\frac{s_1}{s_0} = \frac{T_1^3}{T_0^3}. \tag{2.113}$$

For $m_\phi = 100$ TeV and $T_{\text{RH}} \sim 10^9$ GeV, the dilution factor is $\mathcal{O}(10^{10})$. This requires a primordial baryon asymmetry of $n_{\text{B}}/s \sim 1$ to give the correct abundances at late times.

One method of efficient baryogenesis is Affleck-Dine leptogenesis [46, 44] along a flat direction with non-zero N and Standard Model lepton number. If the entropy generated from the decay of the flat direction is larger than that from the inflaton, then n_B/s can be of order unity [44]. The baryon asymmetry is

$$\frac{n_{\text{B}}}{s} \approx \frac{n_{\text{B}}}{n_{\text{FD}}} \frac{T_{\text{RH}}}{m_{\text{FD}}} \left(\frac{m_{\text{FD}}}{M_{\text{Pl}}}\right)^{2/(n-2)}, \tag{2.114}$$

where $n_{\text{B}}/n_{\text{FD}} \sim \mathcal{O}(1)$ in the standard Affleck-Dine set-up. For $m_{\text{FD}} \sim$ TeV, $T_{\text{RH}} \sim 10^9$ GeV, and $n \geq 7$, then $n_{\text{B}}/s \sim \mathcal{O}(1)$ and the dilution from moduli decay leads to the correct baryon asymmetry at late times. Examples of a flat direction lifted at dimension-8 and invariant under the Standard Model and U(1)$'$ gauge groups include: $\phi_{\text{FD}}^4 = NLL\bar{E}$ and $N\bar{U}\bar{D}\bar{D}$, where we impose R-parity to forbid a lifting term of dimension-4. A detailed account of Affleck-Dine leptogenesis (baryogenesis) and moduli decay can be found in [47]. Other,

highly efficient, non-standard leptogenesis mechanisms (such as resonant leptogenesis [15])
are also possible, but less generic.

If the moduli are instead light, they can be stable on cosmological scales. From cosmic ray
data, the constraint on the dark matter lifetime is $\tau \gtrsim 10^{26}$ seconds [43]. To be conservative,
we require that the moduli also have a longer lifetime than this. Using the moduli decay
rate (2.110), long-lived moduli have masses $m_\phi \lesssim 7$ MeV.

There are additional constraints on moduli masses from the requirement that moduli do
not overclose the universe. If the initial ϕ VEV is $M_{\rm Pl}$ and oscillation begins at a temperature
$T_{\rm osc}$, then ϕ energy density to entropy ratio is

$$\frac{\rho_\phi}{s} \approx \frac{m_\phi^2 M_{\rm Pl}^2}{g_* T_{\rm osc}^3}. \tag{2.115}$$

To avoid overclosing the universe, and so that moduli do not comprise a substantial fraction
of the dark matter, we require that ρ_ϕ/s be less than the value for baryons, $\rho_{\rm B}/s \approx 10^{-10}$
GeV. If oscillation begins when $H(T_{\rm osc}) = m_\phi$, then ϕ overcloses the universe for $m_\phi > 10^{-26}$
eV [48]. Since we expect $m_\phi \sim m_{3/2}$, there are no viable models with such low scales of
SUSY breaking.

If oscillation begins at earlier times, however, the ρ_ϕ per comoving volume is suppressed
and larger ϕ masses are allowed. One example of how this could happen is if the negative
terms proportional to H^2 in the moduli potential (2.88) arise only due to couplings with
inflaton. If this is the case, the mass-squared of ϕ is driven positive when the inflaton decays
and oscillation begins at the time of reheating, giving

$$\frac{\rho_\phi}{s} \approx \frac{m_\phi^2 M_{\rm Pl}^2}{g_* T_{\rm RH}^3} < \frac{\rho_{\rm B}}{s}. \tag{2.116}$$

For example, if $m_\phi = 0.1$ keV and $T_{\mathrm{RH}} = 10^{10}$ GeV in the scenario where oscillation begins at reheating, the present-day moduli density is smaller than the baryon density.

Mixing due to flat directions

Combinations of fields with vanishing $\mathcal{F}-$ or $\mathcal{D}-$terms are also flat and can have large VEVs in the early universe. Such directions are typically lifted by higher-dimensional Planck-suppressed operators. For example, the potential of a flat direction lifted by a superpotential term of dimension 4 is

$$V(\phi) = (m^2 - a^2 H^2)|\phi|^2 + \frac{c}{M_{\mathrm{Pl}}^2}|\phi|^6. \tag{2.117}$$

The interplay between the negative mass-squared coming from the background energy and the ϕ^6 lifting term gives ϕ a VEV for $H > m/a$,

$$\langle \phi \rangle = \left[\frac{M_{\mathrm{Pl}}^2(aH^2 - m^2)}{3c} \right]^{1/4}. \tag{2.118}$$

For $H \gg m/a$, $\langle \phi \rangle \sim H$. This is much smaller than the moduli VEV, which is typically M_{Pl}. As a result, m_{XN} is also suppressed relative to the moduli-induced mass mixing and the asymmetry transfer is out of equilibrium since it was only marginally so for much of the parameter space with mass mixing. The outcome is similar to the case for moduli when $T_{\mathrm{lep}} \ll T_{\mathrm{c}}$ and m_{XN} was suppressed. This favors TeV scale or higher dark matter.

There are additional complications to flat direction VEVs giving mass mixing. The direction coupling to XN cannot be comprised solely of MSSM fields, since the lowest allowed lifting operator would be dimension-4 in the superpotential and lead to rapid dark matter decay. The flat directions can also induce mass mixing between X and other fields in the

theory through renormalizable superpotential couplings, giving X a very large mass and lifting it out of the theory. Such models typically require more complicated field content and symmetries to give large asymmetry transfer from $N \to X$. Although possible, the smaller field values make models more cumbersome so we focus on the simpler cases in this Chapter.

2.3.4   Mixing induced by background energy

An alternate, even more generic origin of mass mixing at early times is through couplings to fields dominating the energy density of the early universe. We consider the specific case of couplings to kinetic terms of relativistic fermions ψ in a thermal background. The higher-dimensional operators are

$$\Delta \mathcal{L} \supset \frac{c}{M_{\mathrm{Pl}}^2} \left(i\psi^\dagger \gamma^\mu D_\mu \psi \right) (XN + \mathrm{h.c.}) . \tag{2.119}$$

In a supersymmetric theory, such terms arise from higher-dimensional corrections to the Kähler potential. If ψ are fields dominating the background density, we have

$$\langle \psi_\Sigma^\dagger \gamma^\mu D_\mu \psi_\Sigma \rangle = \frac{\pi^2}{30} g_* T^4, \tag{2.120}$$

where g_* is the number of relativistic degrees of freedom. We have a mass mixing between scalars

$$m_{XN}^2 = \frac{\pi^2 \, c \, g_* \, T^4}{30 M_{\mathrm{Pl}}^2} \approx \frac{\pi^2 \, c}{82.8} \, H^2 . \tag{2.121}$$

With a higher-dimensional coupling (2.119), the decay rate is suppressed by $(m_X/M_{\mathrm{Pl}})^4$ and for $m_X \lesssim 10^6$ GeV, the dark matter is stable.

Unlike the case of moduli-induced mixing, direct mixing of fermions by a kinetic term occurs only with operators of higher dimension than those inducing scalar mixing. We show below that the asymmetry transfer mechanism between scalars is viable only for very high temperatures (around the GUT scale), and this would be pushed even higher if the mixing were suppressed by an additional power of T/M_{Pl}. Therefore, it is only the scalar mixing through the thermal background that is relevant.

We first estimate the expected parameters that give rise to a viable model and subsequently solve the density matrix evolution equations numerically. The total thermal interaction rate, averaged between X and N, and using the couplings from Section 2.3.3 is approximately

$$\Gamma_0 \sim \frac{1}{8\pi^3}\left(g^4 + \frac{1}{2}y^2\right)T, \tag{2.122}$$

where y and g are Yukawa and gauge couplings given in (2.91). Because the mass mixing is proportional to H, it falls as T^2, and therefore asymmetry transfer is highest when T is large and leptogenesis occurs at a high scale. Consequently, the out-of-equilibrium conditions and neutrino masses are consistent with $y \sim 1$. We therefore expect the hierarchy $yT \gg m_{XN} \gg \mu$ to hold. The mass splittings and mixing angle in this limit are

$$\epsilon \approx \frac{y^2}{6}T, \tag{2.123}$$
$$\sin\theta \approx \frac{m_{XN}^2}{y^2\,T^2}. \tag{2.124}$$

For $g \sim 1$, it is always true that $\Gamma_0 \gg \epsilon$, and so (2.46) reduces to

$$\Gamma_{N\to X^\dagger} = \frac{\epsilon^2}{\Gamma_0}\sin^2\theta\cos^2\theta \approx \frac{2\pi^2\,T}{9(g^4 + y^2/2)}\left(\frac{m_{XN}}{T}\right)^4. \tag{2.125}$$

Integrating over a Hubble time and substituting (2.121) gives

$$\frac{\Gamma_{N \to X^\dagger}}{H} \approx 0.07\pi^7 \, g_*^{3/2} \left(\frac{T}{M_{\mathrm{Pl}}} \right)^3. \tag{2.126}$$

For temperatures around $T_{\mathrm{GUT}} \sim 10^{16}$ GeV, we obtain a fractional X asymmetry (relative to lepton number) of around 5×10^{-4}, which would be the correct asymmetry for a few TeV dark matter candidate. In reality, the accumulated asymmetry is larger by a factor of ~ 5 when we account for integrating over multiple Hubble times, as we find when we solve the full density matrix evolution equations.

We solve the system of equations (2.55) numerically. We present three benchmark points giving $\Omega_{\mathrm{DM}} \approx 5\Omega_{\mathrm{b}}$ with $y = 1$ and $c = 10$:

- $T_{\mathrm{lep}} = 1.8 \times 10^{16}$ GeV, $g = 1$ and $m_X = 1$ TeV,

- $T_{\mathrm{lep}} = 1.8 \times 10^{16}$ GeV, $g = 3$ and $m_X = 10$ TeV,

- $T_{\mathrm{lep}} = 5 \times 10^{16}$ GeV, $g = 10$ and $m_X = 50$ TeV.

We have assumed that higher dimensional operators mix X with all three generations of N. Asymmetries consistent with higher mass dark matter particles are also possible when $T_{\mathrm{lep}} < 10^{16}$ GeV or for $g < 1$, but in these cases, the couplings are insufficiently large to eliminate the symmetric component. Asymmetries consistent with lower masses of X are also possible for higher reheat temperatures, but since T_{RH} is already borderline given the gravitino problem and the risk of reintroducing the flatness and monopole problems [49], we do not consider any higher reheat temperatures.

The temperature scales required for scalar mass mixing are higher than we may typically expect from a supersymmetric theory due to the gravitino problem. The gravitino problem

can be alleviated in theories with very heavy gravitinos, where the gravitinos decay into axions [50] or some other non-Standard Model particle. Alternatively, one may envision a non-supersymmetric theory with mixed scalars whose scales are stabilized by some unknown mechanism.

Note also that the asymmetry transferred by mass mixing is dominant over transfer from thermal scatterings from (2.119). The rate of such processes is

$$\Gamma_{X\Sigma \to N\Sigma} \sim \frac{T^5}{M_{\text{Pl}}^4} < H. \tag{2.127}$$

Integrating the rate over a Hubble time gives $T^3/M_{\text{Pl}}^3 \sim 10^{-7}$ even for the highest temperatures we consider, $T \sim 10^{16}$ GeV and is therefore subdominant to the effect of mass mixing.

2.3.5 Phenomenology

Unlike the two Higgs model in Section 2.2, the minimum interactions necessary between dark matter and the visible sector for the models in this section are Planck-suppressed and there is no built-in mechanism for the annihilation of the symmetric component. As a result, the phenomenology is model-dependent. The main hope of seeing such a model is through the mechanism for annihilation. In Sections 2.3.3 and 2.3.4, we considered a U(1)$'$ gauge interaction under which X and N are charged, although other possibilities exist. Direct detection bounds strongly constrain the strength of this interaction with quarks. As a result, signals would be small at hadron colliders.

As in Section 2.2.6, we do not expect asymmetric dark matter models to have large indirect detection signals. The mechanisms discussed there, however, could yield a non-zero

anti-dark-matter population at late times, and so the model would not necessarily be ruled out by a confirmed indirect signal.

Since our model consists of X mixing with a lepton-number-carrying gauge singlet, as is present in Dirac leptogenesis, the determination of the Dirac or Majorana nature of the neutrino masses can give insight into the components of our model. However, if neutrinos are discovered to have Majorana masses, this will not rule out the models listed above but would favor a more complex model than the minimal Dirac scenario or suggest Affleck-Dine mechanism for generating original asymmetries.

2.4 Conclusions

The global symmetries of the universe could have been very different in the early universe than they are today. In particular, independent dark matter and baryon asymmetries at late times can emerge from a common symmetry at early times and explain the baryon-dark matter near-coincidence. In this Chapter, we show how large field backgrounds in the early universe can induce mass mixings between dark matter and visible matter, sometimes leading to distinctive relations between the dark matter and baryon densities that accommodate a wide range of dark matter masses. Such mixing can arise in renormalizable Lagrangian terms with field VEVs linked to scales already present in the theory, such as the scale of electroweak symmetry breaking. In this case, the dark matter mass is naturally either $\sim$ GeV or in the range $300-500$ GeV. More generically, mixing can also arise from Planck-suppressed operators, which we expect to break the global symmetries present at low scales. This leads to mixing even in scenarios where there is no renormalizable connection between dark and visible matter fields. In this case, the transferred asymmetry is consistent with dark matter

Table 2.1: Moduli mixing results

	Heavy moduli	**Light stable moduli**
DM mass with scalar mixing	$T_{RH} \sim 10^8$ GeV: 90 GeV$-$100 TeV; $T_{RH} \sim 10^{10}$ GeV: $\sim \mathcal{O}(\text{GeV}) - 100$ TeV	Transfer highly suppressed
DM mass with fermion mixing	$T_{RH} \sim 10^8 - 10^{10}$ GeV: $\mathcal{O}(\text{GeV})$	$T_{RH} \sim 10^9$ GeV: $\sim \mathcal{O}(\text{GeV}) - 100$ TeV; $T_{RH} \sim 10^{11}$ GeV: $\sim \mathcal{O}(\text{GeV}) - 100$ TeV

masses above 1 GeV, with weak scale masses preferred in the case of moduli-induced mixing and leptogenesis at the intermediate scale or in the case of mixing due to background energy when leptogenesis happens at the GUT scale. The dark matter masses are typically higher for lower leptogenesis scales, with the only upper bound on the dark matter masses being the requirement that the symmetric component be annihilated by perturbative couplings.

We summarize our results for the various cases below:

- Two-stage phase transition:

    - *Relativistic X*: $\mathcal{O}$ GeV mass

    - *Thermally-suppressed X*: 300-500 GeV mass

    - *Mixing-suppressed X*: 400-500 GeV mass

- Moduli-induced mixing: see Table 2.1

- Background energy induced mixing:

    - *Scalar mixing*: 1-100 TeV mass, requires $T_{\text{RH}} \sim 10^{16}$ GeV

This work expands the range of possible transfer mechanisms in asymmetric dark matter models and provides new considerations for dark matter model building. We see that the range of possible transfer mechanisms in asymmetric dark matter models is broad and a broad range of models and masses are possible. It is important to explore such possibilities and possible means for distinguishing among these and other models so we can eventually learn the true nature of dark matter.

Chapter 3

A WIMPy Baryogenesis Miracle

3.1 Introduction

Generally, baryogenesis and the establishment of the dark matter number density are treated as independent processes. With the notable exception of one class of models [26], it has largely been overlooked that models with symmetric, weakly interacting massive particle (WIMP) dark matter can connect dark matter physics with baryogenesis. We present a new mechanism that creates such a link and is based on a simple premise: if WIMP annihilation satisfies the Sakharov conditions, a non-zero baryon number asymmetry can be generated from dark matter annihilation, and in some instances, can account for the entire observed baryon asymmetry. We call this process WIMPy baryogenesis. Our models are distinct from models of asymmetric dark matter [16, 17, 18, 20, 21, 22, 23, 24, 25, 27], which propose that dark matter and baryons have their origins in a common asymmetry. In our models, the energy densities of baryons and dark matter are more loosely linked but can accommodate the observed dark-matter-to-baryon ratio.

We list below the Sakharov conditions and how they are satisfied in WIMPy baryogenesis:

1. *Baryon number violation:* WIMP annihilations violate baryon or lepton number. A preserved U(1) symmetry is allowed if the baryon asymmetry is balanced by a negative asymmetry in a decoupled sector that restores the net global symmetry. We have such a U(1) symmetry in most models we present.

2. *CP violation:* WIMP couplings to Standard Model fields violate CP.

3. *Departure from thermal equilibrium:* The cooling of the universe provides the necessary departure from thermal equilibrium. Net dark matter annihilation begins around temperatures $T \lesssim m_{\mathrm{DM}}$, resulting in a small deviation of the dark matter number density from its equilibrium value. The annihilations can generate a baryon asymmetry that depends on the amount of dark matter annihilation occurring during washout freeze-out, which is comparable to the dark matter density at that time.

We present models that satisfy all three Sakharov conditions, and that simultaneously generate the observed baryon asymmetry and WIMP relic density. In particular, we find that there exist successful models of WIMPy baryogenesis with $\mathcal{O}(1)$ couplings and CP phases, and weak-scale masses for all new fields. This is an extension of the WIMP miracle to also include baryogenesis, although we show that the size of the generated asymmetry is sensitive to the parameters in the theory and can vary by several orders of magnitude from the observed asymmetry.

Although WIMP annihilation can generate a baryon asymmetry, there are other processes that have the potential to *wash out* the asymmetry, and their freeze-out is crucial to create the observed baryon asymmetry. In our models, the two leading sources of washout are inverse

Figure 3.1: Schematic diagrams showing the evolution of the asymmetry created by dark matter annihilation. **(left)** Model where asymmetry created in exotic antibaryons is sequestered in a sterile sector through baryon-number-conserving decays. **(right)** Model where asymmetry created in exotic antibaryons is converted into a Standard Model baryon asymmetry through baryon-number-violating decays.

annihilations of baryons into dark matter and baryon-to-antibaryon processes. Washout scatterings must be suppressed to generate a sizeable baryon asymmetry because, as we show in Section 3.2, any asymmetry generated prior to washout freeze-out[1] is rapidly damped away. After washout processes freeze out, dark matter annihilations can efficiently create a baryon asymmetry, and the final asymmetry depends on how much dark matter remains when washout scatterings freeze out. Washout freeze-out must occur before that of WIMP annihilation, at which point dark matter annihilation is no longer efficient and no sizeable asymmetry can be created. Thus, we find our central result: *if washout processes freeze out before WIMP freeze-out, then a large baryon asymmetry may accumulate, and its final value is proportional to the WIMP abundance at the time that washout becomes inefficient.*

The early freeze-out of washout processes can occur for kinematic reasons. Inverse annihilations will be Boltzmann-suppressed for $T < m_{\mathrm{DM}}$ because the thermal baryon fields

---

[1]The time of washout freeze-out is defined as when the rate of washout processes falls below the Hubble expansion rate. This is analogous to the freeze-out of WIMP annihilation.

are no longer energetic enough to annihilate back into dark matter. Baryon-antibaryon scatterings, however, can remain rapid at temperatures well below $m_{\rm DM}$. The only way to suppress baryon-to-antibaryon washout is if all washout processes involve a heavy exotic baryon field in the initial state. We illustrate this scenario in Figure 3.1, showing how dark matter annihilates to Standard Model baryons plus an exotic baryon, as well as the possible decays of the exotic baryon (either through baryon-preserving or baryon-violating interactions). If this exotic field has a mass $\gtrsim m_{\rm DM}$, its abundance is Boltzmann-suppressed at $T < m_{\rm DM}$ and suppresses the washout rate. Meanwhile, dark matter annihilations are not kinematically allowed if the heavy baryon field has mass $\gtrsim 2m_{\rm DM}$, so the mass condition $m_{\rm DM} \lesssim m_{\rm exotic\,baryon} \lesssim 2m_{\rm DM}$ is essential to generate a large baryon asymmetry through WIMPy baryogenesis.

Dark matter annihilations generate a positive baryon asymmetry stored in Standard Model quarks along with an equal negative asymmetry stored in the exotic baryon field. It is important that the decays of the exotic baryon do not eliminate the Standard Model baryon asymmetry. In models of WIMPy baryogenesis with a preserved U(1) baryon symmetry, the exotic baryon-number-carrying field is charged under an additional discrete symmetry, while Standard Model fields are uncharged, preventing the exotic baryon from decaying into Standard Model baryons and destroying the asymmetry. The heavy baryon-number-carrying field decays instead into light gauge singlet fields that are charged under the discrete symmetry and decoupled from Standard Model fields at temperatures below the scale of WIMPy baryogenesis. We also present a model where the exotic baryon decays to Standard Model quarks through baryon-number-violating couplings, and such models manifestly satisfy the first Sakharov condition.

For many years, the WIMP miracle – the fact that dark matter fields with weak-scale masses and annihilation cross sections give the correct dark matter thermal relic density – has been a compelling paradigm for dark matter model-building. WIMPy baryogenesis preserves the WIMP miracle while also offering an explanation for the observed baryon asymmetry. While WIMPy baryogenesis models do not predict the precise relationship between the dark matter and baryon number densities, natural models do restrict the baryon asymmetry to a range of about seven orders of magnitude (see Section 3.2), and the observed asymmetry is within this range. Since baryogenesis arises from WIMP annihilations, WIMPy baryogenesis is also necessarily connected to weak-scale physics. While we do not discuss an embedding of WIMPy baryogenesis in a particular solution of the hierarchy problem, we assume that whatever new physics lies at the weak scale stabilizes any scalar potentials in our theory and gives a natural explanation for their weak-scale masses. A consequence of this is that, with weak-scale masses, some of the new fields necessary for baryogenesis may give signals at future experiments. Additionally, the present-day dark matter is symmetric, leading to the possibility of the indirect detection of dark matter annihilations as in conventional WIMP models. This is in contrast with generic asymmetric dark matter models, in which the majority of dark matter annihilations ceased long before the present day, although it is also noteworthy that there do exist scenarios in which the symmetric component of dark matter is regenerated at late times, giving indirect detection signals for some asymmetric dark matter models [38].

A further advantage of this scenario is that bounds on the reheat temperature in supersymmetric models do not constrain WIMPy baryogenesis. Typical reheat temperature constraints come from overproduction of gravitinos and are in the range $T_{\rm RH} \lesssim 10^6 - 10^9$ GeV

[51], and T_{RH} is consequently below the scale required for conventional leptogenesis through the decay of heavy, Majorana right-handed neutrinos. Although low-scale mechanisms for baryogenesis are known, such as electroweak baryogenesis, WIMPy baryogenesis is a new way of generating the baryon asymmetry at $T \sim$ TeV while satisfying the reheat bound.

We discuss the general conditions for successful WIMPy baryogenesis in Section 3.2, finding that interactions washing out the baryon asymmetry must become ineffective prior to WIMP freeze-out in order to generate the observed asymmetry. In Section 3.3, we focus on a particular model where dark matter annihilates through a lepton-number-violating interaction and the asymmetry is subsequently transferred to baryons by sphalerons. Because sphaleron processes are only rapid in the unbroken electroweak phase, such baryogenesis must occur before the electroweak phase transition. We compute the dark matter relic density and baryon asymmetry, and find the range of masses and couplings that agrees with the observed densities of both. We also consider the implications of additional lepton-number-conserving dark matter annihilation channels. In Section 3.4, we consider models with WIMPs annihilating directly to quarks, where baryogenesis can occur over a wider range of temperatures because sphalerons are no longer needed to establish the baryon asymmetry. We discuss experimental constraints and possible signals for models of WIMPy baryogenesis in Section 3.5. Finally, we summarize in Section 3.6.

3.2   General Analysis of WIMPy Baryogenesis

To begin our discussion of WIMPy baryogenesis, we highlight in Section 3.2.1 some of its general features and use an analytic approximation to determine the regimes in which baryogenesis is successful. Our central result is that the final baryon asymmetry from WIMPy

baryogenesis is proportional to the dark matter density at the time when washout processes freeze out. This means that washout scatterings must freeze out at a time when the dark matter density was larger than or comparable to the observed final baryon asymmetry, and that washout freeze-out occurs at such a time when one of the baryon-number-carrying products of WIMP annihilation is heavier than the dark matter mass, as described in the introduction. In Section 3.2.2, we estimate the magnitude of the baryon asymmetry for input parameters consistent with the WIMP miracle and show that it can lie within a range of approximately seven orders of magnitude.

3.2.1 Boltzmann Equations and Solutions

We consider a theory with dark matter species X whose annihilation violates baryon number, creating one quark (or anti-quark) along with other field(s) ψ_i. In this section we will not specify the precise interactions mediating dark matter annihilation in order to avoid specific model dependence. X can be either Majorana or Dirac, and the results derived below remain the same up to $\mathcal{O}(1)$ multiplicative factors. All manifestations of the Boltzmann equation for baryon number evolution in WIMPy baryogenesis models have two important terms: one that describes the annihilation of dark matter and the consequent generation of a baryon asymmetry, and another that drives the asymmetry towards its equilibrium value of zero through baryon-number-violating washout scatterings. The full Boltzmann equations describing the evolution of the various particle abundances are model-dependent and can have many terms, which we give explicitly for concrete models in Sections 3.3 and 3.4. However, in the models of interest to us, namely models where the asymmetry arises predominantly from WIMP annihilations, the overall dynamics are well-described by the

inclusion of only these terms.

Consider the limit where WIMP annihilations are the dominant source of the baryon asymmetry and for which the asymmetry is small as observed. We derive the Boltzmann equations in terms of dimensionless quantities: the number density per comoving volume of field i, $Y_i = n_i/s$ (s is the entropy density), and the temperature, which we express as $x = m_X/T$. The dark matter number density is denoted Y_X and the baryon asymmetry is denoted $Y_{\Delta B}$. The Y_X evolution equation has one term that is important in all models of WIMPy baryogenesis, namely the conventional WIMP annihilation term that is proportional to the annihilation cross section σ_{ann} and drives Y_X to its equilibrium value. This term arises from both $XX \to$ baryon processes and the inverse processes, baryons $\to XX$. The Y_X Boltzmann equation with this term is

$$\frac{dY_X}{dx} = -\frac{2s(x)}{x\,H(x)} \left\langle \sigma_{\mathrm{ann}} v \right\rangle \left[Y_X^2 - (Y_X^{\mathrm{eq}})^2 \right], \tag{3.1}$$

where $H(x)$ is the Hubble scale.

We neglect a back-reaction term in the Y_X Boltzmann equation $\epsilon\, s(x) \left\langle \sigma_{\mathrm{ann}} v \right\rangle Y_{\Delta B} (Y_X^{\mathrm{eq}})^2 / (2 Y_\gamma\, x\, H(x))$, where ϵ is the net baryon number created per dark matter annihilation and is a measure of the magnitude of CP-violation (it is defined more precisely in Section 3.3). This term accounts for the modification of the inverse scattering rate of baryons into X when there is a baryon asymmetry. This approximation is valid because this term is small when $Y_{\Delta B} \ll 1$, as is true in our universe ($Y_{\Delta B} \sim 10^{-10}$). This simplification also decouples the equations for Y_X and $Y_{\Delta B}$, which makes it easier to get an approximate analytic solution for $Y_{\Delta B}$. The equation (3.1) in this limit is the same as the familiar Boltzmann equation for conventional WIMPs. Y_X is then obtained from the

standard WIMP relic density calculation [45] and is approximately inversely proportional to the annihilation cross section.

The Boltzmann equation for the evolution of the baryon asymmetry has two important terms. In the first term, a baryon asymmetry is generated through X annihilations, and is proportional to $\epsilon/2 \times dY_X/dx$, which is the annihilation rate multiplied by the fractional asymmetry generated per annihilation. The factor of $1/2$ arises because the annihilation term in (3.1) includes the sum of annihilation into baryons and antibaryons, whereas the term generating the asymmetry includes the difference. The second term in the baryon asymmetry Boltzmann equation reduces the existing baryon asymmetry and is the *washout* term. It is proportional to $Y_{\Delta B}$ multiplied by the cross section of processes that eliminate the baryon asymmetry σ_{washout}. The Boltzmann equation is

$$\frac{dY_{\Delta B}}{dx} = \frac{\epsilon \, s(x)}{x \, H(x)} \langle \sigma_{\text{ann}} v \rangle \left[Y_X^2 - (Y_X^{\text{eq}})^2 \right] - \frac{s(x)}{x \, H(x)} \langle \sigma_{\text{washout}} v \rangle \frac{Y_{\Delta B}}{2 Y_\gamma} \prod_i Y_i^{\text{eq}}. \tag{3.2}$$

The factor of $Y_{\Delta B}/2Y_\gamma$ comes from the the fact that the chemical potential $\mu_{\Delta B}$ for the baryon asymmetry can be written as $\mu_{\Delta B}/T = Y_{\Delta B}/2Y_\gamma$ [45]. We assume that all species except for X are in equilibrium. There are other terms that we have not included, such as washout terms proportional to $Y_{\text{exotic}-B}^{\text{eq}} Y_X$ that come from scattering of baryon-number-carrying fields off dark matter fields. Typically, the suppression coming from the small value of Y_X for $x \gg 1$ makes this term subdominant to other washout terms. In the models of Section 3.3 and 3.4, the $Y_{\text{exotic}-B}^{\text{eq}} Y_X$ term can be ignored without substantially affecting the numerical results.

As expected, the Boltzmann equations show that the total baryon number is zero when all fields are in equilibrium and with the initial condition $Y_{\Delta B} = 0$. A solution for $Y_{\Delta B}$ can

be written in integral form in terms of the X density:

$$Y_{\Delta B}(x) = \int_0^x dx' \, \frac{\epsilon \, s(x')}{x' \, H(x')} \, \langle \sigma_{\text{ann}} v \rangle \left[Y_X^2 - (Y_X^{\text{eq}})^2 \right](x') \tag{3.3}$$

$$\times \exp \left[- \int_{x'}^x \frac{dx''}{x''} \, \frac{s(x'')}{2 Y_\gamma \, H(x'')} \, \langle \sigma_{\text{washout}} v \rangle \prod_i Y_i^{\text{eq}}(x'') \right]$$

$$\approx -\frac{\epsilon}{2} \int_0^x dx' \, \frac{dY_X(x')}{dx'} \, \exp \left[- \int_{x'}^x \frac{dx''}{x''} \, \frac{s(x'')}{2 Y_\gamma \, H(x'')} \, \langle \sigma_{\text{washout}} v \rangle \prod_i Y_i^{\text{eq}}(x'') \right]. \tag{3.4}$$

Equation (3.4) explicitly shows that $Y_{\Delta B}(x)$ can be expressed in terms of a source term from dark matter annihilations, and an exponential term that attempts to erase any asymmetry generated by WIMP annihilations. The source term can be written as dY_X/dx, as in [52]. At $T \gtrsim m_X$, or $x \lesssim 1$, WIMP annihilations are balanced by inverse scattering processes and $dY_X/dx \approx 0$, meaning no asymmetry is generated according to (3.4). At $x \gtrsim 1$, the expansion and cooling of the universe result in net WIMP annihilations ($dY_X/dx \neq 0$), providing the departure from equilibrium necessary for baryogenesis. The net asymmetry at any x is sensitive to the rate of washout processes during the epoch of WIMP annihilations.

The integrand in the exponent (3.4) is the washout rate $\Gamma_{\text{washout}}(x)$ normalized to the Hubble scale $H(x)$,

$$\frac{\Gamma_{\text{washout}}(x)}{H(x)} = \frac{s(x)}{2 Y_\gamma \, H(x)} \, \langle \sigma_{\text{washout}} v \rangle \prod_i Y_i^{\text{eq}}(x). \tag{3.5}$$

Washout freezes out when $\Gamma_{\text{washout}}/H < 1$. In the limit where Γ_{washout} is a rapidly decreasing function of x, (3.4) takes a particularly simple form. This is true if, for example, the washout rate freezes out because m_i/T becomes large and yields an exponential suppression of Y_i^{eq}.

In this case, we can model the exponential in (3.4) as a step function and obtain

$$Y_{\Delta B}(\infty) \approx -\frac{\epsilon}{2} \int_{x_{\mathrm{washout}}}^{\infty} dx' \frac{dY_X(x')}{dx} = \frac{\epsilon}{2} \left[Y_X(x_{\mathrm{washout}}) - Y_X(\infty) \right], \tag{3.6}$$

where $x_{\mathrm{washout}} = m_X/T_{\mathrm{washout}}$ is the point at which washout processes freeze out, and $Y_X(\infty)$ is the late-time dark matter relic density.

Equation (3.6) has a very clear physical interpretation: after washout scatterings freeze out, all subsequent WIMP annihilations generate a baryon asymmetry with efficiency ϵ. This is why, according to (3.6), $Y_{\Delta B}$ is proportional to ϵ times the total number of WIMP annihilations that happen after x_{washout}, which is $Y_X(x_{\mathrm{washout}}) - Y_X(\infty)$. The observed baryon asymmetry is $Y_{\Delta B} \approx 9 \times 10^{-11}$ [53]. Since dark matter at late times satisfies the relation

$$Y_X(\infty) \approx \frac{(5~\mathrm{GeV})\, Y_{\Delta B}(\infty)}{m_X}, \tag{3.7}$$

we require that $Y_X(\infty) < Y_{\Delta B}(\infty)$ for weak-scale dark matter. Along with the requirement $\epsilon < 1$, (3.7) and (3.6) imply that $Y_X(x_{\mathrm{washout}}) \gg Y_X(\infty)$. In other words, the washout interactions must become ineffective prior to XX annihilation freeze-out in order to generate a sufficiently large baryon asymmetry through WIMPy baryogenesis. As an example of the numerical scales in WIMPy baryogenesis: for a WIMP of mass 1 TeV, $Y_X(\infty) \approx 4 \times 10^{-13}$ and WIMP freeze-out happens at $x_{\mathrm{f.o.}} \approx 27$, or $T \approx 37$ GeV. For $\epsilon = 0.1$, washout scatterings must freeze out at $x_{\mathrm{washout}} \approx 20$ or $T \approx 50$ GeV. The final baryon asymmetry is proportional to the WIMP density at the time when washout ceases to be important, with $Y_{\Delta B}(\infty) \approx 9 \times 10^{-11}$.

For what parameters do we expect washout processes to freeze out prior to WIMP an-

nihilation freeze-out? We compare Γ_{washout} in (3.5) to the corresponding rate of WIMP annihilation, which is [45]

$$\frac{\Gamma_{\text{WIMP}}(x)}{H(x)} = \frac{2s(x)}{H(x)} \langle \sigma_{\text{ann}} v \rangle Y_X(x). \tag{3.8}$$

We then find that

$$\frac{\Gamma_{\text{washout}}(x)}{\Gamma_{\text{WIMP}}(x)} \approx \frac{\langle \sigma_{\text{washout}} v \rangle \prod_i Y_i^{\text{eq}}(x)}{4 \langle \sigma_{\text{ann}} v \rangle Y_X^{\text{eq}}(x) Y_\gamma}. \tag{3.9}$$

This ratio must be less than one at the time of washout freeze-out for washout processes to freeze out prior to WIMP freeze-out. This can be realized if either of the following is true *for every process washing out the baryon asymmetry*:

1. One of the baryon states is heavier than dark matter so $\frac{\prod_i Y_i^{\text{eq}}(x)}{Y_X^{\text{eq}}(x) Y_\gamma} \ll 1$.

2. The baryon-number-violating coupling is small so $\langle \sigma_{\text{washout}} v \rangle \ll \langle \sigma_{\text{ann}} v \rangle$.

The second scenario is challenging to realize, because the same baryon-number-violating couplings appear in both the washout and annihilation cross sections, and $\langle \sigma_{\text{ann}} v \rangle$ is fixed by the dark matter relic density. Furthermore, as we show in Section 3.3.1, suppressing the washout cross section also suppresses the fractional asymmetry generated per annihilation, ϵ, and the resulting baryon asymmetry is typically too small. Therefore, we expect that viable models of WIMPy baryogenesis have at least one baryon-number-carrying field with mass $\gtrsim m_X$.

3.2.2 Estimates of Baryon Asymmetry

In this section, we derive an estimate of the baryon asymmetry generated by a WIMP dark matter candidate with mass $m_X \sim$ TeV, and we determine the size of the baryon energy density compared to the WIMP relic density. In the following, we assume for simplicity that a dark matter field X annihilates into a Standard Model quark Q plus an exotic baryon field ψ (see Sections 3.3 and 3.4 for specific model details). We find that the baryon asymmetry depends strongly on the mass m_ψ and is constrained to lie within a seven or eight order-of-magnitude window, with the observed baryon asymmetry within an order of magnitude of the upper limit. Therefore, WIMPy baryogenesis does not predict the value of the dark matter-baryon ratio, but neither is the relationship between the two energy densities completely arbitrary.

To determine the range of baryon asymmetries obtained from WIMPy baryogenesis, we use the result from the last section that the final baryon asymmetry is proportional to the number of dark matter annihilations that occur after washout freeze-out, as shown in (3.6). The largest possible asymmetry is generated when the exotic baryon field is heavy relative to dark matter ($m_\psi \gtrsim m_X$) so that washout processes freeze out while there is still a large dark matter abundance. To determine the upper bound on the asymmetry, we use the fact that $m_\psi < 2m_X$ for WIMP annihilation to be allowed kinematically, and this limits how many dark matter particles can remain when washout freezes out. By contrast, the baryon asymmetry is small when washout processes turn off at a late time ($m_\psi \ll m_X$) after dark matter annihilation has frozen out. To calculate the lower bound, we determine the rate of residual dark matter annihilation after dark matter freezes out and use this to determine the size of the asymmetry.

For both the upper and lower limits, we first calculate the allowed baryon asymmetry and then determine the corresponding dark matter-baryon ratio. In both scenarios, the baryon asymmetry depends on two time scales: the point of washout freeze-out, $x_{\mathrm{washout}} = m_X/T_{\mathrm{washout}}$, and the point at which WIMP annihilation freezes out, $x_{\mathrm{ann}} = m_X/T_{\mathrm{ann}}$.

Estimate of upper limit: We first estimate the upper limit of the baryon asymmetry generated within our framework, which occurs when m_ψ is heavy to suppress washout and is therefore also at the TeV-scale. Kinematically, dark matter annihilation occurs only if $m_\psi < 2m_X$, which bounds how early x_{washout} can be relative to x_{ann}. For a TeV-scale dark matter field, WIMP annihilation freezes out when the temperature is about $1/30$ of its mass. Therefore $x_{\mathrm{washout}} \approx x_{\mathrm{ann}}(m_X/m_\psi) \gtrsim 15$. We also know that, when washout freezes out while WIMP annihilation is still active, $Y_X(x_{\mathrm{washout}}) \gg Y_X(\infty)$. We then obtain from (3.6):

$$Y_{\Delta B}(\infty) \approx \frac{\epsilon}{2} Y_X(x_{\mathrm{washout}}) < \frac{\epsilon}{2} Y_X^{\mathrm{eq}}(15) \approx \epsilon \times 10^{-8}. \qquad (3.10)$$

According to (3.10), the asymmetry is independent of m_X and depends only on the ratio $x_{\mathrm{washout}} \approx m_\psi/m_X$, with a large asymmetry when m_ψ is comparable to or larger than m_X.

To compare the baryon density to the dark matter energy density, recall that the WIMP density changes little after annihilation freezes out, and so $Y_X(\infty) \approx Y_X(x_{\mathrm{ann}}) \approx Y_X(30)$. We then find that

$$\frac{\Omega_B}{\Omega_X} = \frac{m_{\mathrm{proton}} Y_{\Delta B}(\infty)}{m_X Y_X(\infty)} \approx \frac{\epsilon}{2} \frac{Y_X(x_{\mathrm{washout}})}{Y_X(x_{\mathrm{ann}})} \left(\frac{\mathrm{GeV}}{m_X}\right) \approx \frac{\epsilon}{2} \frac{Y_X^{\mathrm{eq}}(15)}{Y_X^{\mathrm{eq}}(30)} \left(\frac{\mathrm{GeV}}{m_X}\right) \lesssim 10 \left(\frac{\epsilon}{10^{-2}}\right) \left(\frac{\mathrm{TeV}}{m_X}\right). \qquad (3.11)$$

Therefore, for a model with weak-scale m_X, $\mathcal{O}(1)$ couplings (in accordance with the WIMP miracle), and the loop-suppressed $\epsilon \sim 10^{-2}$ as in (3.24), we find that the energy density of

baryons can be at most an order of magnitude larger than the energy density of dark matter.

Estimate of lower limit: In deriving the upper bound, we assumed that m_ψ saturated the bound $m_\psi < 2m_X$ and we found that dark matter annihilation could generate the observed baryon asymmetry. When $m_\psi \ll 2m_X$, washout processes remain in equilibrium until after dark matter freeze-out, and the asymmetry from WIMPy baryogenesis is too small to account for the observed asymmetry. We now estimate the full range of baryon asymmetries achieved in our models when $m_\psi \ll 2m_X$. In this case, the equilibrium number density of X is much smaller than the actual, frozen-out X abundance. As a result of this overabundance of X relative to its equilibrium value, some residual dark matter annihilations continue at late times, even though the annihilation rate is insufficient to appreciably change Y_X after x_{ann}. Such annihilations can, however, generate a small baryon asymmetry. According to (3.6), this asymmetry can be estimated by calculating $Y_X(\infty) - Y_X(x_{\mathrm{washout}})$, where $x_{\mathrm{washout}} > x_{\mathrm{ann}}$.

To determine the asymmetry, we solve the Boltzmann equation (3.1), neglecting the subdominant term $(Y_X^{\mathrm{eq}})^2$ in equation (3.1). Furthermore, if XX annihilation is s-wave, then $\langle \sigma_{\mathrm{ann}} v \rangle$ is approximately constant in the domain $x_{\mathrm{ann}} < x < x_{\mathrm{washout}}$. The only x-dependence comes from the factor

$$\frac{s(x)}{x\,H(x)} = \frac{s(x_{\mathrm{ann}})}{H(x_{\mathrm{ann}})}\,\frac{x_{\mathrm{ann}}}{x^2}. \tag{3.12}$$

Integrating (3.1) from $x = x_{\mathrm{washout}}$ to $x = \infty$ gives

$$Y_X(x_{\mathrm{washout}}) - Y_X(\infty) \approx \frac{2s(x_{\mathrm{ann}})x_{\mathrm{ann}}\,\langle \sigma_{\mathrm{ann}} v \rangle\, Y_X(x_{\mathrm{ann}})^2}{H(x_{\mathrm{ann}})}\,\frac{1}{x_{\mathrm{washout}}}. \tag{3.13}$$

Using the definition of Γ_{WIMP} in (3.8), together with the fact that $\Gamma_{\text{WIMP}}(x_{\text{ann}}) = H(x_{\text{ann}})$, gives the simple result

$$Y_X(x_{\text{washout}}) - Y_X(\infty) \approx \frac{2x_{\text{ann}}}{x_{\text{washout}}} Y_X(x_{\text{ann}}) \approx \frac{2x_{\text{ann}}}{x_{\text{washout}}} Y_X(\infty). \tag{3.14}$$

Notice that for $x_{\text{washout}} > x_{\text{ann}}$, Y_X is constant at leading order from x_{washout} to ∞. Also as mentioned earlier, by assuming both X and ψ have weak-scale masses and interactions, $x_{\text{ann}}/x_{\text{washout}} \sim m_\psi/m_X$. We can then obtain an estimate for the baryon asymmetry:

$$Y_{\Delta B} \approx \frac{\epsilon \, x_{\text{ann}}}{x_{\text{washout}}} Y_X(\infty) \approx \epsilon \left(\frac{m_\psi}{m_X} \right) Y_X(\infty). \tag{3.15}$$

We see that the baryon asymmetry decreases linearly with m_ψ when $m_\psi \ll m_X$.

The ratio of the baryon energy density to the dark matter energy density is

$$\frac{\Omega_B}{\Omega_X} \sim 10^{-3} \times \epsilon \left(\frac{m_\psi}{m_X} \right) \left(\frac{\text{TeV}}{m_X} \right). \tag{3.16}$$

If there is no large hierarchy in m_X and m_ψ (i.e. $m_\psi/m_X \gtrsim 0.1$), and using our earlier estimate of $\epsilon \sim 10^{-2}$ for $\mathcal{O}(1)$ couplings that give the correct WIMP relic density, we find that $\Omega_B/\Omega_X \gtrsim 10^{-6}$. We emphasize, however, that even smaller asymmetries are possible if the imaginary parts of the couplings are tuned to be small or if there exist hierarchies in the masses of the new fields.

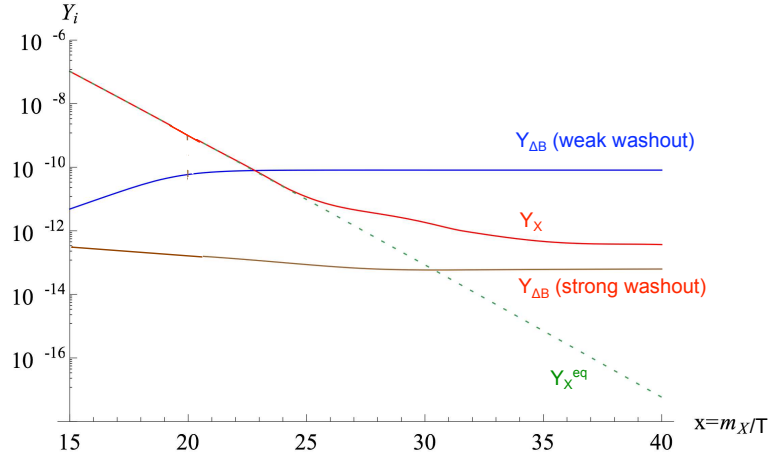Considering equations (3.11) and (3.16), we find that the expected range for the baryon-

Figure 3.2: The evolution of the number density per comoving volume for field i (Y_i) as a function of $x = m_X/T$. The numerical solutions shown here are based on the WIMPy leptogenesis model discussed in Section 3.3, where the dominant annihilation process is $XX \to L\psi$ and the dominant washout is $L\psi \to L^\dagger \psi^\dagger$. The input parameters are $y_X = 2.7$, $\lambda_L = 0.8$, $\epsilon = 0.2$, $m_X = 3$ TeV, and $m_S = 5$ TeV. $m_\psi = 4$ TeV gives the behavior when washout freezes out well before WIMP annihilation freezes out ("weak washout"). $m_\psi = 2$ TeV gives the behavior when washout becomes ineffective subsequent to WIMP freeze-out ("strong washout").

to-dark matter ratio in WIMPy baryogenesis is

$$10^{-6} \lesssim \frac{\Omega_B}{\Omega_X} \lesssim 10, \tag{3.17}$$

assuming $\mathcal{O}(1)$ couplings, and weak-scale masses for all new fields, i.e. $m_X, m_\psi \sim \mathcal{O}(0.1 - 1\text{TeV})$. The observed value of $\Omega_B/\Omega_X \approx 0.2$ falls within this range, and thus WIMPy baryogenesis can account for the entire observed baryon asymmetry, but it does fall toward the upper end of the allowed region.

To summarize, models of WIMPy baryogenesis predict a dark matter relic density inversely proportional to the WIMP annihilation cross section, as in conventional WIMP models, and a baryon asymmetry proportional to the dark matter density at the time when

washout processes freeze out. In Figure 3.2, we illustrate the evolution of the dark matter abundance and the baryon asymmetry in one model of WIMPy baryogenesis for the two limiting washout cases.

3.3   WIMP Annihilation to Leptons

3.3.1   Model Overview

We have discussed baryogenesis in the generalized sense of either the direct production of a baryon asymmetry through WIMP annihilation or leptogenesis, in which a lepton asymmetry is produced by WIMP annihilation and converted to a baryon asymmetry through sphalerons. In this section, we present a model of leptogenesis, where the lepton asymmetry is generated above the electroweak phase transition while sphalerons are still active. We discuss the field content and symmetries of the model Section 3.3.1, and we calculate the efficiency of generating a lepton number asymmetry in Section 3.3.1. As we showed in Section 3.2, the final baryon asymmetry is determined by the time at which washout processes freeze out. We address washout in Section 3.3.1, discussing the implications for the WIMPy leptogenesis parameter space. Finally, we give the Boltzmann equations in Section 3.3.1.

Field Content and Lagrangian

We consider a simple model with the minimal ingredients for WIMPy leptogenesis. Dark matter consists of a pair of gauge singlet Dirac fermions[2] X and $\bar{X}$ that annihilate to the Standard Model lepton doublet L_i and new weak-scale fields ψ_i. X annihilates through weak-

---

[2]A Majorana dark matter field X does not work in this case because X must carry a complex charge for the model to generate a non-zero lepton asymmetry, as we show later in this section.

scale gauge singlet pseudoscalars[3] S_α. By gauge invariance, ψ_i has charge $(2, 1/2)$ under the $\mathrm{SU}(2)_\mathrm{L} \times \mathrm{U}(1)_Y$ gauge interactions. The Lagrangian is

$$\mathcal{L} = \mathcal{L}_\mathrm{kin} + \mathcal{L}_\mathrm{mass} - \frac{i}{2} \left(\lambda_{X\alpha} X^2 + \lambda'_{X\alpha} \bar{X}^2 \right) S_\alpha + i\, \lambda_{L\,\alpha i}\, S_\alpha L_i \psi_i + \mathrm{h.c.} \qquad (3.18)$$

To satisfy the Sakharov conditions, dark matter annihilation must also violate CP, and $\lambda_{L\alpha i}$ must be complex. To have physical CP violation, there must be more than one scalar S_α so there is a relative phase in their amplitudes. XX annihilation can then generate an asymmetry in L_i, and the lepton asymmetry is subsequently converted to a baryon asymmetry by sphalerons. Because the symmetry preserved by sphalerons is $B - L$, a negative lepton asymmetry must be generated to account for the observed positive baryon asymmetry.

A positive lepton number asymmetry also accumulates in ψ_i, and it is important that this positive asymmetry does not erase the negative asymmetry in Standard Model leptons. In our model, ψ_i decays into light gauge singlets n_i that are decoupled from Standard Model fields at low temperatures. The asymmetry produced in ψ is therefore sequestered in a sterile sector and the Standard Model asymmetry persists to the present time[4]. A Z_4 symmetry, with charges in Table 3.1, forbids other operators that allow ψ to decay directly into Standard Model leptons, thus preventing the erasure of the Standard Model lepton asymmetry. The Z_4 symmetry also makes dark matter stable.

---

[3]We consider pseudoscalars instead of scalars because they do not have a velocity-suppressed XX annihilation cross section. A scalar S with couplings to X that are CP-violating with a large imaginary part would work as well.

[4]If $m_\psi > m_S$, then ψ can decay into $S + L^\dagger$ and wipe out the lepton asymmetry. However, S then subsequently decays into either $L + H + n^\dagger$ or $L^\dagger + H^* + n$ (when $XX \to L\psi$ is kinematically allowed, $S \to XX$ is kinematically forbidden because $2m_X > m_\psi > m_S$), and the difference in the rates of these decays generates another lepton asymmetry. If the efficiency of asymmetry generation from S decays is comparable to that from XX annihilations, the asymmetry is comparable to the original asymmetry created from $XX \to L\psi$.

Table 3.1: Z_4 charges (WIMP annihilation to leptons)

	X	X	ψ	ψ	S	n	Standard Model
Z_4	$+i$	$-i$	-1	-1	-1	-1	$+1$

In the simplest model, ψ_i decays to $n_i + H$ through the interaction

$$\Delta\mathcal{L} = \lambda_i\, H^\dagger n_i \psi_i + \text{h.c.} \tag{3.19}$$

We assume that ψ_i is vectorlike with a partner $\bar{\psi}_i$ in order to more readily satisfy electroweak precision constraints. Its mass is restricted by the LEP bound $m_\psi \gtrsim 100$ GeV (see Section 3.5.2).

After electroweak symmetry breaking, ψ_i mixes with the sterile neutrino n_i, and we must ensure that the sterile neutrino satisfies overclosure constraints. Since ψ is Dirac, we also include $\bar{\psi}$ when diagonalizing the mass matrix and find that there remains a massless eigenstate even after the Higgs condenses. This is good, because light, weakly interacting thermal relics (such as sterile neutrinos) with masses $\gtrsim \mathcal{O}(\text{eV})$ would overclose the universe. n could have a Majorana mass $m_n \lesssim$ eV and still satisfy observational constraints, since the light eigenstate would have a mass $\lesssim$ eV as well, but we take n to be massless in our model.

The Lagrangian (3.18) is also invariant under a $\text{U}(1)^3$ lepton flavor symmetry that prohibits flavor-changing neutral currents but allows flavor-dependent couplings. L_i, n_i, and ψ_i have charges $+1$, $+1$, and -1, respectively, under the $\text{U}(1)_i$ factor of the flavor symmetry. We assume that the only source of flavor-breaking in the low-energy theory is through the neutrino mass matrices, and this effect is very small.
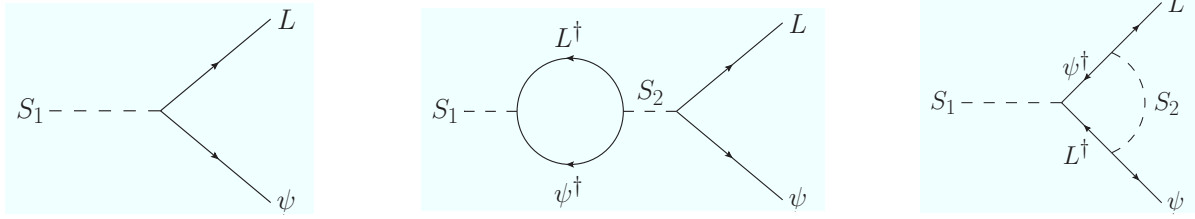
Figure 3.3: Diagrams of tree and loop contributions to S decay. The difference between these rates and their conjugates generates a lepton asymmetry.
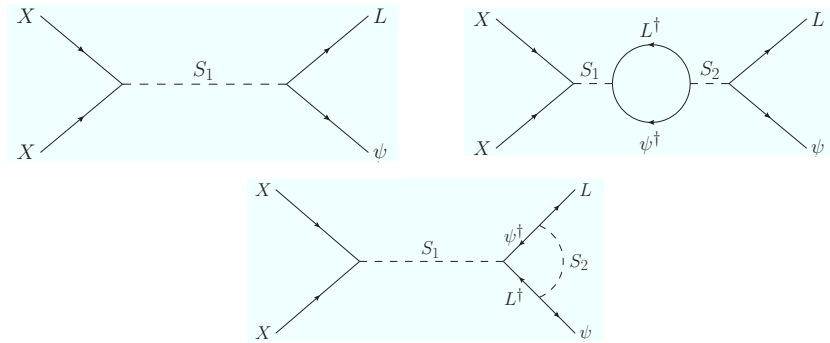

Figure 3.4: Diagrams of tree and loop contributions to the XX annihilation cross section. The difference between these rates and their conjugates generates a lepton asymmetry.

Asymmetry generation

In this model, a lepton asymmetry can in principle be generated through two processes: the more conventional process of S_α decay into $L_i\psi_i$ and their conjugates (or directly into $L_i + n_i + H$ if $m_\psi > m_S$), and XX annihilation into the same final states. We show these in Figures 3.3 and 3.4, respectively, assuming that decay and annihilation occur predominantly through the lightest scalar S_1. Existing work discusses the relevant processes for generating a lepton asymmetry through $2 \to 2$ scattering [54], although the authors consider only high-scale models ($T \gtrsim 10^9$ GeV) with qualitatively different features than WIMPy leptogenesis. CP-violating phases in our model appear in the interference between tree-level and one-loop

diagrams. We define asymmetry factors for the decay of the lightest scalar S_1 and for WIMP annihilations, respectively, in the manner of conventional leptogenesis:

$$\epsilon_1 = \frac{\Gamma(S_1 \to \psi_i L_i) - \Gamma(S_1 \to \psi_i^\dagger L_i^\dagger)}{\Gamma(S_1 \to \psi_i L_i) + \Gamma(S_1 \to \psi_i^\dagger L_i^\dagger)}, \tag{3.20}$$

$$\epsilon_2 = \frac{\sigma(XX \to \psi_i L_i) + \sigma(\bar{X}\bar{X} \to \psi_i L_i) - \sigma(XX \to \psi_i^\dagger L_i^\dagger) - \sigma(\bar{X}\bar{X} \to \psi_i^\dagger L_i^\dagger)}{\sigma(XX \to \psi_i L_i) + \sigma(\bar{X}\bar{X} \to \psi_i L_i) + \sigma(XX \to \psi_i^\dagger L_i^\dagger) + \sigma(\bar{X}\bar{X} \to \psi_i^\dagger L_i^\dagger)}. \tag{3.21}$$

ϵ_1 gives the fractional asymmetry generated per S_1 decay, while ϵ_2 gives the fractional asymmetry generated per XX annihilation. The precise values of ϵ_1, ϵ_2 in this case depend on the masses $m_{S\alpha}$ and the couplings $\lambda_{\alpha i}$.

To reduce the number of arbitrary parameters in our analysis, we make the following assumptions:

- Dark matter annihilation occurs dominantly to only one flavor of lepton, and the couplings of all other leptons to S_α are zero. The non-zero couplings of the single lepton flavor are denoted $\lambda_{L\alpha}$.

- Dark matter annihilation and washout occur mostly through the lightest scalar, S_1, and we consider the rates of only these processes in our analysis. For concreteness, we require that the corresponding cross sections with intermediate S_2 to be less than 20% of the corresponding cross sections with S_1, giving roughly

$$\frac{\lambda_{L2}^4}{m_{S2}^4} \lesssim \frac{\lambda_{L1}^4}{5m_{S1}^4}, \tag{3.22}$$

$$\frac{\lambda_{X2}^2 \lambda_{L2}^2}{m_{S2}^4} \lesssim \frac{\lambda_{X1}^2 \lambda_{L1}^2}{5m_{S1}^4}. \tag{3.23}$$

We also assume that $m_{S1} \ll m_{S2}$, so that the loop integrals in ϵ_1 and ϵ_2 can be put in

a simple analytic form (3.24).

- The physical CP phases are large i.e. $\text{Im}(a) \approx a$ where a is some product of couplings appearing in scattering and decay amplitudes.

None of these assumptions are required by WIMPy leptogenesis, and we make them only to simplify the analysis and its interpretation. Relaxing these assumptions would introduce much complexity into the Boltzmann equations while giving qualitatively similar results. The phenomenology does, however, depend to some extent on the flavor of leptons to which dark matter predominantly annihilates (see Section 3.5 for details). With the above assumptions[5],

$$\epsilon_2 \approx -\frac{1}{6\pi} \frac{\text{Im}(\lambda_{L1}^2 \lambda_{L2}^{*2})}{|\lambda_{L1}|^2} \frac{(2m_X)^2}{m_{S2}^2} \left[7 - 15 \left(\frac{m_\psi}{2m_X} \right)^2 + 9 \left(\frac{m_\psi}{2m_X} \right)^4 - \left(\frac{m_\psi}{2m_X} \right)^6 \right]. \quad (3.24)$$

The expression for ϵ_1 is the same but with $2m_X \to m_{S1}$. Since we are most interested in the asymmetry from annihilation, ϵ_2 is the relevant parameter for WIMPy baryogenesis and we denote its asymmetry factor by $\epsilon \equiv \epsilon_2$. ϵ is suppressed by $1/m_{S2}^2$ from the S_2 propagator, and is proportional to $(2m_X)^2$ because the momentum flowing through the S_1 propagator in XX annihilation is $\sqrt{\hat{s}} = 2m_X + \mathcal{O}(T)$, where $T \ll m_X, m_{S1}$ at freeze-out. Note that (3.24) vanishes when $m_\psi = 2m_X$, at which point the particles in the loop cannot go on shell and there is no imaginary part of the amplitude (and, hence, no CP violation).

---

[5]This expression is derived in the narrow-width approximation. For TeV WIMPs, $\lambda_X \gtrsim 1$ is often necessary to obtain the correct dark matter relic abundance, which may lead to $\Gamma_{S1}, \Gamma_{S2} \sim m_S$. When $2m_X > m_{S1}$, S_1 is kinematically forbidden from decaying into XX and the S_1 width is narrow (because typically $\lambda_L \lesssim 1$). S_2 may be broad, but the imaginary part of its self-energy correction $\text{Im}\Pi(p^2)$ as substituted into (3.24) must be evaluated at $p^2 = 4m_X^2 \ll m_{S2}^2$ and satisfies $\text{Im}\Pi(4m_X^2) \sim 4m_X^2 \ll m_{S2}^2$. Similarly, if $2m_X < m_{S1}$, then the partial width of S_1 to X can be very large for $2m_X \ll m_{S1}$, but once again $\text{Im}\Pi$ is evaluated in (3.24) as $\text{Im}\Pi(4m_X^2) \sim 4m_X^2 < m_{S1}^2$. Therefore, the narrow-width approximation holds true to a degree sufficient for our purposes.

Using (3.22), (3.24), and the assumption of large CP phases, we can bound ϵ from above:

$$|\epsilon| \lesssim \frac{2\lambda_{L1}^2}{3\pi\sqrt{5}} \frac{m_X^2}{m_{S1}^2} \left[7 - 15 \left(\frac{m_\psi}{2m_X} \right)^2 + 9 \left(\frac{m_\psi}{2m_X} \right)^4 - \left(\frac{m_\psi}{2m_X} \right)^6 \right]. \tag{3.25}$$

We treat ϵ as a free parameter, subject to (3.25), and we can now express all rates and cross sections in terms of $\lambda_X \equiv \lambda_{X1}$, $\lambda_L \equiv \lambda_{L1}$, ϵ, m_X, m_ψ, and $m_S \equiv m_{S1}$.

We have assumed that the lepton asymmetry from XX annihilations dominates over that from S decays. We find that this assumption is true whenever $m_X < m_S$. Since the asymmetry is proportional to the number density of X or S at the time of washout freeze-out, the ratio of asymmetry from decay vs. annihilation is the same as the ratio of the number of S particles to the number of X particles at the time of washout freeze-out. The assumption of annihilation-dominated asymmetry is therefore equivalent to $m_X < m_S$.

Washout

As we demonstrated in Section 3.2, the final baryon asymmetry depends on the time of washout freeze-out. We now discuss the implications for WIMPy leptogenesis, finding that we need $m_\psi \gtrsim m_X$ for successful WIMPy leptogenesis. We show the lepton number washout processes in Figure 3.5. They include inverse annihilations, lepton $\to$ antilepton scatterings, and $\psi X \to L^\dagger X$ processes. The dominant washout is typically from $L\psi \to L^\dagger \psi^\dagger$ scatterings, because the inverse annihilation $L\psi \to XX$ is kinematically suppressed for $T < m_X$ and $\psi X \to L^\dagger X$ gets more Boltzmann suppression. Applying (3.5) for the specific model of WIMPy leptogenesis, the washout rate is proportional to

$$\Gamma_{\text{washout}}(x) \approx \frac{s(x)}{Y_\gamma} \langle \sigma_{L\psi \to L^\dagger \psi^\dagger} v \rangle Y_L^{\text{eq}} Y_\psi^{\text{eq}}(x), \tag{3.26}$$
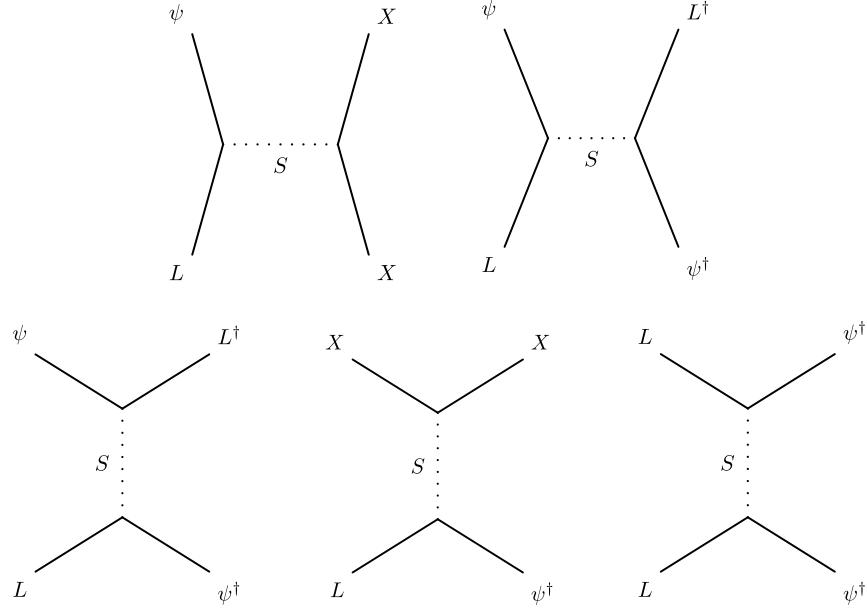
Figure 3.5: Diagrams leading to washout of the lepton number from (top row) s-channel and (bottom row) t-channel scatterings.

where $s(x)$ is the entropy density at x. Washout freezes out when its rate is about equal to the Hubble scale, $\Gamma_{\text{washout}}(x_{\text{washout}}) \approx H(x_{\text{washout}})$. $\Gamma_{\text{washout}}(x_{\text{washout}})$ can be small for one of two reasons:

1. $m_\psi \gtrsim m_X$ so that $Y_\psi^{\text{eq}}(x_{\text{washout}})$ is Boltzmann-suppressed while dark matter is annihilating.

2. $\langle \sigma_{L\psi \to L^\dagger \psi^\dagger} v \rangle$ is small relative to the annihilation cross section so that washout freezes out before annihilation. The washout cross section can be small if $\lambda_L \ll 1$.

One of these two conditions must hold for each washout process. We find that option #1 leads to viable WIMPy leptogenesis. Option #2, on the other hand, does not give a large asymmetry. According to (3.25), the asymmetry efficiency factor ϵ is also suppressed when $\lambda_L \ll 1$, and the potential gain in the baryon asymmetry from early washout freeze-out
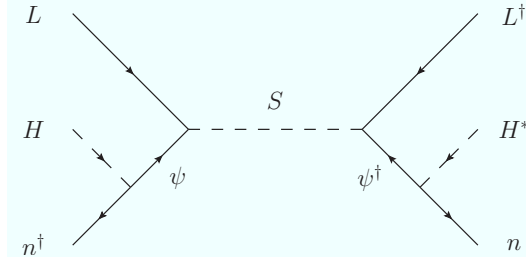
Figure 3.6: $3 \to 3$ washout process that can dominate over $2 \to 2$ scattering when $T \ll m_\psi$.

in option #2 is offset because leptogenesis occurs less efficiently. Therefore, $m_\psi \gtrsim m_X$ is generally required to generate the observed baryon asymmetry.

When m_ψ is much larger than m_X (we find this is typically true for $m_\psi \gtrsim 2m_X$), the exponential suppression of Y_ψ is so large that $3 \to 3$ scatterings of $L\,n\,H \to L^\dagger\,n^\dagger\,H^*$ become important (see Figure 3.6). This region is, however, kinematically inaccessible in WIMPy leptogenesis since $2m_X > m_\psi$ for efficient annihilation to occur, and we neglect $3 \to 3$ processes.

Boltzmann equations

We consider the evolution of a single component L_a, where a is a gauge index (flavor indices are suppressed since we consider only one flavor). We define Br_L (Br_X) as the total branching fraction of S into leptons (X), with $\mathrm{Br}_L + \mathrm{Br}_X = 1$. Also, $\xi = 1 + \mu_{\psi_a}/\mu_{L_a}$, where μ are chemical potentials, and η is defined as the amount of L_a asymmetry generated for each L_a directly created/annihilated (this accounts for the fact that the asymmetry spreads among all baryons and leptons by rapid thermalization). We calculated the cross sections and widths analytically and checked them with CalcHEP [55].

The Boltzmann equations describing the evolution of the various particle species and the

asymmetry in **one** of the components of the L_a doublet are

$$\frac{H(m_X)}{x}\frac{dY_X}{dx} = -4s\langle\sigma_{XX\to L_a\psi_a}v\rangle[Y_X^2-(Y_X^{\mathrm{eq}})^2]-2s\epsilon\frac{\xi Y_{\Delta L_a}}{Y_\gamma}\langle\sigma_{XX\to L_a\psi_a}v\rangle(Y_X^{\mathrm{eq}})^2$$

$$-\mathrm{Br}_X^2\langle\Gamma_S\rangle Y_S^{\mathrm{eq}}\left(\frac{Y_X}{Y_X^{\mathrm{eq}}}\right)^2+\mathrm{Br}_X\langle\Gamma_S\rangle(Y_S-\mathrm{Br}_L Y_S^{\mathrm{eq}})$$

$$-\epsilon\frac{\xi Y_{\Delta L_a}}{2Y_\gamma}\mathrm{Br}_X\mathrm{Br}_L\langle\Gamma_S\rangle Y_S^{\mathrm{eq}}; \tag{3.27}$$

$$\frac{H(m_X)}{x}\frac{dY_S}{dx} = -\langle\Gamma_S\rangle Y_S+\langle\Gamma_S\rangle Y_S^{\mathrm{eq}}\left[\mathrm{Br}_L+\mathrm{Br}_X\left(\frac{Y_X}{Y_X^{\mathrm{eq}}}\right)^2\right]; \tag{3.28}$$

$$\frac{H(m_X)}{x\,\eta}\frac{dY_{\Delta L_a}}{dx} = \frac{\epsilon}{2}\mathrm{Br}_L\langle\Gamma_S\rangle\left[Y_S+Y_S^{\mathrm{eq}}\left(1-2\mathrm{Br}_L-\mathrm{Br}_X\left[1+\frac{Y_X^2}{(Y_X^{\mathrm{eq}})^2}\right]\right)\right] \tag{3.29}$$

$$+2s\,\epsilon\langle\sigma_{XX\leftrightarrow L_a\psi_a}v\rangle\left[Y_X^2-(Y_X^{\mathrm{eq}})^2\right]$$

$$-\frac{s\,\xi Y_{\Delta L_a}}{Y_\gamma}\left[\langle\sigma_{XX\leftrightarrow L_a\psi_a}v\rangle(Y_X^{\mathrm{eq}})^2+2\langle\sigma_{L_a\psi_b\leftrightarrow L_b^\dagger\psi_a^\dagger}v\rangle Y_L^{\mathrm{eq}}Y_\psi^{\mathrm{eq}}\right]$$

$$-\frac{2s\,\xi Y_{\Delta L_a}}{Y_\gamma}\left[\langle\sigma_{L_a\psi_a\leftrightarrow L_a^\dagger\psi_a^\dagger}v\rangle+\langle\sigma_{L_a\psi_a\leftrightarrow L_b^\dagger\psi_b^\dagger}^{(a\neq b)}v\rangle]Y_L^{\mathrm{eq}}Y_\psi^{\mathrm{eq}}\right]$$

$$-\frac{s\,\xi Y_{\Delta L_a}}{Y_\gamma}\left[\langle\sigma_{X\psi_a\leftrightarrow XL_a^\dagger}v\rangle Y_X Y_\psi^{\mathrm{eq}}+2\langle\sigma_{\psi_a\psi_a\leftrightarrow L_a^\dagger L_a^\dagger}v\rangle(Y_\psi^{\mathrm{eq}})^2\right]$$

$$-\frac{2s\,\xi Y_{\Delta L_a}}{Y_\gamma}\langle\sigma_{\psi_a\psi_b\leftrightarrow L_a^\dagger L_b^\dagger}^{(a\neq b)}v\rangle(Y_\psi^{\mathrm{eq}})^2$$

$$+\frac{\xi Y_{\Delta L_a}}{4Y_\gamma}\mathrm{Br}_L\langle\Gamma_S\rangle Y_S^{\mathrm{eq}}\left(\epsilon^2\mathrm{Br}_L+\mathrm{Br}_X\right). \tag{3.30}$$

We assume that all abundances are in thermal equilibrium at $x=1$ and that all fields remain in equilibrium except for S and X. In the evolution of the scalar S, we only include the decay terms, as they dominate over SS annihilation for $T\ll m_S$.

To determine the relationship between μ_{ψ_a} and μ_{L_a}, we assume that all abundances other than S, X and ΔL_a are in thermal equilibrium and that all processes except those involving S are in chemical equilibrium. We also take sphaleron processes to be in equilibrium. The non-S couplings in (3.18) distribute the L and ψ asymmetries among the light fields. Solving

the chemical potential relations gives

$$\xi = \frac{16 + 12\, n^{\text{eq}}_{\psi_a}/n^{\text{eq}}_{L_a}}{3 + 12\, n^{\text{eq}}_{\psi_a}/n^{\text{eq}}_{L_a}}, \tag{3.31}$$

$$\eta = \frac{2(7 + 28\, n^{\text{eq}}_{\psi_a}/n^{\text{eq}}_{L_a})}{79 + 355\, n^{\text{eq}}_{\psi_a}/n^{\text{eq}}_{L_a}}. \tag{3.32}$$

The precise values of ξ and η are model-dependent.

The assumption of thermal equilibrium for ψ is consistent provided the decay width $\Gamma_\psi > H(T_{\text{lep}})$, which in our model constrains

$$\lambda_i^2 \gtrsim \frac{16\pi H(T_{\text{lep}})}{m_{\psi\, i}} \approx \frac{80\sqrt{g_*}\, T^2_{\text{lep}}}{M_{\text{Pl}}\, m_{\psi\, i}}. \tag{3.33}$$

For $T_{\text{lep}} = 100$ GeV and $m_{\psi\, i} = 2$ TeV, this gives $\lambda_i \gtrsim 3 \times 10^{-8}$. This is not a very stringent requirement, since this value is smaller than any of the Standard Model Yukawa couplings.

The final lepton asymmetry is also determined by the chemical potential relations. The relation between the total lepton asymmetry ΔL_{tot} and the asymmetry in a single component of the doublet field ΔL_a as determined by equation (3.30) is

$$Y_{\Delta L\, \text{tot}} = \frac{51 + 243 n^{\text{eq}}_{\psi_a}/n^{\text{eq}}_{L_a}}{7 + 28 n^{\text{eq}}_{\psi_a}/n^{\text{eq}}_{L_a}} Y_{\Delta L a}. \tag{3.34}$$

The final baryon asymmetry $Y_{\Delta B}$ follows from the sphaleron chemical potential relations, and is

$$Y_{\Delta B}(x) = -4\left(\frac{7 + 28 n^{\text{eq}}_{\psi_a}/n^{\text{eq}}_{L_a}}{51 + 243 n^{\text{eq}}_{\psi_a}/n^{\text{eq}}_{L_a}}\right) Y_{\Delta L\, \text{tot}} = -4 Y_{\Delta L_a}. \tag{3.35}$$

In the limit $x \to \infty$, the ratio of total baryon to lepton number reduces to the same expression as conventional leptogenesis [33].

The total dark matter relic abundance is

$$Y_{\mathrm{DM}}(\infty) = Y_X(\infty) + Y_{\bar{X}}(\infty) = 2Y_X(\infty). \tag{3.36}$$

3.3.2 Numerical Results

There are six free parameters in our model: three masses (m_S, m_X, and m_ψ) and three dimensionless parameters (λ_X, λ_L, and ϵ). To determine over what range of parameters WIMPy leptogenesis can be successful, we perform scans over two parameters at a time while holding others fixed. In particular, we are interested to see what range of masses is allowed, and if any tuning of the mass and coupling constant relations is necessary to generate the correct baryon asymmetry and WIMP relic density.

Range of allowed masses: We hold m_S fixed and determine for which m_X and m_ψ masses there exists *some* perturbative couplings that give the observed dark matter density and baryon asymmetry. We place no other restrictions on the couplings. If $m_\psi > m_S$, we assume that the S width is dominated by the three-body decay $S \to L H n$. We show in Figure 3.7 the masses that give rise to successful WIMPy leptogenesis. The viable ψ masses satisfy $m_\psi \approx (1-2)m_X$, while there is no correlation between m_X and m_S as long as $m_X < m_S$. For smaller values of m_ψ/m_X, the Boltzmann suppression of the washout rate is insufficient to generate the observed baryon asymmetry, while $m_\psi \gtrsim 2m_X$ is not allowed because dark matter annihilation is not kinematically allowed and because the asymmetry efficiency ϵ is zero (CP violation is zero if L and ψ cannot go on-shell in the dark matter annihilation loop diagrams).

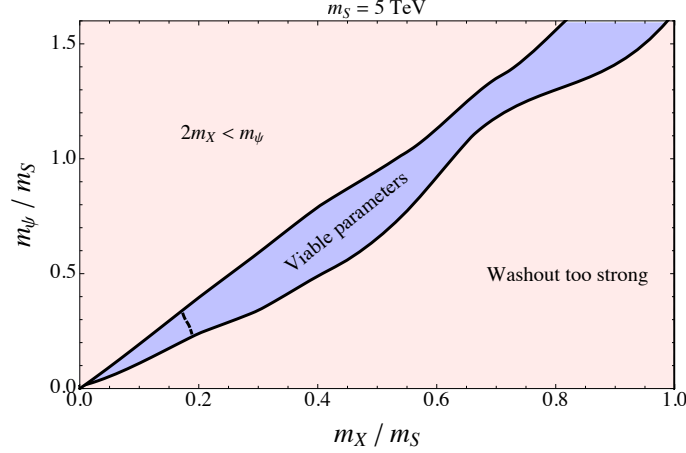The lower boundary of the allowed region has a meandering shape around $m_\psi \approx m_S$.

Figure 3.7: Regions in the m_X-m_ψ plane with the correct WIMP relic density and baryon asymmetry from WIMPy leptogenesis, with $m_S = 5$ TeV and some choice of perturbative couplings. The masses giving both observed abundances are shown in blue (middle stripe). We plot the ratios m_X/m_S, m_ψ/m_S to show the relationship between the X and ψ masses and the mediator scale m_S. The excluded regions are shown in red: the upper region is not viable because $2m_X < m_\psi$ and the thermal annihilation cross section is Boltzmann-suppressed, while the lower region has Y_ψ too large to prevent rapid washout of the asymmetry. The dashed line indicates the lower boundary of allowed m_X and m_ψ; below the line, the electroweak phase transition occurs before the baryon asymmetry is large enough to account for the observed value. For $m_X/m_S > 1$, the asymmetry is dominated by S decay.

The reason is that s-channel washout processes have a resonant enhancement in this region, leading to a smaller baryon asymmetry and a restricted parameter space. Above resonance, t-channel washout processes are also important, explaining why the bend in the curve is centered at m_ψ slightly larger than m_S.

The principal reason that it is difficult to generate a large baryon asymmetry is because the efficiency of asymmetry generation ϵ is tied to the washout cross section through its dependence on λ_L^2 in (3.25). A large asymmetry can only be generated when washout effects are also large, limiting how much of an asymmetry can be generated. The viable parameter space is larger if (3.25) can be relaxed, as is the case when S_1 and S_2 are nearly degenerate

and the asymmetry is resonantly enhanced, but this is not a required feature of WIMPy leptogenesis.

In leptogenesis, the asymmetry must be generated prior to the electroweak phase transition, at which point sphalerons decouple and the conversion of a lepton asymmetry into a baryon asymmetry ceases. Since WIMPy leptogenesis is a weak-scale model, the timing of the asymmetry generation relative to the phase transition is important. To illustrate this, we computed the critical temperature T_c of the phase transition assuming a Standard Model Higgs with mass $m_h = 120$ GeV, and we required that the baryon asymmetry at T_c be equal to the observed asymmetry[6]. This typically yields a much smaller baryon asymmetry than lepton asymmetry at late times because the baryon asymmetry stops accumulating at T_c. Accounting for the effects of the phase transition, the allowed region is above the dashed line in Figure 3.7. If the phase transition is modified by additional Higgs fields or other new physics, then this boundary line changes.

Range of allowed couplings: We choose representative values of the masses, with $m_S = 5$ TeV for all cases, and m_X and m_ψ chosen in the middle of the allowed bands in Figure 3.7. For one set of parameters, dark matter annihilates above the S resonance, with parameters $m_X = 4.25$ TeV, $m_\psi = 7.5$ TeV, and $|\epsilon| = 0.075$, and we determine the dark matter relic abundance and baryon asymmetry as functions of the two couplings. We also study XX annihilation below resonance, with $m_X = 1.5$ TeV, $m_\psi = 2.25$ TeV, and $|\epsilon| = 0.0075$. We plot the results in Figure 3.8 as contours of constant relic density and baryon asymmetry. We

---

[6]Since the Standard Model phase transition is of second order, sphalerons do not suddenly shut off, and a more proper treatment would account for the gradual departure from equilibrium of the sphaleron effects. Since the asymmetry is typically generated over a very short time period (we find numerically that it is on the order of $\Delta x \sim 2 - 3$ or $\Delta T \sim 5 - 10$ GeV), the dynamics of sphaleron shut-off are largely irrelevant and the most important factor is the rate of $L \to B$ transfer at the washout freeze-out time x_{washout}.
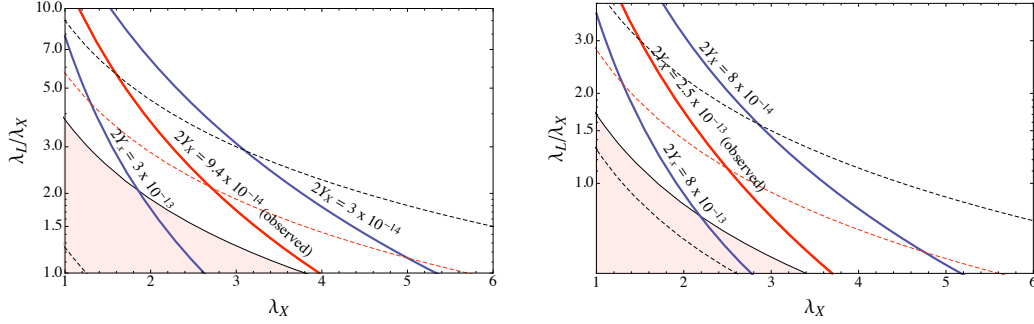
Figure 3.8: Dark matter relic density *(solid lines)* and baryon asymmetry *(dotted lines)* as functions of couplings λ_X and λ_L/λ_X. We consider two sets of massses, with $m_S = 5$ TeV for both: **(left)** $m_X = 4.25$ TeV, $m_\psi = 7.5$ TeV, and $|\epsilon| = 0.075$; **(right)** $m_X = 1.5$ TeV, $m_\psi = 2.25$ TeV, and $|\epsilon| = 0.0075$. The asymmetry contours are, from top to bottom: **(left)** $Y_{\Delta B} = 5 \times 10^{-11}$, 8.5×10^{-11} (observed asymmetry), and 3×10^{-10}; **(right)** $Y_{\Delta B} = 3 \times 10^{-11}$, 8.5×10^{-11} (observed asymmetry), and 3×10^{-10}. The dark matter abundances are printed on the plots. In the shaded regions, the numerical value of ϵ is not consistent with our assumptions according to the bound (3.25).

focus on the ratio λ_L/λ_X because we are interested in seeing if any relationship between these two theoretically unrelated quantities is required to obtain a particular relic abundance and asymmetry. In both cases shown, WIMPy leptogenesis gives the correct dark matter relic abundance and asymmetry when both couplings are $\mathcal{O}(1)$. Thus, a perfectly natural choice of couplings, and the very same couplings that satisfy the WIMP miracle, can also generate the correct baryon asymmetry if CP phases are large! Specifically, with $m_X = 4.25$ TeV, $m_\psi = 7.5$ TeV, and $|\epsilon| = 0.075$, the observational constraints are satisfied with $\lambda_X = 2.7$ and $\lambda_L = 5.7$; with $m_X = 1.5$ TeV, $m_\psi = 2.25$ TeV, and $|\epsilon| = 0.0075$, the couplings are $\lambda_X = 2.8$, $\lambda_L = 2.5$.

In deriving our results, we assumed that dark matter only annihilates through lepton-number-violating interactions. In a more general model, dark matter may also have lepton-
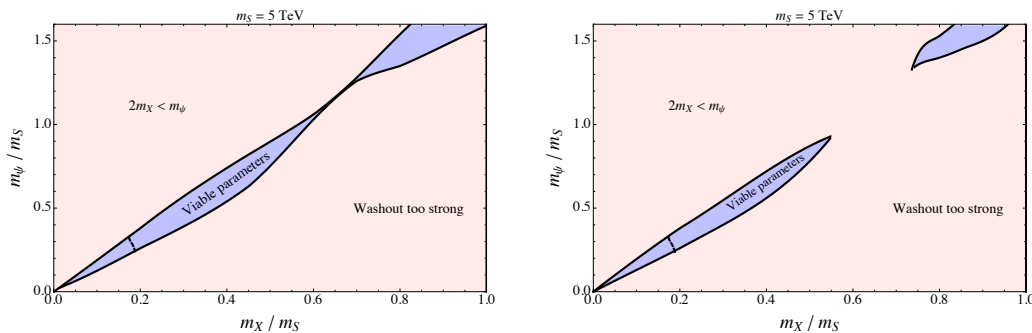
Figure 3.9: Regions in the m_X-m_ψ plane for viable WIMPy leptogenesis with additional lepton-number-preserving dark matter annihilation modes: **(left)** $\alpha = 2$, **(right)** $\alpha = 3$. The masses giving the correct dark matter density and baryon asymmetry for some choice of perturbative coupling are shown in blue (middle stripe). As the lepton-number-preserving annihilation cross section increases, the efficiency of asymmetry generation drops, and the marginal regions of parameter space become inaccessible, particularly the enhanced washout region $m_\psi \sim m_S$. The descriptions of the regions on the plot are the same as those in Figure 3.7.

number-preserving interactions that contribute to the total annihilation cross section. We parameterize this possibility with the quantity

$$\alpha \equiv \frac{\langle \sigma_{XX \to \text{anything}} \, v \rangle}{\langle \sigma_{XX \to L\psi} \, v \rangle} \geq 1. \qquad (3.37)$$

When $\alpha > 1$, the asymmetry generated by WIMPy leptogenesis is smaller, because only $1/\alpha$ of dark matter annihilations proceed through lepton-number-violating couplings and can create an asymmetry[7]. As a result, the viable parameter space for WIMPy leptogenesis is reduced. In Figure 3.9, we show the masses m_X, m_ψ giving successful WIMPy leptogenesis with $\alpha > 1$. In particular, we find that the lepton asymmetry from WIMPy leptogenesis is

---

[7]When $\alpha > 1$, the WIMP annihilation cross section is also larger, and λ_X, λ_L are smaller to give the same WIMP relic density. As discussed in Section 3.3.1, however, decreasing the couplings results in *both* a smaller washout rate and a smaller efficiency of generating an asymmetry. These two effects counteract one another, and the change in couplings for $\alpha > 1$ does not substantially affect the asymmetry.

too small in regions with large washout ($m_\psi \sim m_S$, where wash-out scattering is on-shell). While WIMPy leptogenesis is possible with lepton-preserving annihilation channels, m_ψ lies in a more restricted region when $\alpha > 1$.

To summarize, we have presented a model of WIMPy leptogenesis where the WIMP miracle has been extended to the WIMPy baryogenesis miracle: the correct baryon asymmetry and WIMP relic density can be generated simultaneously with TeV-scale masses and $\mathcal{O}(1)$ couplings. We find that, depending on the ratio m_ψ/m_X and the Yukawa couplings, larger and smaller asymmetries are also possible over a range of about seven orders of magnitude. Generating the observed baryon asymmetry does require some correlation between m_X and m_ψ, which may be explained if the masses have some common dynamical origin. For m_X lighter than about 1 TeV, sphalerons decouple in the middle of asymmetry generation and the resulting baryon asymmetry is typically smaller than the observed $Y_{\Delta B}$.

3.4 WIMP Annihilation to Quarks

3.4.1 Model Overview

If the final products of dark matter annihilation are quarks, WIMP annihilation can directly generate a baryon number asymmetry. The lower bound of $\sim$ TeV on m_X in WIMPy leptogenesis (the dashed line in Figure 3.7) does not apply when WIMPs annihilate to quarks, since the production of baryon number no longer depends on efficient sphaleron interactions. Just as the leptogenesis model included new weakly charged vectorlike doublets, this model requires new vectorlike colored states to couple to quarks. Such states can be pair-produced at the LHC, leading to much stronger constraints and better detection prospects, which we

discuss in Section 3.5.2.

The model content is similar to the leptogenesis model discussed in Section 3.3: vectorlike gauge singlet dark matter X and $\bar{X}$, singlet pseudoscalars S_α, and vectorlike exotic quark color triplets ψ_i and $\bar{\psi}_i$. The Lagrangian is

$$\mathcal{L} = \mathcal{L}_{\text{kin}} + \mathcal{L}_{\text{mass}} - \frac{i}{2}\left(\lambda_{X\alpha}X^2 + \lambda'_{X\alpha}\bar{X}^2\right)S_\alpha + i\lambda_{B\,\alpha}\,S_\alpha \bar{u}\psi. \tag{3.38}$$

A baryon asymmetry can be generated in $\bar{u}$ along with an equal negative baryon asymmetry in ψ. ψ must decay, because it would otherwise overclose the universe and violate bounds on stable colored particles.

The negative baryon asymmetry in ψ must not destroy the positive baryon asymmetry in $\bar{u}$ when it decays. This can happen in two ways:

1. ψ decays into a sector decoupled from Standard Model quarks at low energies. Total baryon number is preserved, but the negative baryon number carried by ψ is sequestered from quarks at late times and does not eliminate the Standard Model asymmetry.

2. ψ decays into Standard Model quarks through baryon-number-violating couplings. The final baryon asymmetry is different from the asymmetry created initially in $\bar{u}$ from WIMP annihilations because ψ decays give an additional contribution to the baryon asymmetry.

We now implement each of the above scenarios.

1. ψ_i decays to light, baryon-number-carrying singlets n_i plus Standard Model antiquarks. It can do so through a colored scalar ϕ with Standard Model gauge representation

$(3, 1, -1/3)$. The additional terms in the Lagrangian are

$$\Delta\mathcal{L} = \lambda_i \, \bar{\psi}_i \, \bar{d}_i \, \phi^* + \lambda'_i \, \phi \, \bar{d}_i \, n_i + \text{h.c.} \tag{3.39}$$

A Z_4 symmetry prevents ψ from decaying directly into Standard Model quarks through a $QH\bar{\psi}$ term and eliminating the baryon asymmetry. We show the charges in Table 3.2. This Lagrangian has a U(1)^3 flavor symmetry and satisfies all quark flavor constraints. In particular, $\bar{u}_i$, ψ_i, and n_i have charges -1, $+1$, and -3, respectively, under the U(1)$_i$ factor of the flavor symmetry. ϕ has charge -2 under all U(1) flavor symmetries. We assume that the only sources of flavor violation are the Standard Model Yukawa matrices.

2. In this scenario, ψ_i also decays to two antiquarks plus a singlet n, but n is a Majorana fermion that does not carry any charge. Baryon number is now explicitly violated, and dark matter annihilations generate -1 unit of baryon number for each $\psi + \bar{u}$ produced from dark matter annihilations (because $\psi \to \bar{d}\bar{d}n$). There is a new colored scalar $\tilde{d}_i$ in the $(3, 1, -1/3)$ representation of the Standard Model gauge group that mediates ψ decays. The additional terms in the Lagrangian are

$$\Delta\mathcal{L} = \lambda \, \epsilon^{ijk} \, \bar{\psi}_i \, \bar{d}_j \, \tilde{d}_k^* + \lambda'_i \, \bar{d}_i \, \tilde{d}_i \, n + \text{h.c.} \tag{3.40}$$

A Z_4 symmetry, with charges given in Table 3.2, prevents ψ from decaying to Standard Model quarks through other interactions that would destroy the baryon asymmetry. This Lagrangian can be naturally realized in supersymmetric models, where $\tilde{d}$ is the down squark and n is the neutralino, although this is not the only possible realization

Table 3.2: Z_4 charges (WIMP annihilation to quarks)

	X	$\bar{X}$	ψ	$\bar{\psi}$	S	$\bar{u}$	$\bar{d}$	$\phi/\tilde{d}$	Q	H	n	leptons
Z_4	$+i$	$-i$	$+1$	$+1$	-1	-1	-1	-1	-1	$+1$	$+1$	$+1$

of this scenario. (3.40) has a U(3) flavor symmetry, which is the diagonal subgroup of the full $\mathrm{U}(3)_u \times \mathrm{U}(3)_d$ flavor group. The quark, ψ_i and $\tilde{d}_i$ fields transform in the fundamental of U(3). The Yukawa couplings between $S\bar{u}\psi$ in (3.38) have a flavor-independent piece and a flavor-dependent piece proportional to the up Yukawa matrix Y_u, consistent with minimal flavor violation.

In both scenarios, ψ decays to a singlet n plus quarks. Operators allowing ψ to decay entirely to quarks (such as $\phi^*\bar{d}\,\bar{u}$ or $\tilde{d}^*\bar{d}\,\bar{u}$) are forbidden by the Z_4 symmetry. The Z_4 symmetry also ensures the stability of dark matter and of the proton. The proton is stable provided $m_\mathrm{p} < 2m_X, m_S$ because baryons have charge $(-1)^3 = -1$ and can never decay into the lighter meson and lepton fields, which are uncharged under the Z_4.

The Z_4 symmetry in principle allows neutral baryons to oscillate into one another. For scenario #1, the generalized baryon number symmetry prohibits neutron-antineutron oscillation. In scenario #2, the baryon-number-violating term is antisymmetric in flavor indices, and the dominant contribution to neutron-antineutron mixing involves loops of W bosons and off-diagonal CKM matrix element insertions V_{bd} and V_{sd}. Since the bound on the neutron-antineutron oscillation operator $c/\Lambda^5(\bar{u}\bar{d}\bar{d})^2$ is $\Lambda \gtrsim 10 - 100$ TeV for $c = 1$ [56], the loop- and CKM-suppression is sufficient to lower the oscillation rate well below current constraints for m_S, m_ψ, $m_{\tilde{d}} \sim$ TeV and $\mathcal{O}(1)$ couplings.

The Boltzmann equations for WIMP annihilation to quarks are changed only by group theory factors from the corresponding equations for leptons. Similarly, the chemical poten-
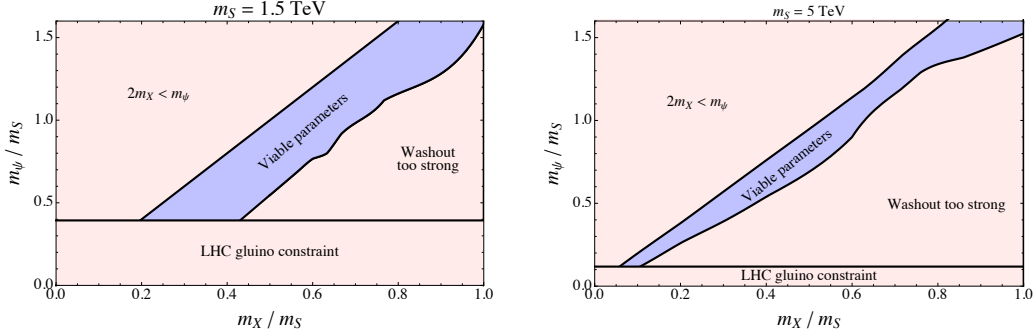
Figure 3.10: Regions in the m_X-m_ψ plane with the correct WIMP relic density and baryon asymmetry from WIMPy baryogenesis, with **(left)** $m_S = 1.5$ TeV and **(right)** $m_S = 5$ TeV, and any choice of perturbative couplings. The masses giving both observed abundances are shown in blue (middle stripe). The descriptions of the regions on the plot are the same as those in Figure 3.7.

tials relations are modified to reflect the new interactions (3.39) or (3.40).

As with WIMPy leptogenesis, we assume that ψ is in equilibrium, and this places constraints on the couplings through which it decays. In scenario #1, we considered the decay of ψ according to interactions given in equation (3.39). If $m_\psi > m_\phi$, the ψ decay is two-body and the constraint (3.33) applies, giving $\lambda_i \gtrsim 6 \times 10^{-8}$. If $m_\psi < m_\phi$, ψ undergoes a three-body decay to $\bar{d}\,\bar{d}\,n$, and the constraint is

$$(\lambda_i \lambda_i')^2 \gtrsim \frac{80\sqrt{g_*}\,T_{\mathrm{lep}}^2\,m_\phi^2}{M_{\mathrm{Pl}} m_\psi^3}. \tag{3.41}$$

For $T_{\mathrm{lep}} = 50$ GeV and $m_\psi = 1$ TeV, we find that the constraint on the geometric mean of the couplings is

$$\sqrt{\lambda_i \lambda_i'} \gtrsim 6 \times 10^{-5} \sqrt{\frac{m_\phi}{2\ \mathrm{TeV}}}. \tag{3.42}$$

The constraints on scenario #2 are comparable.

3.4.2   Numerical Results

Because of its similarity to leptogenesis, we use the quark flavor structure of scenario #1 in our analysis, since it allows for a more direct comparison of numerical results in both cases. We consider two scenarios: $m_S = 5$ TeV, to compare the results for quarks with that for leptons, and $m_S = 1.5$ TeV, because dark matter can be much lighter than in WIMPy leptogenesis since there are no constraints from sphaleron decoupling. For simplicity, we consider sphalerons to be out of equilibrium for the 1.5 TeV case and in equilibrium for the 5 TeV case to avoid considering sphaleron decoupling effects, although the calculation can be easily extended to include them.

<u>Range of allowed masses</u>: We show the range of allowed masses in Figure 3.10. Gluino searches at the LHC constrain this scenario (see Section 3.5.2), in contrast with the leptogenesis model, for which the entire parameter space is unconstrained by collider searches. This is particularly true for $m_S = 1.5$ TeV, where LHC searches will cover almost the entire parameter space for dark matter annihilation to quarks during the 14 TeV run. The WIMP mass is already constrained to be $m_X \gtrsim 295$ GeV by the gluino bound discussed in Section 3.5.2 along with the kinematic requirement that $2m_X > m_\psi$. This is true independent of all other parameters.

In both cases, the results are qualitatively similar to leptogenesis. With WIMP annihilation to quarks, the annihilation and washout cross sections are enhanced because the final states are charged under $\text{SU}(3)_\text{C}$. As a result, the baryon asymmetry is suppressed by the increased washout rate. This is partially offset by the fact that the self-energy contribution to ϵ is enhanced by a group theory factor as well. With $m_X = 0.9$ TeV, the parameter space is actually larger than for $m_X = 4.25$ TeV or WIMPy leptogenesis. Since in this case,
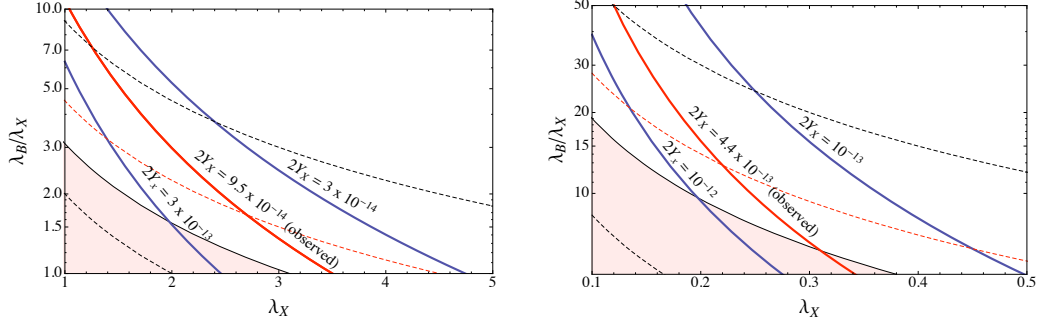
Figure 3.11: Dark matter relic density (solid lines) and baryon asymmetry (dotted lines) as functions of couplings λ_X and λ_B/λ_X. We consider two sets of massses: **(left)**, $m_X = 4.25$ TeV, $m_\psi = 7.25$ TeV, $m_S = 5$ TeV, and $|\epsilon| = 0.075$. The asymmetry contours are, from top to bottom: $Y_{\Delta B} = 4 \times 10^{-11}$, 8.5×10^{-11} (observed asymmetry), and 1.5×10^{-10}. **(right)** $m_X = 0.9$ TeV, $m_\psi = 1.2$ TeV, $m_S = 1.5$ TeV, and $|\epsilon| = 0.075$; the asymmetry contours are, from top to bottom: $Y_{\Delta B} = 5 \times 10^{-11}$, 8.5×10^{-11} (observed asymmetry), and 3×10^{-10}. In the shaded regions, ϵ is not consistent with our assumptions according to the bound (3.25).

sphalerons no longer inter-convert baryon and lepton number, the asymmetry created in quarks is distributed among fewer fields, enhancing the asymmetry.

Range of allowed couplings: We do the same analysis as in Section 3.3.2. To compare the results of direct baryon asymmetry production with those for WIMPy leptogenesis, we choose a set of parameters used in the leptogenesis analysis: $m_X = 4.25$ TeV, $m_\psi = 7.25$ TeV, $m_S = 5$ TeV, and $|\epsilon| = 0.075$. We also consider a corresponding point with light S and broken phase chemical potential relations: $m_X = 0.9$ TeV, $m_\psi = 1.2$ TeV, $m_S = 1.5$ TeV, and $|\epsilon| = 0.075$. We show the results in Figure 3.11. The parameter points giving the correct dark matter density and baryon asymmetry are $\lambda_X = 2.7$, $\lambda_B = 4.5$ for $m_X = 4.25$ TeV, and $\lambda_X = 0.22$, $\lambda_B = 2.8$ for $m_X = 0.9$ TeV.

Table 3.3: Experimental prospects

	Annihilation to leptons	Annihilation to quarks
Direct detection	−−	$m_X \lesssim 5$ TeV for some parameters [8] $(\sigma_{X-\text{nucleon}} \sim 10^{-46} - 10^{-44}$ cm$^2)$
Indirect detection (antideuterons)	$m_X \lesssim 200$ GeV	$m_X \lesssim 1$ TeV
Colliders	$m_\psi \lesssim$ few hundred GeV, possible improvements with targeted searches	$m_\psi \lesssim 1.44$ TeV with 100 fb^{-1} LHC (14 TeV)
EDM	−−	−−

3.5 Experimental Constraints and Prospects

In this section, we survey the possible experimental constraints and signals for models of WIMPy baryogenesis, considering both annihilation to leptons and annihilation to quarks. For WIMP annihilation to leptons, the experimental bounds on m_X and m_ψ are too weak to constrain leptogenesis because $m_X, m_\psi \gtrsim$ TeV are required to generate a sufficiently large baryon asymmetry. The prospects are better for WIMP annihilation to quarks, which predicts signals at indirect and direct detection experiments, as well as at the LHC. We first give a preview of our results for current and near-future experiments in Table 3.3. In this table, '−−' indicates no signal in that particular search channel.

We provide details for each class of experiment in the following sections.

---

[8]Precise reach depends on m_ψ, m_S, λ_X, λ_B, and ϵ.
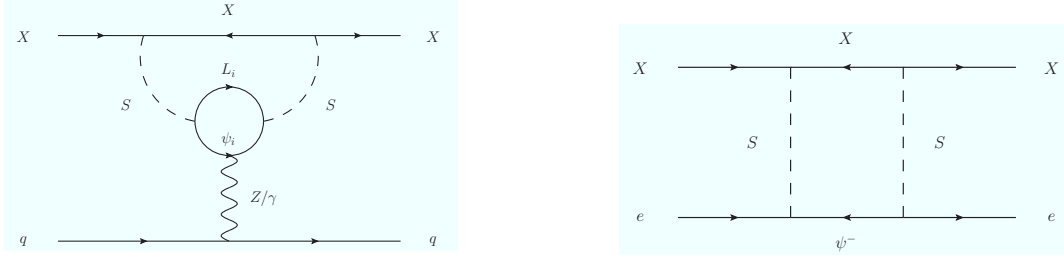
Figure 3.12: Feynman diagrams for dark matter scattering off **(left)** nucleons and **(right)** electrons in direct detection experiments for WIMPy leptogenesis.

3.5.1   Dark Matter Detection

Direct Detection

Dark matter direct detection experiments are typically important probes of weak-scale dark matter models. As we show in this section, however, only WIMPy baryogenesis with dark matter annihilation to quarks is expected to give a signal in conventional direct detection experiments. This is because the dark matter scattering cross section is suppressed by loops of heavy fields, and it is only when dark matter couples directly to quarks that the WIMP-nucleon cross section is large enough to give a signal in upcoming experiments. We assume in this section that dark matter annihilates predominantly to first generation quarks/leptons. The baryon-number-violating interactions in WIMPy baryogenesis can also induce proton decay due to WIMP scattering, but we find that our models are consistent with all current and projected experimental bounds.

We first present the Feynman diagrams for the leading processes relevant to direct detection. With WIMP annihilation to leptons, we show the diagrams for scattering in direct detection experiments in Figure 3.12. We show the corresponding diagrams with WIMP annihilation to quarks in Figure 3.13.
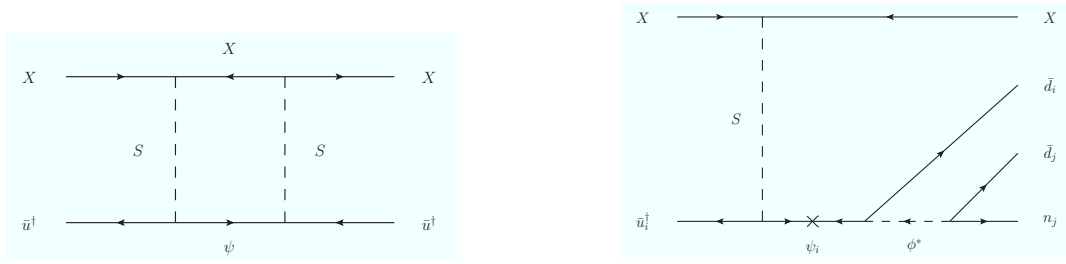
Figure 3.13: Feynman diagrams for dark matter scattering off nucleons in direct detection experiments when WIMPs annihilate to quarks: **(left)** standard signal and **(right)** inelastic induced nucleon decay.

<u>WIMP annihilation to leptons</u>: X can elastically scatter off electrons at one loop and nucleons at two loops. However, direct detection experiments are on the verge of testing dark matter models with nucleon scattering at one loop [35, 17, 23, 27] and electron scattering at tree level [36]. Therefore, the elastic scattering signals from our models are too small to be detected at near-future experiments.

As we discussed in Section 3.3.2, there can be lepton-number-preserving dark matter annihilation channels in addition to those responsible for baryogenesis, although the parameter space is more restricted in this case. The lepton-number-preserving WIMP interactions can lead to conventional WIMP signals in direct detection experiments, but do not probe the WIMP's lepton-number-violating couplings, which are the crucial ingredients of WIMPy leptogenesis.

<u>WIMP annihilation to quarks</u>: The dominant contribution to the direct detection cross section is the one-loop scattering of dark matter off the right-handed up quark. We estimate

the dark matter-nucleon cross section:

$$\sigma_{X-N} \sim \frac{1}{16\pi} \left(\frac{\lambda_B^2 \lambda_X^2}{16\pi^2} \right)^2 \frac{\mu^2}{m_X^4},$$
(3.43)

where μ is the reduced mass of the dark matter-nucleon system[9]. In our models, $m_X \gg m_N$, where m_N is the nucleon mass, so $\mu \approx m_N$.

We determine the direct detection cross section for the benchmark points in Section 3.4.2. For the point $m_X = 4.25$ TeV, $m_\psi = 7.25$ TeV, $m_S = 5$ TeV, $\lambda_X = 2.7$ and $\lambda_B = 4.5$, we find $\sigma_{X-N} \approx 1 \times 10^{-44}$ cm^2. For the point $m_X = 0.9$ TeV, $m_\psi = 1.2$ TeV, $m_S = 1.5$ TeV, $\lambda_X = 0.22$ and $\lambda_B = 2.8$, we find $\sigma_{X-N} \approx 4 \times 10^{-46}$ cm^2. The current limits from the XENON100, CDMS experiments [8, 9] on dark matter direct detection have a minimum bound of $\sim 10^{-44}$ cm^2 for WIMPs with masses of ~ 50 GeV. The upper limit on the cross section for a TeV WIMP is $\sim 10^{-43}$ cm^2. We therefore see that the cross sections for our benchmark points are below current bounds but are large enough that they can give a signal in upcoming direct detection experiments such as XENON1T [57]. We leave a detailed study of the direct detection reach for future work.

There also exists an inelastic scattering process that converts an up-type quark to two down-type antiquarks, as we show in the right-hand graph in Figure 3.13. Such an inelastic process can lead to nucleon decays induced by WIMP scattering. The dominant process is $X p \to X n \pi^+$, along with the corresponding processes with strange quark production (b quark production is kinematically suppressed). To avoid conflict with proton decay experiments, the induced proton decay rate should satisfy bounds outlined in [58]. Comparing our

---

[9]Because the masses of all fields running in the loop are similar in mass, there is no significant mass suppression to the cross section from evaluating the loop integral.

model to the Hylogenesis model in [58], we find that the operator giving rise to induced proton decay in our model is dimension-9 ($X^2 \bar{u} d \bar{d} n / \Lambda^5$), whereas the corresponding Hylogenesis operator is dimension-7. At the hadronic level, the Hylogenesis process is $2 \rightarrow 2$, in contrast with our $2 \rightarrow 3$ process, which gives our model a relative phase space suppression $\sim 1/(2\pi)^3$. Furthermore, the Hylogenesis model has a dark matter mass $\sim \mathcal{O}(\text{GeV})$, while the dark matter mass in WIMPy baryogenesis is $m_X \sim \mathcal{O}(\text{TeV})$. As a result, the dark matter number density is smaller by a factor of (GeV/TeV) in WIMPy baryogenesis, and the incident flux of dark matter particles is suppressed. Taking into account all factors, the induced proton decay rate for WIMPy baryogenesis has a $\sim \left(\frac{1}{2\pi}\right)^3 \left(\frac{\text{GeV}}{\text{TeV}}\right)^5 \sim 10^{-17}$ suppression compared to that of Hylogenesis. Since induced proton decay is on the verge of current bounds for Hylogenesis models with a heavy scale $\Lambda \sim \text{TeV}$, the proton lifetime in our model is safely above the current bound, and not within the reach of near-future proton decay experiments.

To summarize, models with WIMP annihilation to leptons typically predict the absence of a signal in conventional dark matter direct detection experiments, while models with WIMP annihilation to quarks have WIMP-nucleon cross sections below the current bounds but accessible in upcoming experiments. Baryon/lepton-number-preserving WIMP interactions can also give a signal in direct detection experiments, but such models have a smaller viable parameter space. WIMP scattering can induce nucleon decay in WIMPy baryogenesis models, but the proton decay rate is far lower than current experimental constraints.

Indirect Detection

Models of WIMPy baryogenesis have indirect detection prospects similar to those in conventional WIMP scenarios because the dark matter relic abundance is symmetric and is

established by thermal freeze-out. This is in contrast with many asymmetric dark matter models, which typically have suppressed indirect detection signals due to the fact that dark matter is largely asymmetric today. The only asymmetric dark matter models with indirect detection signals are those in which the symmetric component is regenerated after WIMP freeze-out [38]. In the following summary, we assume that WIMPs annihilate predominantly through the interactions that generate the baryon asymmetry.

We find that indirect detection is most promising with WIMPy baryogenesis with dark matter annihilating to quarks. In this scenario, the final states are color-connected quarks and sterile fields n_i, and the quarks hadronize in the dark matter rest frame. This populates the low-energy anti-deuteron spectrum, leading to a clean, low-background signal at GAPS and AMS-02. The mass reach in this scenario is $m_X \lesssim 1$ TeV. Annihilation of dark matter in WIMPy leptogenesis also leads to $q\bar{q}$ production via Higgs decay, but the quarks hadronize in the Higgs rest frame. Fewer low-energy antideuterons are produced, and the mass reach is only $m_X \lesssim 200$ GeV, which is too low for viable models of WIMPy leptogenesis. We give more details below.

WIMP annihilation to leptons: The indirect detection signals are energetic neutrinos, positrons, and secondary photons from the leptons produced in WIMP annihilations, along with antiprotons and antideuterons ($\bar{D}$) from $\psi^0 \to h + n \to b\bar{b} + n$. Unfortunately, the dark matter mass of $\mathcal{O}(\text{TeV})$ in leptogenesis gives a flux lower than the sensitivities of most upcoming indirect direction experiments. With the standard cross section for thermal WIMP annihilation ($\langle \sigma_{\text{ann}} \rangle \approx 3 \times 10^{-26}$ cm^3/s), the reach of most current experiments like Fermi-LAT [59] is in the mass range $\lesssim \mathcal{O}(100 \text{ GeV})$. One exception is in the scenario with a very steep

dark matter profile in the galactic center, which occurs in halo models favored by hydro-dynamical simulations. In this case, HESS measurements of gamma rays from the galactic center are within a factor of two of constraining a 3 TeV WIMP with standard annihilation cross section to leptonic final states [60]. Based on the HESS analysis, it is likely that with more data Fermi-LAT could rule out WIMPy leptogenesis models with masses $\lesssim$ few TeV if the similar assumptions on dark matter distribution are applied. Such constraints suffer from large uncertainties in the dark matter profile, however, and we caution that such strong limits on WIMP masses may not be possible.

According to the general analysis performed in [61], the mass reach of low energy an-tideuteron detection experiments at AMS-02 and GAPS could be up to ~ 1TeV if hadroniza-tion happens mostly in the rest frame of dark matter annihilation, as occurs in the gg channel in [61]. However, hadronic decay products in the leptogenesis scenario are secondary or ter-tiary, and hadronization typically happens in the boosted frame, similar to the WW channel in the same reference. The resulting mass reach could be only ~ 200 GeV, which is too low for WIMPy leptogenesis because sphalerons are decoupled during the era of asymmetry generation for dark matter masses in this range.

WIMP annihilation to quarks: The possible signals are $\bar{p}$, $\bar{D}$, and γ. In contrast with lep-togenesis, the baryon asymmetry can be generated after the electroweak phase transition and the dark matter mass can be as low as ~ 290 GeV according to the bound in Section 3.5.2. This is promising for detection at upcoming experiments, particularly low energy anti-deuteron searches. Because the primary products of WIMP annihilation now involve color-connected u and ψ, a large proportion of hadronization proceeds in the rest frame,

resulting in a larger rate of $\bar{D}$ production [61]. This extends the mass reach at GAPS and AMS-02 [62] to ~ 1 TeV and covers a large part of the WIMPy baryogenesis parameter space. Higher WIMP mass regions ($\sim$ TeV) may be constrained by Fermi-LAT gamma ray observations of the galactic center, but as discussed above with WIMPy leptogenesis, these constraints are highly dependent on the dark matter profile [60].

In general, models of WIMPy baryogenesis and leptogenesis satisfy all current constraints from indirect detection experiments, and future searches for antideuterons are promising discovery channels for models with WIMP annihilation to quarks.

3.5.2   Collider Detection

We consider the LHC constraints and detection prospects for new charged particles predicted in WIMPy baryogenesis. We find that the LHC can strongly constrain the scenario with WIMP annihilation to quarks but may not constrain WIMP annihilation to leptons. Searches for supersymmetry (SUSY) with missing energy are relevant to our models, since WIMPy baryogenesis predicts new charged fields decaying to Standard Model particles and neutral fermions. We focus on existing LHC searches for SUSY and leave for later work the optimization of collider searches for the particular charged fields found in our models.

The strongest LHC constraints are bounds on new colored fields, such as gluinos and squarks. Current searches at the LHC therefore constrain the scenario with WIMP annihilation to quarks, which has new colored fields ψ. The luminosity at the LHC is not yet large enough to bound electroweak production of new particles, due to the smaller production cross section, and softer jets and missing energy. As a result, current collider constraints on
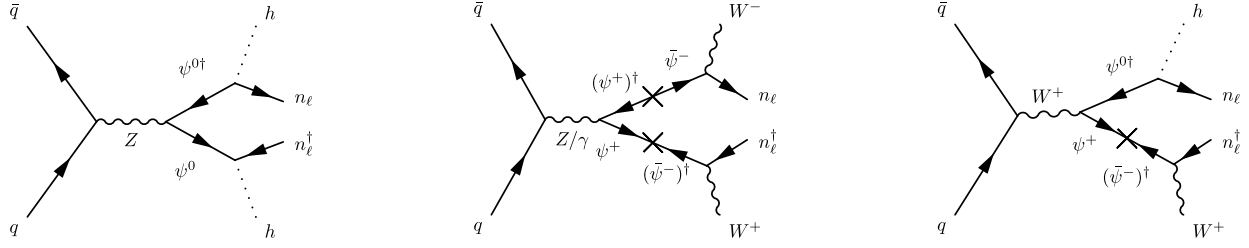
Figure 3.14: LHC electroweak pair production of ψ and its subsequent decay in the model with WIMP annihilation to leptons. ψ^0 decays to a Higgs boson and the light neutral fermion n_ℓ, while $\psi^\pm$ decays to $W^\pm$ and n_ℓ.

m_ψ in the scenario with dark matter annihilation to leptons are well below the range needed for viable WIMPy leptogenesis. Higher luminosity and new targeted searches can improve the LHC reach for m_ψ depending on its decay modes.

We now consider each scenario in more detail.

WIMP annihilation to leptons: A characteristic feature of the WIMPy leptogenesis model in section 3.3 is the presence of an exotic vectorlike $\mathrm{SU(2)_L}$ doublet ψ. The neutral and charged components of ψ can be pair-produced via electroweak gauge bosons. According to our arguments in Section 3.3.1, ψ decays promptly.

The dominant decay of ψ^0 is to Higgs $+ n_\ell$ through the interactions in (3.18), where n_ℓ is the light neutral mass eigenstate after Higgs-induced mixing between ψ and n. The resulting collider signature for pair production is $\psi^0\psi^0 \to 4b(4j) + \not{E}_\mathrm{T}$. The charged component, $\psi^\pm$, decays to $W^\pm + n_\ell$, with a collider signature for pair production of $\psi^+\psi^- \to W^+W^- + \not{E}_\mathrm{T}$. The relevant diagrams are shown in Figure 3.14.

Searches at LEP constrain the masses of the charged and neutral components of ψ with bounds on pair production of charginos ($\tilde{\chi}^\pm \to W^\pm \tilde{\chi}^0$), $m_{\chi^\pm} \gtrsim 100$ GeV [63]. $\psi^\pm$ decays look

identical to chargino decays, so $m_{\psi\pm} \gtrsim 100$ GeV as well. Hadronic chargino decays, which have a $4j + \not{E}_T$ final state, constrain the ψ^0 mass. The LEP bound groups hadronic chargino decays with other decay modes, so the bound is not directly applicable to ψ^0. A more careful analysis (that we leave for future work) is needed to determine the precise bound on ψ^0, but we expect it to be on the order of 100 GeV as well. The bounds on both $\psi^\pm$ and ψ^0 are well below the typical m_ψ required for WIMPy leptogenesis.

With the current luminosity of 5 fb^{-1} at $\sqrt{s} = 7$ TeV, the LHC bounds the masses of weakly charged particles appearing in cascade decays of colored particles, but does not constrain particles such as ψ that are only produced directly from electroweak gauge bosons. Therefore, the LHC does not bound m_ψ at present, and the LEP constraint remains the most important. Searches for direct chargino and slepton production with future LHC data will improve the bounds on m_ψ to masses on the order of a few hundred GeV, but this is still smaller than m_ψ needed in WIMPy leptogenesis.

New LHC searches at 14 TeV could possibly yield stronger constraints. For example, If the Higgs mass is known, we could require a reconstruction of the Higgs mass among final state jet pairs, greatly reducing backgrounds. If $m_\psi \gg m_h$, the final state Higgses are boosted and can be studied with jet substructure techniques, as suggested in [64].

In summary, the collider constraints on ψ are currently too weak to place any bounds on WIMPy leptogenesis models. Future LHC running will improve the bounds on m_ψ, and we have outlined some of the possible signals here. A more detailed collider analysis is deferred to later work.

WIMP annihilation to quarks: As with WIMP annihilation to leptons, there are new charged
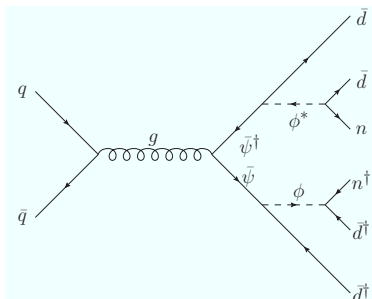
Figure 3.15: LHC pair production of $\bar{\psi}$ and its subsequent decay in the model with WIMP annihilation to quarks.

states at the weak scale. In this model, ψ carries color charge, and the bounds are consequently much stronger than for WIMPy leptogenesis: $m_\psi \gtrsim 590$ GeV as inferred from the current LHC gluino search at 7 TeV. The phenomenology depends on how ψ decays, and we outlined two possible models in (3.39) and (3.40). In both, ψ decays to two jets plus a singlet, and so the collider phenomenology is identical. For the purposes of notation in this section, we assume that ψ decays through an intermediate colored scalar ϕ to 2 Standard Model quarks and a singlet fermion, n.

ψ can be pair-produced at the LHC with the signature $pp \to \psi\bar{\psi} \to 4j + \not{E}_\mathrm{T}$. We show the relevant diagram in Figure 3.15.

Gluino searches at LHC7 bound the ψ mass. Both gluinos and ψ decay to $jj + \not{E}_\mathrm{T}$, and the bounds on both gluinos and ψ are comparable, as their cross sections differ only by a group theory factor. We correct the gluino bounds for this factor. We apply simplified model searches from ATLAS, which place bounds on gluino and squark masses in the presence of a massless neutralino [65]. The corresponding fields in WIMPy baryogenesis are ψ, the colored scalar ϕ, and the massless singlet fermion n. The lower bound on the ψ mass is $m_\psi \gtrsim 590$ GeV, which comes from the gluino bound when the squark is much heavier than the gluino.

In our scenario, this means that $m_\psi \gtrsim 590$ GeV when $m_\phi \gg m_\psi$ (numerically, $m_\phi \gtrsim 1.2$ TeV). The bounds on m_ψ cut significantly into the allowed parameter space for dark matter because $2m_X > m_\psi$, and so $m_X \gtrsim 295$ GeV for heavy ϕ. The bounds are stronger for lighter ϕ because ϕ and ψ can be jointly produced. For example, the bound on m_ψ is about 30% higher for $m_\phi = 1$ TeV.

The LHC search reach for gluinos is expected to be $m_{\tilde{g}} \approx 1.44$ TeV at 100 fb^{-1} and $\sqrt{s} = 14$ TeV [66] (with the assumptions of mSUGRA and heavy squarks), so models of WIMPy baryogenesis will be strongly constrained by future running of the LHC. The LHC will not reach the highest-mass regions of WIMPy baryogenesis, but will exclude models with masses $m_\psi \lesssim 2$ TeV, $m_X \lesssim 1$ TeV, and $\mathcal{O}(1)$ couplings.

LHC searches also constrain the mass of the colored scalar ϕ. Since m_ϕ is not directly relevant to the outcome of WIMPy baryogenesis (apart from the requirement that it be light enough for ψ decays to be in thermal equilibrium), bounds on m_ϕ do not directly constrain WIMPy baryogenesis. Nevertheless, the production rate of ϕ is comparable to that of squarks and is very high at the LHC. With the interaction (3.39), ϕ decays to $d_i + \not{E}_{\mathrm{T}}$ and has an event topology identical to squark pair production in the MSSM: two jets (possibly b-tagged) plus missing energy. The current model-independent constraint is $m_\phi \gtrsim 875$ GeV for degenerate squarks of the first two generations [65]. In WIMPy baryogenesis, however, only a single field ϕ is necessary, so the bound can be relaxed. Since ϕ can decay into b, the bound is approximately that of a sbottom squark from DØ, $m_{\tilde{b}} > 250$ GeV [67]. Future LHC running at 14 TeV will improve the bound to ~ 2 TeV at 100 fb^{-1} [66], and has the potential to discover colored scalars in the mass range of WIMPy baryogenesis.
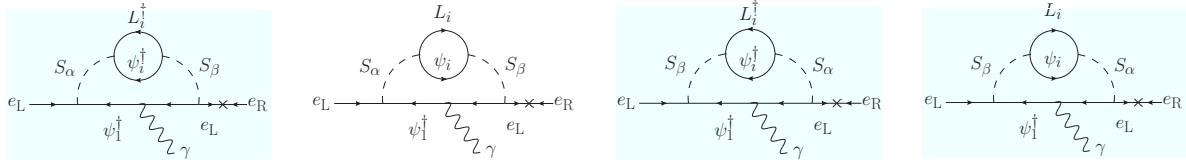
Figure 3.16: A set of two-loop contributions to the electron EDM that vanishes when summed together.

3.5.3 Electric Dipole Moment Constraints

A viable mechanism for baryogenesis necessitates the existence of new CP phases. Bounds on the electron and neutron electric dipole moments (EDMs) strongly constrain many new sources of CP-violation, but we find CP phases in WIMPy baryogenesis are not constrained by EDM experiments. The minimal models of WIMPy baryogenesis presented in this Chapter couple new fields to *either* left-handed or right-handed light fermions (but not both), resulting in suppressed EDMs that are consistent with current observations. As a result, minimal models of WIMPy baryogenesis do not have the CP problem often associated with models of weak-scale physics.

In the models presented in Sections 3.3 and 3.4, the fields S and ψ couple exclusively to either left-handed or right-handed quarks and leptons. As a result, loops contributing to light fermion EDMs are helicity-preserving with an even number of Yukawa couplings, half of which are of the form $\lambda_{\alpha i}$ and the other half $\lambda^*_{\beta j}$. By summing over all permutations of different flavors of S, L and ψ on the internal lines, it can be shown that all one- and two-loop diagrams appear in pairs that are complex conjugates of one another. Summing over each set of pairs leads to a result that is real, and hence a vanishing EDM. As an example, we show in Figure 3.16 a set of four diagrams contributing to the electron EDM: the sum of the first two is proportional to $\lambda_{L\alpha 1}\lambda^*_{L\beta 1}$, while the sum of the second two is proportional

to $\lambda_{L\,\alpha1}^{*}\lambda_{L\,\beta1}$. Therefore, the sum of all four is real and does not contribute to the electron EDM.

The two-loop EDM in the Standard Model vanishes for the same reason as in WIMPy baryogenesis: CP-violation arises only in couplings to one chirality of fermion. In both the Standard Model and WIMPy baryogenesis, the neutron EDM is non-zero at three loops, and we show the relevant diagrams in Figure 3.17. The principal difference between the two is that CP violation vanishes in the Standard Model with fewer than three generations, so the Standard Model EDM is suppressed by mixings involving all three generations. By contrast, WIMPy baryogenesis has a contribution to the EDM with only two generations of quarks that couple to more than one flavor of S, and if the model is minimally flavor violating, the EDM will be suppressed by $\sin^2\theta_{\rm c} \approx 0.05$, the square of the Cabibbo angle. The naïve estimate for the neutron EDM in WIMPy baryogenesis with $\mathcal{O}(1)$ couplings is

$$\frac{d_n}{e} \sim \frac{\sin^2\theta_{\rm c}}{(16\pi^2)^3}\frac{m_u}{m_S^2}. \tag{3.44}$$

Substituting $m_S \sim 5$ TeV and $m_f \sim$ MeV gives $d_n/e \lesssim 5\times 10^{-32}$ cm, which is well below the current experimental bound of $d_n/e < 2.9\times 10^{-26}$ cm [68]. The electron EDM from WIMPy leptogenesis is even smaller than this, as flavor-changing effects in the charged lepton sector are suppressed by neutrino masses, and the EDM is also well below the experimental bound of $d_e/e < 1.05 \times 10^{-27}$ cm [69].

Phases from WIMPy leptogenesis can also contribute to EDMs via other new, weak-scale fields not included in our minimal models. Since these contributions are model-dependent, we do not consider them further.

Minimal models of WIMPy baryogenesis do not suffer from a CP problem and are con-
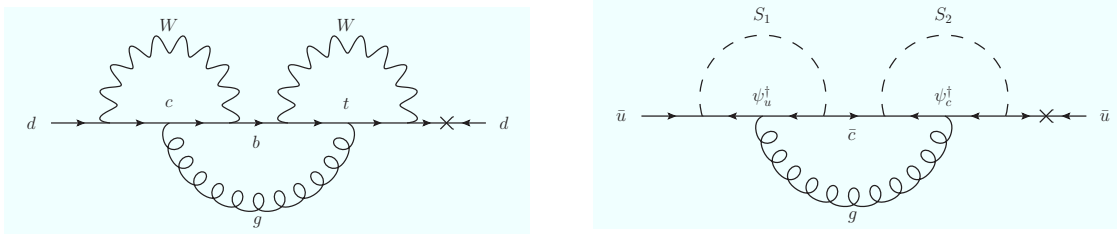
Figure 3.17: **(left)** Three loop EDM in the Standard Model. **(right)** The analogous diagram for quark EDMs in WIMPy baryogenesis. The photon line attaches to any charged internal fields.

sistent with low-energy experiments, but it is possible that other, model-dependent contributions to the EDM could be constrained by and give rise to signals in electron and neutron EDM experiments.

3.6 Conclusions

In this Chapter, we explored a novel scenario called WIMPy baryogenesis that extends the WIMP miracle by generating the observed baryon asymmetry through annihilations of weak-scale dark matter and provides a dynamical connection between the dark matter and baryon abundances. We found that natural couplings and weak-scale masses for the new fields can lead to the correct baryon asymmetry. As a by-product of linking baryogenesis with dark matter annihilation, we introduced a new mechanism for weak-scale baryogenesis, avoiding any conflicts with reheat bounds in supersymmetric theories.

The key observation is that, if dark matter annihilation proceeds via $CP-$ and (Standard Model) $B-$ or $L-$violating operators, all Sakharov conditions for baryogenesis are satisfied. Successful models also suppress washout prior to dark matter freeze-out. In our models, such suppression results from the heaviness of the field ψ carrying Standard Model gauge charges

and $B-$ or $L-$number that is one of the final states in dark matter annihilation. Additional discrete symmetries forbid such exotic fields from decaying back to Standard Model fields. We presented models where dark matter annihilates to either quarks or leptons, and found viable parameter spaces with natural couplings and TeV-scale masses in both scenarios.

In models where dark matter annihilates to leptons, the lepton asymmetry must be generated before the electroweak phase transition so that the asymmetry can be transferred to baryons via sphalerons. As a result, dark matter and ψ masses must be $\mathcal{O}(\text{TeV})$. Because the new states are heavy and dark matter does not couple directly to quarks, dark matter in this set-up is not in reach of near-future direct and indirect detection experiments. In this scenario, ψ is charged only under weak interactions, making LHC searches challenging, although targeted searches at high integrated luminosity may allow discovery.

If dark matter annihilates to quarks, baryogenesis can occur after the electroweak phase transition, allowing smaller dark matter and ψ masses. With lighter new states and colored objects, dark matter in these models can be within reach of direct detection experiments and indirect detection searches for antideuterons. LHC searches for ψ are similar to gluino searches and can exclude $m_\psi \lesssim 1.44$ TeV at 100 fb^{-1} and $\sqrt{s} = 14$ TeV.

In both scenarios, WIMPy baryogenesis models can generate both the correct dark matter relic density and the baryon asymmetry at the weak scale. Such models predict new weak-scale particles that can lead to signals in dark matter direct and indirect detection experiments, and that may be accessible at the LHC.

Appendix A

Two Higgs model vacua

A.1 Vacua and stability

The vacua of the potential can be determined by finding the extrema of the potential. Here, we follow the analysis of [30]. We perform the analysis at finite temperature and then discuss the particular case of the zero temperature vacua.

Extremizing the potential gives

$$\langle h \rangle = 0, \quad \frac{1}{2}\sqrt{\frac{4\mu_1^2 - 2k_3\langle\phi\rangle^2 - \alpha_1 T^2}{k_1}}, \tag{A.1}$$

$$\langle \phi \rangle = 0, \quad \frac{1}{2}\sqrt{\frac{4\mu_2^2 - 2k_3\langle h\rangle^2 - \alpha_2 T^2}{k_2}}. \tag{A.2}$$

At a given temperature, there are four distinct critical points of the potential:

1.

$$\langle h \rangle = \langle \phi \rangle = 0, \tag{A.3}$$

2.

$$\langle h \rangle = 0, \ \ \langle \phi \rangle = \frac{1}{2}\sqrt{\frac{4\mu_2^2 - \alpha_2 T^2}{k_2}}, \tag{A.4}$$

3.

$$\langle \phi \rangle = 0, \ \ \langle h \rangle = \frac{1}{2}\sqrt{\frac{4\mu_1^2 - \alpha_1 T^2}{k_1}}, \tag{A.5}$$

4.

$$\langle h \rangle = \sqrt{\frac{8k_2\mu_1^2 - 4k_3\mu_2^2 + (\alpha_2 k_3 - 2\alpha_1 k_2)T^2}{8k_1 k_2 - 2k_3^2}}, \tag{A.6}$$

$$\langle \phi \rangle = \sqrt{\frac{8k_1\mu_2^2 - 4k_3\mu_1^2 + (\alpha_1 k_3 - 2\alpha_2 k_1)T^2}{8k_1 k_2 - 2k_3^2}}. \tag{A.7}$$

For extrema 2 and 3, the vacuum is only well-defined if

$$T^2 < T_{\text{c}i}^2 \equiv \frac{4\mu_i^2}{\alpha_i}. \tag{A.8}$$

These temperatures are sufficiently important that we label them *critical temperatures* and they indicate the point at which the fields h and ϕ can condense.

We now examine the stability of the extrema of the potential.

1. The symmetric vacuum is only stable for $T^2 > \max(T_{\text{c}1}^2, T_{\text{c}2}^2)$. Below these temperatures, the negative mass-squared parameter in the Lagrangian dominates and tends to drive the fields to non-zero values. At high temperature, the scalars begin in the symmetric phase and later condense when T passes below one of the threshold temperatures.

2. The vacuum where $\langle h \rangle = 0$ and $\langle \phi \rangle \neq 0$ is stable given $T < T_{\text{c}2}$ and $k_3\alpha_2(T_{\text{c}2}^2 - T^2) >$

$2k_2\alpha_1(T_{c1}^2 - T^2)$. For $T_{c2} > T > T_{c1}$, this condition is automatically satisfied. If $T < T_{c1}$ and T_{c2}, then the vacuum is only stable down to the temperature

$$T_0^2 = \frac{4(2k_2\mu_1^2 - k_3\mu_2^2)}{k_2\alpha_1 - k_3\alpha_2}, \tag{A.9}$$

at which point this extremum becomes a saddle point.

3. The vacuum where $\langle\phi\rangle = 0$ and $\langle h\rangle \neq 0$ is exactly the same as the one in vacuum #2, except with indices $1 \leftrightarrow 2$.

4. Finally, the conditions for a stable vacuum at both h and ϕ non-zero are

$$2k_2\alpha_1(T_{c1}^2 - T^2) - k_3\alpha_2(T_{c2}^2 - T^2) > 0, \tag{A.10}$$

$$2k_1\alpha_2(T_{c2}^2 - T^2) - k_3\alpha_1(T_{c1}^2 - T^2) > 0, \tag{A.11}$$

$$4k_1k_2 - k_3^2 > 0. \tag{A.12}$$

It is not immediately apparent whether this is stable or not, but we demonstrate below out that for all parameters of interest to us (namely those that give a two stage phase transition), the conditions are be violated and this is be a saddle point.

Because extremum # 4 is a saddle point, there is only one non-zero VEV in any vacuum. This gives us two options: the first is that the field that initially condenses is also the field with a VEV at zero temperature (we want this to be h) and hence there is only a one stage phase transition. The other possibility is that the initial field to condense (ϕ) has a higher zero-temperature energy when condensed than the vacuum with non-zero h, and so at late times there is a phase transition where the ϕ VEV shuts off and the h VEV is turned on.

Because there is a classical energy barrier between these two minima of the potential, this generally leads to a first-order phase transition (see Appendix B).

A.1.1   Parameter constraints

In this section, we determine the parameters that lead to a viable two stage phase transition. We begin by matching the parameters onto the known zero temperature physics. In particular, we would like $\langle \phi \rangle = 0$ and $\langle h \rangle = v$ at zero temperature, where $v = 246$ GeV. To ensure that h condenses instead of ϕ, we require the vacuum energy in the state where h is condensed to have a lower energy than the state where ϕ is condensed. The vacuum energy in the $\langle \phi \rangle = 0$ vacuum at zero temperature is

$$V_1(T = 0) = -\frac{\mu_1^4}{k_1} \tag{A.13}$$

and similarly for the $\langle h \rangle = 0$ vacuum energy V_2. For the former to be lower, we require $|V_1(T = 0)| > |V_2(T = 0)|$ or, alternately,

$$\frac{\mu_1^4}{\mu_2^4} > \frac{k_1}{k_2}. \tag{A.14}$$

Imposing this constraint, and therefore being in the $\langle \phi \rangle = 0$ vacuum at zero temperature, we can determine the physical Higgs mass from the quadratic term,

$$m_h^2 = 8\mu_1^2. \tag{A.15}$$

The zero temperature Higgs mass has not yet been determined, but electroweak fits prefer a value as close as possible to the LEP bound of 115 GeV, so we choose $m_H = 120$ GeV. We can then determine the parameters μ_1 and k_1 using

$$\mu_1 = \frac{m_h}{\sqrt{8}} \approx 42.4 \text{ GeV}, \tag{A.16}$$

$$k_1 = \frac{1}{8}\left(\frac{m_h}{v}\right)^2 \approx 0.0297. \tag{A.17}$$

Meanwhile, ϕ gets a mass due to the $\phi^2 h^2$ term, and its value is

$$m_\phi^2 = 2\mu_1^2 \frac{k_3}{k_1} - 4\mu_2^2. \tag{A.18}$$

This gives us our second constraint,

$$k_3 > \frac{2\mu_2^2}{\mu_1^2} k_1, \tag{A.19}$$

which requires that the mixed quartic term be large enough to compensate for the negative ϕ mass-squared term. If (A.19) is not satisfied, then ϕ is also driven to a non-zero value (vacuum #4 above).

In order to have a two stage phase transition, we would like the system to first condense in the ϕ direction. This imposes the requirement that $T_{c1} < T_{c2}$, which can be expressed as

$$\frac{\mu_1^2}{\mu_2^2} < \frac{\alpha_1}{\alpha_2}; \tag{A.20}$$

combining this with (A.14) gives

$$\sqrt{\frac{k_1}{k_2}} < \frac{\mu_1^2}{\mu_2^2} < \frac{\alpha_1}{\alpha_2}. \tag{A.21}$$

Thus, we see that the mass terms are constrained to be roughly close in magnitude to one another in order to have a two stage phase transition.

Appendix B

The two Higgs phase transition and bubble nucleation

B.1 Tunneling and bubble nucleation

There exists a potential barrier between the true and false vacua in our two Higgs model. The vacua become degenerate at the temperature

$$T_{\mathrm{d}}^2 = \frac{4\left(\sqrt{k_2}\mu_1^2 - \sqrt{k_1}\mu_2^2\right)}{\sqrt{k_2}\alpha_1 - \sqrt{k_1}\alpha_2}. \tag{B.1}$$

Below this temperature, the system can transition from the false vacuum to the true vacuum. The phase transition between the two vacua, should it occur, satisfies the following conditions:

1. It occurs at the very latest before big bang nucleosynthesis ($T \gg 10$ MeV) to satisfy observational constraints.

2. The ϕ VEV must turn off sufficiently rapidly that the asymmetry relation from mass mixing is not disturbed. This means either that the fields directly tunnel into the $\phi = 0$ vacuum, or in the case where the system tunnels to a non-zero ϕ vev, that ϕ is rapidly damped to zero (on a time shorter than the rate of asymmetry transfer) following tunneling.

3. The expansion of the bubble wall should be faster than the asymmetry transfer rate from thermal scattering.

To begin, we calculate the temperature at which bubble nucleation occurs. At large temperature, when the bubble wall $r_{\mathrm{w}} \gg \beta$, we can take the bubble solution to be constant in the period Euclidean time, τ. The bounce solution is then given by the O(3) symmetric function minimizing the Euclidean action

$$S(T, \phi, h) = \frac{4\pi}{T} \int dr \, r^2 \left[\frac{1}{2} \left(\frac{d\phi}{dr} \right)^2 + \frac{1}{2} \left(\frac{dh}{dr} \right)^2 + V(\phi, h, T) \right]. \tag{B.2}$$

The semi-classical probability P of nucleating a bubble inside of a casual volume during the temperature interval dT is [?]

$$P \approx 16 \, \omega \, \xi^4 \frac{M_{\mathrm{Pl}}^4}{T^5} \, e^{-S(T)} \, \Delta T, \tag{B.3}$$

where ω is a dimensionless coefficient given by functional determinants from the path integral and $\xi \approx 1/34$ is a numerical factor coming from the Hubble constant. The result is dominated by the action S in the exponential, making the precise value of ω irrelevant. Taking $\omega \sim 1$, $T \sim 30$ GeV and $\Delta T \sim 10$ GeV (for reasons that will be shown later), we find that $S \approx 140$ gives a probability of nucleation equal to one. We take this as our benchmark for determining

when nucleation occurs.

It is difficult to find the bounce solution to (B.2) numerically since there are two fields involved. Because we are simply interested in an estimate of the action, we instead make an ansatz that eliminates one of the fields. We take $h = f(\phi)$, with f to be determined from $V(\phi, h)$, giving

$$S(T, \phi) = \frac{4\pi}{T} \int dr\, r^2 \left[\frac{1}{2} \left(1 + f'(\phi)^2 \right) \left(\frac{d\phi}{dr} \right)^2 + V(\phi, T) \right]. \tag{B.4}$$

The resulting equation of motion is

$$\frac{d^2\phi}{dr^2} + \frac{2}{r} \frac{d\phi}{dr} = \frac{1}{1 + f'(\phi)^2} \left[\frac{\partial V}{\partial \phi} - \left(\frac{d\phi}{dr} \right)^2 f'(\phi) f''(\phi) \right]. \tag{B.5}$$

The initial condition $\phi(0)$ is chosen to satisfy the bounce boundary conditions $\phi'(0) = 0$ and $\phi(\infty) = \phi_{\text{false}}$. This equation can be solved numerically using the "overshoot-undershoot" method [**?**].

The ansatz $h = f(\phi)$ is chosen as the curve in $\phi - h$ space such that the smallest possible potential barrier is crossed while tunneling. We determine this curve by slicing the potential along lines of constant ϕ and determining the value of h that minimizes V. While we cannot guarantee that this is the minimum action, it is plausible that it is among the curves that gives the smallest action, and it gives an upper bound on the action. If we find rapid bubble nucleation from our ansatz, then bubble nucleation *does* occur, even if the exact instanton configuration is slightly different from the one determined here.

Bubble nucleation does not occur for all choices of parameters; for a particular choice of k_3, k_2 must be chosen sufficiently large to reduce the barrier between vacua. Numerical

solutions are presented in Section 2.2.4.

To address point #2 above, we find that tunneling does not, in fact, take ϕ to zero but instead to some non-zero value. ϕ then undergoes damped oscillations about its minimum, $\phi = 0$. The damping due to the Hubble constant, $H \sim 10^{-13}$ GeV, is negligible. The dominant source of damping is decays of $\phi \to X + L$ and the conjugate process. These decays do not change the asymmetry in the X or L sectors, since it is CP-conserving. We require that $\Gamma_\phi \gg \Gamma_{L \to X}$ to avoid eliminating the asymmetry in X by the residual mass mixing due to non-zero ϕ. We can estimate Γ_ϕ by

$$\Gamma_\phi \sim \frac{y_X^2}{4\pi} m_\phi \sqrt{1 - \frac{m_X^2}{m_\phi^2}}. \tag{B.6}$$

The asymmetry washout term is 2.7, with Γ_0 given by the larger of

$$\Gamma_X \ \sim \ \frac{y_X^4}{8\pi^3} \frac{m_X^2}{m_\phi^4} T^3, \tag{B.7}$$

$$\Gamma_L \ \sim \ \frac{g_{\rm w}^4}{8\pi^3} T. \tag{B.8}$$

The first interaction comes from $XX \to LL$ through an intermediate ϕ, while the second is L^0 interacting with W bosons, whose mass is given dominantly by the h VEV. For a benchmark point with $y_X = 1$, $m_X = 400$ GeV, $m_\phi = 450$ GeV and $T_{\rm N} = 60$ GeV (as is a typical scale for bubble nucleation), we get $\Gamma_\phi = 16$ GeV while $\Gamma_0 \approx \Gamma_L = 7.6 \times 10^{-2}$ GeV. Thus, the VEV of ϕ safely damps away before the asymmetry relation from mass mixing is altered.

Finally, the bubble wall must sweep over a particle without it undergoing any thermal interactions. There is approximately one particle in a region with length $1/T$. The bubble

wall takes a time $t_{\mathrm{w}} = (2\delta r + 1/T)/v_{\mathrm{w}}$ to pass over the cube, where δr is the bubble wall thickness and v_{w} is the velocity. This time must satisfy $t_{\mathrm{w}} \ll 1/\Gamma_{L \to X}$. We find that the wall thickness is always $\lesssim 1 \text{ GeV}^{-1}$. Using the rates of interaction in the false vacuum phase and assuming a small mixing angle, we determine that $v_{\mathrm{w}} > 10^{-3}$ for the bubble wall passage to be out of equilibrium. This is easily satisfied for variants of the Standard Model with a first-order phase transition (the drag from top quarks in that case is similar to the drag for this bubble wall) [?]. Therefore, the transition is strongly first-order and our instantaneous approximation for the state projection is valid.

For GeV-scale dark matter, where the mixing angle is large, there is no thermal suppression of any of the modes ($n_{\bar{X}'} = n_{L'}$) and neither the number densities nor the asymmetries change during the phase transition.

B.2   Back-reaction on phase transition

So far, we have neglected the back-reaction of the mass terms on the evolution of the bubble expansion at the first-order phase transition. In the limit of $T_{\mathrm{t}} \ll M$, the dark matter energy density present after the phase transition is entirely given by the repopulation of the heavy states due to the mass mixing. We must also concern ourselves with the "drag" associated with the top quarks becoming massive at the phase transition.

The energy density of the light mass eigenstates that become heavy X fields following the phase transition is given by

$$\rho_X = m_X \sin^2 \theta n_{L'} = \frac{2}{\pi^2} \sin^2 \theta m_X T_{\mathrm{N}}^3, \tag{B.9}$$

while the mass energy density of the top quarks following the phase transition is

$$\rho_t = m_t n_t = \frac{12}{\pi^2} \left(\frac{v_h(T_{\rm N})}{246 \text{ GeV}} \right) m_t T_{\rm N}^3. \tag{B.10}$$

The contribution from top quarks dominates over the contribution from X even for the largest viable masses for our model $m_X \sim 500$ GeV, since there are six top quark degrees of freedom, giving an "effective" top quark mass of $6m_t \sim$ TeV.

At high temperature, the quarks have a large kinetic energy and this can be used to offset the vacuum energy expended to impart mass to the quarks. The energy density from the kinetic energy of the quarks (using $\langle p \rangle \approx 3T$) is

$$\rho_{\rm k} = \frac{36}{\pi^2} T_{\rm N}^4, \tag{B.11}$$

and so for $T_{\rm t} > 50$ GeV, we find that the mass of the top quarks can be accounted for entirely from the kinetic energy and so this does not affect the progress of the phase transition.

In the region 30 GeV $< T_{\rm t} <$ 50 GeV, the situation is slightly more subtle. The energy density that goes into creating masses for the top quarks is comparable to the energy difference between the vacua immediately after $T_{\rm t}$. We must therefore not use $T_{\rm t}$ as the tunneling temperature and use instead the temperature at which the energy difference between the vacua is equal to the energy density from top quark masses. For a benchmark point with $y_X = 0.4$, $k_2 = 0.5$, $k_3 = 0.7$ and $\mu_2 = 80$ GeV, we find that $T_{\rm N} = 34$ GeV, whereas the temperature where the energy difference between vacua is ρ_t is $T = 30$ GeV, corresponding to an approximately 10% difference. Similar results are found for nearby benchmark points.

Bubble nucleation rarely occurs below 30 GeV, so we do not consider this range further.

Fortunately, this does not significantly alter our results, since in the mass mixing-dominated limit, the final X density is fixed only by $\tan^2 \theta$, which has only a weak dependence on T. In fact, this gives us slightly more flexibility as the temperature for bubble nucleation can be about 10% lower than before, giving more thermal suppression and a broader range of parameter space where the X density is dominated by mass mixing.

Appendix C

Review of Dirac leptogenesis

We review a mechanism for realistic Dirac leptogenesis [39]. As the universe cools below the temperature $T = M_\psi$, ψ and $\bar\psi$ decay in two ways:

$$\psi \quad \to \quad N^\dagger H_u^\dagger, \tag{C.1}$$

$$\psi \quad \to \quad L\chi; \tag{C.2}$$

$$\bar\psi \quad \to \quad N\, H_u, \tag{C.3}$$

$$\bar\psi \quad \to \quad L^\dagger \chi^\dagger. \tag{C.4}$$

The total decay rates of ψ and $\bar\psi$ are equal, but they can decay with different rates into N and L. This can give rise to an asymmetry of L over $L^\dagger$. Because total lepton number is conserved by these interactions (assuming ψ carries $L = 1$), this asymmetry is equal and opposite to the asymmetry of N over $N^\dagger$. Thus, there is an N asymmetry that is directly correlated with the Standard Model lepton asymmetry (and hence related to the baryon asymmetry by sphaleron processes). N and L ultimately come into equilibrium due to oscillations once

H_u and χ have VEVs (see [32]).

Eventually, N and L come into thermal equilibrium and the lepton asymmetry is destroyed at the time of equilibriation. This must happen after the time of BBN, since strong constraints exist on the Standard Model lepton asymmetry in that era. Fortunately, this equilibriation rate is suppressed by neutrino masses and is not important until $T \sim$ eV. We can see that this is true below M_ψ by integrating out ψ, giving an effective superpotential

$$W_{\text{eff}} \supset \frac{y_L \, y_N}{M_\psi} N H_u L \chi. \tag{C.5}$$

At low temperatures, χ and H_u have weak scale VEVs (which come about due to interactions with the SUSY breaking sector), giving neutrino masses

$$m_\nu \sim \frac{y_L \, y_N \, v \langle \chi \rangle}{M_\psi} < \text{eV}, \tag{C.6}$$

meaning that $y_L \, y_N \sim 0.1-1$ for $M_\psi \sim 10^{15}$ GeV and weak scale $\langle \chi \rangle$, while it is $y_L \, y_N \sim 10^{-5}$ for $M_\psi \sim 10^{10}$ GeV.

Bibliography

[1] G. W. Bennett *et al.* [Muon G-2 Collaboration], Phys. Rev. D **73**, 072003 (2006) [hep-ex/0602035].

[2] T. Aaltonen *et al.* [CDF Collaboration], Phys. Rev. D **83**, 112003 (2011) [arXiv:1101.0034 [hep-ex]]; V. M. Abazov *et al.* [D0 Collaboration], Phys. Rev. D **84**, 112005 (2011) [arXiv:1107.4995 [hep-ex]].

[3] R. Aaij *et al.* [LHCb Collaboration], Phys. Rev. Lett. **108**, 111602 (2012) [arXiv:1112.0938 [hep-ex]].

[4] K. Nakamura *et al.* [Particle Data Group Collaboration], J. Phys. G G **37**, 075021 (2010).

[5] G. Isidori, Y. Nir and G. Perez, Ann. Rev. Nucl. Part. Sci. **60**, 355 (2010) [arXiv:1002.0900 [hep-ph]].

[6] D. Larson, J. Dunkley, G. Hinshaw, E. Komatsu, M. R. Nolta, C. L. Bennett, B. Gold and M. Halpern *et al.*, Astrophys. J. Suppl. **192**, 16 (2011) [arXiv:1001.4635 [astro-ph.CO]].

[7] J. L. Feng, Ann. Rev. Astron. Astrophys. **48**, 495 (2010) [arXiv:1003.0904 [astro-ph.CO]].

[8] E. Aprile *et al.* [XENON100 Collaboration], Phys. Rev. D **84**, 052003 (2011) [arXiv:1103.0303 [hep-ex]].

[9] Z. Ahmed *et al.* [The CDMS-II Collaboration], Science **327**, 1619 (2010) [arXiv:0912.3592 [astro-ph.CO]].

[10] T. Lin, H. -B. Yu and K. M. Zurek, Phys. Rev. D **85**, 063503 (2012) [arXiv:1111.0293 [hep-ph]].

[11] A. Rajaraman, W. Shepherd, T. M. P. Tait and A. M. Wijangco, Phys. Rev. D **84**, 095013 (2011) [arXiv:1108.1196 [hep-ph]]; P. J. Fox, R. Harnik, J. Kopp and Y. Tsai, Phys. Rev. D **85**, 056011 (2012) [arXiv:1109.4398 [hep-ph]].

[12] J. M. Cline, hep-ph/0609145.

[13] S. Davidson and A. Ibarra, Phys. Lett. B **535**, 25 (2002) [hep-ph/0202239].

[14] M. E. Shaposhnikov, JETP Lett. **44**, 465 (1986) [Pisma Zh. Eksp. Teor. Fiz. **44**, 364 (1986)].

[15] A. Pilaftsis, T. E. J. Underwood, Nucl. Phys. **B692**, 303-345 (2004). [arXiv:hep-ph/0309342 [hep-ph]].

[16] S. Nussinov, Phys. Lett. **B165**, 55 (1985).

[17] D. E. Kaplan, M. A. Luty, K. M. Zurek, Phys. Rev. **D79**, 115016 (2009). [arXiv:0901.4117 [hep-ph]].

[18] M. R. Buckley, L. Randall, JHEP **1109**, 009 (2011). [arXiv:1009.0270 [hep-ph]].

[19] A. Falkowski, J. T. Ruderman and T. Volansky, JHEP **1105**, 106 (2011) [arXiv:1101.4936 [hep-ph]].

[20] H. An, S. -L. Chen, R. N. Mohapatra, Y. Zhang, JHEP **1003**, 124 (2010). [arXiv:0911.4463 [hep-ph]]; E. J. Chun, Phys. Rev. **D83**, 053004 (2011). [arXiv:1009.0983 [hep-ph]]; P. -H. Gu, M. Lindner, U. Sarkar and X. Zhang, Phys. Rev. D **83**, 055008 (2011) [arXiv:1009.2690 [hep-ph]]; Z. Kang, J. Li, T. Li, T. Liu, J. Yang, [arXiv:1102.5644 [hep-ph]]; D. E. Kaplan, G. Z. Krnjaic, K. R. Rehermann and C. M. Wells, JCAP **1110**, 011 (2011) [arXiv:1105.2073 [hep-ph]].

[21] R. Allahverdi, B. Dutta, K. Sinha, Phys. Rev. **D83**, 083502 (2011). [arXiv:1011.1286 [hep-ph]];

[22] N. F. Bell, K. Petraki, I. M. Shoemaker and R. R. Volkas, Phys. Rev. D **84**, 123505 (2011) [arXiv:1105.3730 [hep-ph]]; C. Cheung and K. M. Zurek, Phys. Rev. D **84**, 035007 (2011) [arXiv:1105.4612 [hep-ph]].

[**?**] S. Dodelson, L. M. Widrow, Phys. Rev. Lett. **64**, 340-343 (1990). S. M. Barr, R. S. Chivukula, E. Farhi, Phys. Lett. **B241**, 387-391 (1990); S. M. Barr, Phys. Rev. **D44**, 3062-3066 (1991); D. B. Kaplan, Phys. Rev. Lett. **68**, 741-743 (1992); R. Foot, R. R. Volkas, Phys. Rev. **D69**, 123510 (2004). [hep-ph/0402267]; D. Hooper, J. March-Russell, S. M. West, Phys. Lett. **B605**, 228-236 (2005). [hep-ph/0410114]; S. B. Gudnason, C. Kouvaris, F. Sannino, Phys. Rev. **D74**, 095008 (2006). [hep-ph/0608055].

[23] T. Cohen, K. M. Zurek, Phys. Rev. Lett. **104**, 101301 (2010). [arXiv:0909.2035 [hep-ph]].

[24] Y. Cai, M. A. Luty, D. E. Kaplan, [arXiv:0909.5499 [hep-ph]]; P. -H. Gu, Phys. Rev. D **81**, 095002 (2010) [arXiv:1001.1341 [hep-ph]]; T. Cohen, D. J. Phalen, A. Pierce, K. M. Zurek, Phys. Rev. **D82**, 056001 (2010). [arXiv:1005.1655 [hep-ph]]; J. Shelton, K. M. Zurek, Phys. Rev. **D82**, 123512 (2010). [arXiv:1008.1997 [hep-ph]]; H. Davoudiasl, D. E. Morrissey, K. Sigurdson, S. Tulin, Phys. Rev. Lett. **105**, 211304 (2010). [arXiv:1008.2399 [hep-ph]]; N. Haba and S. Matsumoto, Prog. Theor. Phys. **125**, 1311 (2011) [arXiv:1008.2487 [hep-ph]]; M. Blennow, B. Dasgupta, E. Fernandez-Martinez, N. Rius, JHEP **1103**, 014 (2011). [arXiv:1009.3159 [hep-ph]]; L. J. Hall, J. March-Russell, S. M. West, [arXiv:1010.0245 [hep-ph]]; B. Dutta, J. Kumar, Phys. Lett. **B699**, 364-367 (2011). [arXiv:1012.1341 [hep-ph]]; M. T. Frandsen, S. Sarkar and K. Schmidt-Hoberg, Phys. Rev. D **84**, 051703 (2011) [arXiv:1103.4350 [hep-ph]]; J. March-Russell and M. McCullough, JCAP **1203**, 019 (2012) [arXiv:1106.4319 [hep-ph]]; C. Arina and N. Sahu, Nucl. Phys. B **854**, 666 (2012) [arXiv:1108.3967 [hep-ph]].

[25] M. L. Graesser, I. M. Shoemaker and L. Vecchi, JHEP **1110**, 110 (2011) [arXiv:1103.2771 [hep-ph]].

[26] J. McDonald, Phys. Rev. **D83**, 083509 (2011); J. McDonald, Phys. Rev. D **84**, 103514 (2011) [arXiv:1108.4653 [hep-ph]].

[27] Y. Cui, L. Randall, B. Shuve, JHEP **1108**, 073 (2011). [arXiv:1106.4834 [hep-ph]].

[28] Y. Cui, L. Randall and B. Shuve, arXiv:1112.2704 [hep-ph].

[29] S. Weinberg, Phys. Rev. **D9**, 3357-3378 (1974).

[30] D. Land, E. D. Carlson, Phys. Lett. **B292**, 107-112 (1992). [hep-ph/9208227]; A. Ham-

merschmitt, J. Kripfganz, M. G. Schmidt, Z. Phys. **C64**, 105-110 (1994). [hep-ph/9404272].

[31] A. D. Linde, Phys. Lett. **B259**, 38-47 (1991); A. R. Liddle, D. H. Lyth, Phys. Rept. **231**, 1-105 (1993). [astro-ph/9303019]; A. D. Linde, Phys. Rev. **D49**, 748-754 (1994). [astro-ph/9307002]; E. J. Copeland, A. R. Liddle, D. H. Lyth, E. D. Stewart, D. Wands, Phys. Rev. **D49**, 6410-6433 (1994). [astro-ph/9401011]; E. D. Stewart, Phys. Lett. **B345**, 414-415 (1995). [astro-ph/9407040]; L. Randall, M. Soljacic, A. H. Guth, Nucl. Phys. **B472**, 377-408 (1996). [hep-ph/9512439].

[32] A. Manohar, Phys. Lett. **186B**, 370 (1987).

[33] J. A. Harvey, M. S. Turner, Phys. Rev. **D42**, 3344-3349 (1990).

[34] G. Abbiendi *et al.* [OPAL Collaboration], Eur. Phys. J. **C32**, 453-473 (2004). [hep-ex/0309014].

[35] S. A. Raby, G. West, Nucl. Phys. **B292**, 793 (1987).

[36] J. Kopp, V. Niro, T. Schwetz, J. Zupan, Phys. Rev. **D80**, 083502 (2009). [arXiv:0907.3159 [hep-ph]].

[37] S. I. Bityukov, N. V. Krasnikov, Phys. Atom. Nucl. **62**, 1213-1225 (1999). [hep-ph/9712358].

[38] M. R. Buckley and S. Profumo, Phys. Rev. Lett. **108**, 011301 (2012) [arXiv:1109.2164 [hep-ph]]; M. Cirelli, P. Panci, G. Servant and G. Zaharijas, JCAP **1203**, 015 (2012) [arXiv:1110.3809 [hep-ph]]; S. Tulin, H. -B. Yu and K. M. Zurek, arXiv:1202.0283 [hep-ph].

[39] K. Dick, M. Lindner, M. Ratz, D. Wright, Phys. Rev. Lett. **84**, 4039-4042 (2000). [hep-ph/9907562]; H. Murayama, A. Pierce, Phys. Rev. Lett. **89**, 271601 (2002). [hep-ph/0206177].

[40] G. Gelmini, E. Roulet, Rept. Prog. Phys. **58**, 1207-1266 (1995). [hep-ph/9412278].

[41] R. Foot, M. J. Thomson, R. R. Volkas, Phys. Rev. **D53**, 5349-5353 (1996). [hep-ph/9509327].

[42] A. D. Dolgov, F. L. Villante, Nucl. Phys. **B679**, 261-298 (2004). [hep-ph/0308083].

[43] P. Meade, M. Papucci, A. Strumia and T. Volansky, Nucl. Phys. B **831**, 178 (2010) [arXiv:0905.0480 [hep-ph]].

[44] M. Dine, L. Randall, S. D. Thomas, Nucl. Phys. **B458**, 291-326 (1996). [hep-ph/9507453].

[45] E. W. Kolb, M. S. Turner, Front. Phys. **69**, 1-547 (1990).

[46] I. Affleck, M. Dine, Nucl. Phys. **B249**, 361 (1985).

[47] M. Kawasaki, K. Nakayama, Phys. Rev. **D76**, 043502 (2007). [arXiv:0705.0079 [hep-ph]].

[48] J. P. Conlon, F. Quevedo, JCAP **0708**, 019 (2007). [arXiv:0705.3460 [hep-ph]].

[49] B. A. Bassett, S. Tsujikawa, D. Wands, Rev. Mod. Phys. **78**, 537-589 (2006). [astro-ph/0507632].

[50] T. Asaka, T. Yanagida, Phys. Lett. **B494**, 297-301 (2000). [hep-ph/0006211].

[51] M. Y. .Khlopov, A. D. Linde, Phys. Lett. **B138**, 265-268 (1984); J. R. Ellis, J. E. Kim, D. V. Nanopoulos, Phys. Lett. **B145**, 181 (1984); M. Kawasaki, T. Moroi, Prog. Theor. Phys. **93**, 879-900 (1995). [hep-ph/9403364, hep-ph/9403061].

[52] E. W. Kolb, S. Wolfram, Nucl. Phys. **B172**, 224 (1980).

[53] E. Komatsu *et al.* [WMAP Collaboration], Astrophys. J. Suppl. **192**, 18 (2011). [arXiv:1001.4538 [astro-ph.CO]].

[54] L. Bento, Z. Berezhiani, Phys. Rev. Lett. **87**, 231304 (2001). [hep-ph/0107281]; P. - H. Gu, U. Sarkar, Phys. Lett. **B679**, 118-121 (2009). [arXiv:0903.3473 [hep-ph]]; C. R. Das, L. V. Laperashvili, H. B. Nielsen, A. Tureanu, Phys. Lett. **B696**, 138-144 (2011). [arXiv:1010.2744 [hep-ph]].

[55] A. Pukhov, [hep-ph/0412191].

[56] R. N. Mohapatra, J. Phys. G **G36**, 104006 (2009). [arXiv:0902.0834 [hep-ph]].

[57] E. Aprile, http://www.physics.ucla.edu/hep/dm10/talks/aprile.pdf.

[58] H. Davoudiasl, D. E. Morrissey, K. Sigurdson, S. Tulin, [arXiv:1106.4320 [hep-ph]].

[59] T. F. -L. collaboration, [arXiv:1108.3546 [astro-ph.HE]].

[60] K. N. Abazajian and J. P. Harding, JCAP **1201**, 041 (2012) [arXiv:1110.6151 [hep-ph]].

[61] Y. Cui, J. D. Mason, L. Randall, JHEP **1011**, 017 (2010). [arXiv:1006.0983 [hep-ph]].

[62] S. P. Ahlen, V. M. Balebanov, R. Battiston, U. Becker, J. Burger, M. Capell, H. F. Chen, H. S. Chen *et al.*, Nucl. Instrum. Meth. **A350**, 351-367 (1994).

[63] R. Barate *et al.* [ALEPH Collaboration], Eur. Phys. J. **C11**, 193-216 (1999); D. Fouchez, "Search for charginos and neutralinos with the ALEPH experiment at LEP-2."

[64] G. D. Kribs, A. Martin, T. S. Roy, M. Spannowsky, Phys. Rev. **D81**, 111501 (2010). [arXiv:0912.4731 [hep-ph]]; G. D. Kribs, A. Martin, T. S. Roy, M. Spannowsky, Phys. Rev. **D82**, 095012 (2010). [arXiv:1006.1656 [hep-ph]].

[65] G. Aad *et al.* [ATLAS Collaboration], arXiv:1109.6572 [hep-ex].

[66] H. Baer, C. Balazs, A. Belyaev, T. Krupovnickas, X. Tata, JHEP **0306**, 054 (2003). [hep-ph/0304303].

[67] V. M. Abazov *et al.* [D0 Collaboration], Phys. Lett. **B693**, 95-101 (2010). [arXiv:1005.2222 [hep-ex]].

[68] C. A. Baker, D. D. Doyle, P. Geltenbort, K. Green, M. G. D. van der Grinten, P. G. Harris, P. Iaydjiev, S. N. Ivanov *et al.*, Phys. Rev. Lett. **97**, 131801 (2006). [hep-ex/0602020].

[69] J. J. Hudson, D. M. Kara, I. J. Smallman, B. E. Sauer, M. R. Tarbutt, E. A. Hinds, Nature **473**, 493-496 (2011).